MODIFYING NANOPARTICLE SHAPE BY CHOICE OF SYNTHETIC METHOD: NANORODS, SPHERES, MUTIPODS, AND GELS

By

KHADGA M. SHRESTHA

B. S., TRIBHUVAN UNIVERSITY, KATHMANDU, NEPAL, 1993
M. S., TRIBHUVAN UNIVERSITY, KATHMANDU, NEPAL, 1995

AN ABSTRACT OF A DISSERTATION

submitted in partial fulfillment of the requirements for the degree

DOCTOR OF PHILOSOPHY

Department of Chemistry
College of Arts and Sciences

KANSAS STATE UNIVERSITY
Manhattan, Kansas

2012

Abstract

A series of nanoparticle synthesis methods were devised with the aim of controlling shape. CuO nanorods were synthesized by a hydrothermal treatment with different chemical combinations. Physical parameters: concentration, temperature, and aging time greatly affected the size, morphology and the composition of nanorods. These CuO nanomaterials were reduced to metallic copper at elevated temperature by 4% H_2 diluted in helium while preserving the morphology. The CuO and Cu nanomaterials were employed for near infra-red (NIR) diffuse reflectance. Among them, CuO nanorods were found to be the best NIR diffuse reflectors, indicating potential application as NIR obscurants.

Cu_2O and its comoposite samples with different morphologies, some with unique morphologies, were synthesized by reducing Cu^{2+} precursors without using any surfactant. The effects of change of Cu-precursors, reducing agents, and other physical conditions such as temperature and pressure were investigated. Since Cu_2O is a semiconductor (E_g ~ 2.1 eV), these samples were used as photocatalyst for the degradation of methyl violet B solution under UV-vis light and as dark catalysts for decomposition of H_2O_2 to investigate the effect of morphology. The photocatalytic activity was found to be morphology dependent and the dark catalytic activity was found to be dependent on both surface area and morphology.

Mixed oxides of MgO and TiO_2 with different ratios, and pure TiO_2 were synthesized by two methods—flame synthesis and aerogel. These mixed oxides were employed as photo-catalysts under UV-vis light to oxidize acetaldehyde. The mixed oxides with low content of MgO (~ 2 mole %) were found to be more UV active photo-catalysts for the degradation of acetaldehyde

than the degradation by TiO_2. The mixed oxides prepared by the aerogel method were found to be superior photo-catalysts than the mixed oxides of equal ratio prepared by flame synthesis.

Silica aerosol gels were prepared by two methods: detonation and flame synthesis. Hexamethyldisiloxane (HMDSO) was used as a precursor during the detonation at different conditions. Interestingly, spherical silica nanoparticles were found to be formed by the detonation. Relatively smaller silica nanoparticles with larger volume fraction were found to be favorable for the formation of silica aerosol gels. During the flame synthesis, the silicon precursors, dimethoxydimethylsilane (DMDMS) and HMDSO, were used. Different shapes—spherical, oval, and non-spherical—and sizes of silica particles were formed. These silica nanomaterials were almost amorphous, and they might have many potential applications.

MODIFYING NANOPARTICLE SHAPE BY CHOICE OF SYNTHETIC METHOD: NANORODS, SPHERES, MUTIPODS, AND GELS

by

KHADGA M. SHRESTHA

B. S., TRIBHUVAN UNIVERSITY, KATHMANDU, NEPAL, 1993
M. S., TRIBHUVAN UNIVERSITY, KATHMANDU, NEPAL, 1995

A DISSERTATION

submitted in partial fulfillment of the requirements for the degree

DOCTOR OF PHILOSOPHY

Department of Chemistry
College of Arts and Sciences

KANSAS STATE UNIVERSITY
Manhattan, Kansas

2012

Approved by:

Major Professor
Kenneth J. Klabunde

Copyright

Abstract

A series of nanoparticle synthesis methods were devised with the aim of controlling shape. CuO nanorods were synthesized by a hydrothermal treatment with different chemical combinations. Physical parameters: concentration, temperature, and aging time greatly affected the size, morphology and the composition of nanorods. These CuO nanomaterials were reduced to metallic copper at elevated temperature by 4% H_2 diluted in helium while preserving the morphology. The CuO and Cu nanomaterials were employed for near infra-red (NIR) diffuse reflectance. Among them, CuO nanorods were found to be the best NIR diffuse reflectors, indicating potential application as NIR obscurants.

Cu_2O and its comoposite samples with different morphologies, some with unique morphologies, were synthesized by reducing Cu^{2+} precursors without using any surfactant. The effects of change of Cu-precursors, reducing agents, and other physical conditions such as temperature and pressure were investigated. Since Cu_2O is a semiconductor (E_g ~ 2.1 eV), these samples were used as photocatalyst for the degradation of methyl violet B solution under UV-vis light and as dark catalysts for decomposition of H_2O_2 to investigate the effect of morphology. The photocatalytic activity was found to be morphology dependent and the dark catalytic activity was found to be dependent on both surface area and morphology.

Mixed oxides of MgO and TiO_2 with different ratios, and pure TiO_2 were synthesized by two methods—flame synthesis and aerogel. These mixed oxides were employed as photo-catalysts under UV-vis light to oxidize acetaldehyde. The mixed oxides with low content of MgO (~ 2 mole %) were found to be more UV active photo-catalysts for the degradation of acetaldehyde

than the degradation by TiO_2. The mixed oxides prepared by the aerogel method were found to be superior photo-catalysts than the mixed oxides of equal ratio prepared by flame synthesis.

Silica aerosol gels were prepared by two methods: detonation and flame synthesis. Hexamethyldisiloxane (HMDSO) was used as a precursor during the detonation at different conditions. Interestingly, spherical silica nanoparticles were found to be formed by the detonation. Relatively smaller silica nanoparticles with larger volume fraction were found to be favorable for the formation of silica aerosol gels. During the flame synthesis, the silicon precursors, dimethoxydimethylsilane (DMDMS) and HMDSO, were used. Different shapes—spherical, oval, and non-spherical—and sizes of silica particles were formed. These silica nanomaterials were almost amorphous, and they might have many potential applications.

Table of Contents

List of Figures

List of Tables

Acknowledgements

I would like to acknowledge many people for helping me to complete my Ph. D. studies. First of all, I would like to express my sincere gratitude to my doctorate supervisor, Professor Kenneth J. Klabunde, for continuous support and prominent guidance in his wonderful research group. He always encouraged me to think critically and work scientifically. I highly appreciate him for providing me a greater extent of academic freedom to work in his group. His kind nature always directed me to be self-motivated, and let me work in a pleasant environment. I have learned many qualities and research disciplines from him and his research group. Furthermore, I would like to thank him for helping me with paper-writing and allowing conference participacipation.

I would like to thank my committee members: Dr. Eric M. Maatta, Dr. Xiuzhi Susan Sun, Dr. Viktor Chikan, Chairperson Dr. Kevin Lease, and my major adviser Dr. Kenneth J. Klabunde. Thank you very much for your valuable time, discussions, and suggestions.

I would like to acknowledge Prof. Christopher M. Sorensen for his help for the synthesis of silica aerosol gels prepared by detonation and flame synthesis in his laboratory in the Department of Physics. He also helped me for interpretation of some research data. I am thankful as I learned some interdisciplinary research activities.

I would like to express my gratitude to Dr. Shyamala Rajagopalan of Nanoscale Corporation for her friendly help to work in a joint project so that I got a chance to learn some industrial research disciplines.

I would like to praise my past and current research group members: Dr. Zhiqiang Yang, Dr. Dambar B. Hamal, Dr. Sreeram Cingarappu, Dr. Yenting Kuo, Dr. Deepa Jose, Manindu Peiris, Yijun Sun for working in friendly environment and for their every help.

I would like to thank Earline Dikeman for her help in teaching courses, and departmental staff. I would like to express my gratitude to Mr. Tobe Eggers, Mr. Jim Hodgson, Dr. John Desper, Mr. Kent Hampton, Dr. Dan Boyle, Mr. Ron Jackson for fixing and providing the equipment to complete my research projects. I would like to acknowledge US Army Research, Targeted Excellence, Nanoscale Corporation, Department of Energy, National Science Foundation (EPSCoR) for funding. Furthermore, I am thankful to the Department of Chemistry and Graduate School for the admission at K-State.

Lastly, I would like to thank my all family members, specially my encouraging wife Meena Pradhan for her continuous support and my lovely son Deepankar Shrestha providing me a pleasing environment all the time. Moreover, I would like to thank my father-in-law Man B. Shrestha, mother-in-law Janaki Shrestha, and brother-in-law Gopal M. Pradhan for their unforgettable supports to earn higher education from USA.

Dedication

To my parents

Mother Nir Maya Shrestha and Late Father Ganesh Dash Shrestha

To my wife

Meena Pradhan

For their unlimited love, encourage, and support

Preface

Controlling the Shape and Properties of Nanoscale Materials by Synthetic Methods: CuO, Cu, Cu_2O, Cu_2O-Cu, Cu_2O-Cu, MgO-TiO_2, and SiO_2.

Chapter 1 - Introduction

Properties of materials depend upon their intensive atomic/molecular structure, composition, interface, defects, and other physical and chemical parameters. On the basis of their properties, various materials have been widely exploited for many purposes in the long course of time, especially using their bulk properties. In the last two decades, nanoscience and nanotechnology have been developed extensively due to the available tools and techniques for synthesis and characterization.[1] Nanoscience and technology deal with design and fabrication of nanomaterials, primarily with synthesis, characterization, applications. Nanomaterials fall in the range of those materials whose size is 1-100 nm at least in one dimension. Nanometer scale is a very small scale, for example, 10 H-atoms can be placed on the line segment of 1 nm so that 10,000,000,000 H-atoms can be set in a line segment of 1 m.[2] Nanomaterials contain a significant fraction of atoms on the surface. They give some transitional properties between bulk and atomic/molecular levels; so we observe some unique properties than their bulk counterparts. Many physical properties—optical, electronic, magnetic, melting point, color, solubility—are found to be different; for an example, melting point of nanomaterials can be lowered by 1000 ^{o}C, and their lattice constant also gets decreased. Ferroelectricity and ferromagnetism can be lost by nanomaterials. Bulk semiconductor materials can converted to insulator in nanoscale. Absorption and emission properties, color, and catalytic nature of nanomaterials can be different from bulk materials. Interestingly, the properties can be manipulated with change in size and morphology of nanomaterials. The new properties of nanomaterials can be exploited for various purposes. People of different fields of science have been involved in designing and exploiting new

properties of nanomaterials in their related fields; so nanoscience and technology has been an interdisciplinary and multidisciplinary field.[3]

Nanomaterials, as bulk matetials, can be classified into metals, semiconductors, and insulators. The study of semiconductor nanomaterials is one of the most investigated research field in the last two decandes. A semiconductor has special electrical properties; its conductivity lies between insulator and conductor. Semiconductor has two energy levels; lower energy level is called valence band and higher energy level is called conduction band. The electrons in valence are not available for the conduction; they can conduct when they are promoted to the conduction band, and some thermally promoted electrons can be conducted if electric field is provided. The electrons in the valence band can also be promoted to the conduction band after the absorption of an appropriate photon. The energy gap between conduction band and valence is called the band gap energy (E_g). After transition of an electron from valence band to conduction band, a positive charge called a hole is formed at the valence band; an electron at the conduction band and hole at valence band is called the electron-hole pair. At atomic or molecular level, the band gap is high, and the band gap is relatively low in bulk materials. Interestingly, the band gap of a semiconductor namaterials lies between those two levels. After the absorption of a photon, the electron-hole pair is loosely bound, and usually moves a longer distance than the lattice constant. Their lower energy state of an electrostatically bound electron-hole pair is called an exciton. The exciton, defined by the Bohr exciton radius (a_B), has a finite size—1nm to more than 100 nm depending on the material—within the crystal. If the size of a semiconductor is smaller than an exciton, the charge carrier becomes confined, raising the energy. Nanoscale semiconductor materials are interesting and important due to the quantum confinement. If the particle size is reduced below the exciton Bohr radius, this would lead to an increase the band gap energy.

Moreover, valence band and conductance band energy levels are quantized.[4] In the confinement regime, crystal size < a_B, there would be size-dependent photon absorption and fluorescence spectra with discrete electronic transition. For example, CdSe (a_B= 9.6 nm, E_g= 1.76 eV) can be tuned through quantum confinement to emit fluorescent light throughout the visible spectrum (Fig. 1, 2). Such small crystalline particles exhibit size-dependent optical and electronic properties. For example, CdSe semiconductor nanocrystals behave differently for the absorption and emission spectra in the visible range with the change in particle size.[5]

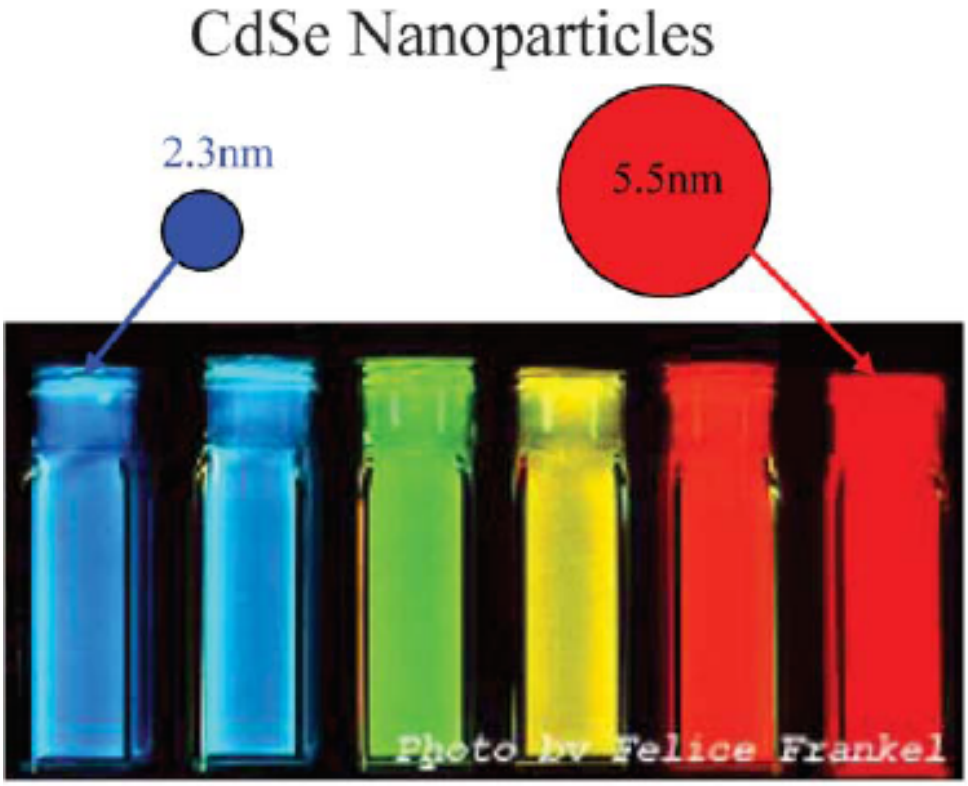

(Sample colors: deep blue, blue, green, yellow, red, and deep red from left to right)

Figure 1.1 Fluorescence emission of (CdSe)ZnS quantum dots of various sizes.[7b]

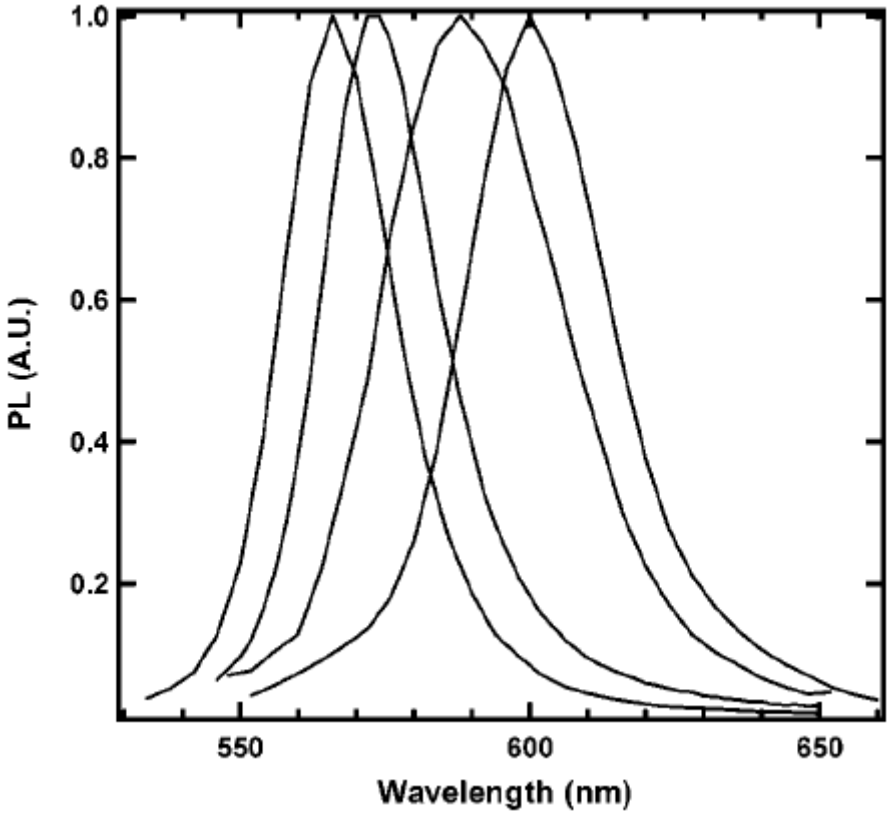

Figure 1.2 Photoluminescence spectra of 3.7 (±0.2) nm wide CdSe quantum rods with lengths of 9.2, 11.5, 28.0, and 37.2 nm, respectively (from left to right), excited at 450 nm.[5b]

Metal nanoparticles also show interesting properties in the nano regime. In small nanoparticles of metals, band structures disappear and discrete energy levels become dominant which can be explained on the basis of quantum mechanics.[6] Metal nanoparticles also show size dependent properties. Some physical properties such as melting point, color, magnetic and electrical properties of metal particles in nano regime might be different with change in particle size. For examples, bulk gold is yellow and silver is white, while gold nanoparticles appear red and silver nanoparticles appear yellow. Gold nanoparticles absorb strongly with broad band at different wavelengths in the visible region as size or shape of gold nanoparticle is changed (Fig. 3 and 4).

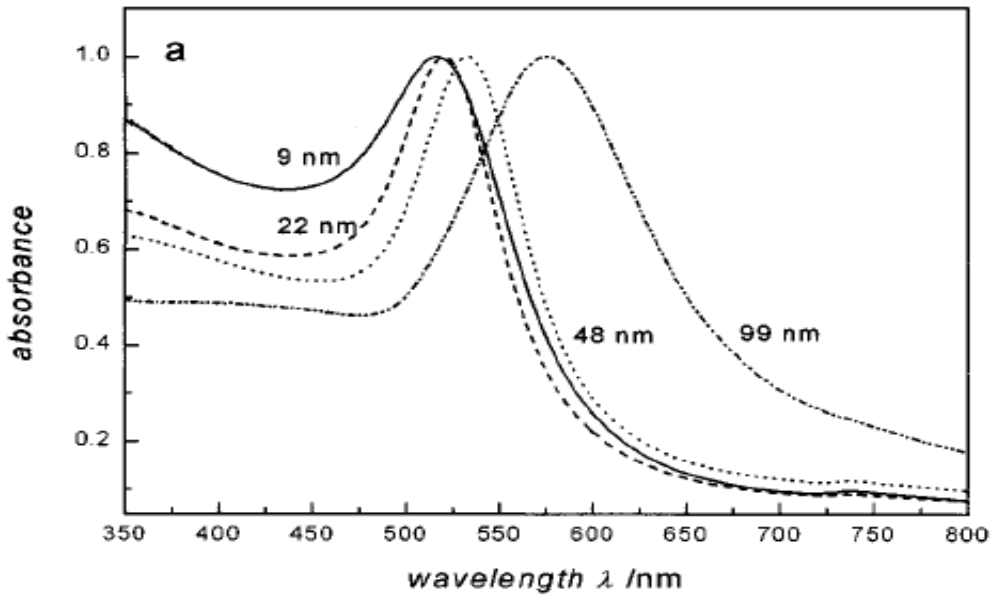

Figure 1.3 Absorption spectra of gold nanoparticles with various size.[7a]

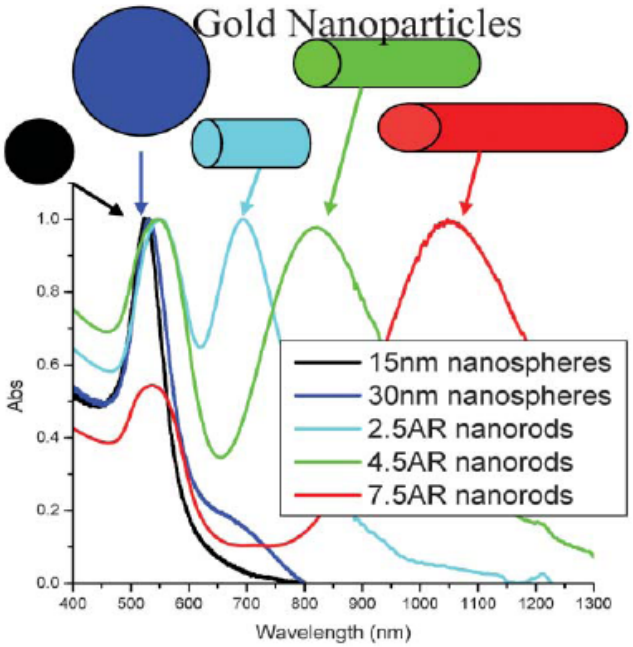

(Shape Colors: Black sphere, blue spheres, turquoise rod, green rod, and red rod from left to right.)

Figure 1.4 Absorption spectra of gold nanoparticles with various shapes.[7b]

The strong absorption in visible light is due to surface plasmon resonance; the surface plasmon resonance is due to the collective oscillation of electrons in the conductance band, and oscillation frequencies of gold and silver nanoparticles lie in the visible region. The surface plasmon resonance of gold nanoparticles can be tuned according to their particle size. Such properties of metal nanoparticles have many potential applications.[7,8]

Another important class of materials is ceramics (insulator). The band gap of ceramic materials is relatively too high; so the quantum size effect of insulator nanoparticles is less obvious. However, the surface properties can be significantly important. There are extensive researches about synthesis and characterization of this class of nanomaterials. Many investigations were carried out in the field of surface area, textural property, destructive adsorption, and catalytic property. Most of insulators are ionic in nature, and due to their ionic nature, it is likely to form stable defect sites such as edge, corners, and anion/cation vacancies, unsaturated surface.[9-13] These properties of ceramic materials might lead for the catalytic and destructive adsorption of some of unfriendly chemicals.

The properties of nanomaterials can be exploited in various applications. The research of nanomaterials has covered a large domain of scientific research; the study of nanomaterials has been the new field of research in physics, chemistry, biology, engineering, and medicine. Researchers have investigated cancer fighting nanoparticles.[14] About half of drug formulations have not been introduced to patients due to the lack of solubility in the blood stream.[15] Nanoparticles are small particles that can be dispersed in aqueous medium; so those drugs can be designed to nanoscale and can be brought in use. Nanomaterials can be used for the information storage.[16] Nanomaterials have appeared as strong agents for the destructive adsorbents of chemical and biological warfare agents.[17-18] They can be also used as new materials for

environmental remediation. Many pollutants can be removed by adsorption and dark and photocatalytic mechanisms.[19] One of the most important potential applications of namaterials is in the field of energy. Nanomaterials have been widely investigated in lithium ion batteries, and the results seem promising.[20] Semiconductor nanomaterials have been widely used for the investigation of photovoltaic cells.[21-22] Furthermore, some nanomaterials have been used as photocatalysts for water splitting.[23] Similarly, nanomaterials can be used for the photodecomposition of carbon dioxide to get useful products.[24] Some types of nanoparticles can be used as coloring agents.[25] The nanomaterials have been investigated as nanoelectrodes, smart magnetic fluids, optical computers etc.[26-29] In addition to pure nanomaterials, the study of nanocomposites is also an important field of research. Nanomaterials can be used for the development of polymer nanocomposites which showed better quality than traditional polymers.[30] Metal alloy nanoparticles have been investigated so as to get better properties.[31] People have also investigated the nanocomposites of semiconductor-insulator and insulator-insulator to find new properties and applications.[32-38] People have been paying for the investigation of metal and non-metals doped semiconductor nanomaterials, especially in the field of catalysis.[39]

Although nanomaterials have demonstrated effective results in certain areas, there are many challenges for the effective exploration in all areas of science; so more researches are going on for the development of many applications. There are different aspects of nanomaterials such as synthesis, characterization, and applications. One of the important aspects is to design and develop effective nanomaterials which depend upon the condition of synthesis; so it is important to develop a method for the synthesis of nanoparticles that would be well established and

commercially viable. There are some well established methods for the synthesis of various nanomaterials. There are some established methods as listed below.

1. Solgel method: aerogel and xerogel
2. Hydrothermal method
3. Flame synthesis
4. Electrolysis
5. Solvated metal atom dispersion (SMAD)
6. Digestive ripening
7. Chemical vapor deposition
8. Detonation
9. Inverse micelle method
10. Photodeposition
11. Microwave synthesis
12. Laser ablation
13. Template method

There is no universal method for the synthesis of all types of nanoparticles. A method for the synthesis depends upon nature of a nanomaterial, and its precursors. According to nature of nanomaterials and precursors, we can use one or more methods. Size, morphology, and properties of nanomaterials might be different according to choice of a method.

In this context, we synthesized some oxide nanomaterials. Among them, some are insulators, some are semiconductors, and some are composites of semiconductor and insulator oxide materials. The nanorods and nanoparticles of CuO, a semiconductor with Eg = 1.2 eV, were synthesized by a hydrothermal process; these semiconductor nanomaterials were reduced with

H_2 at elevated temperature to copper nanorods and nanopaticles while preserving their morphology. An optical property—the diffuse reflectance at near infrared region—of these CuO and Cu nanomaterials were measured and compared. Furthermore, Cu_2O samples, another semiconductor material with band gap = 2.2 eV, with different morphologies were synthesized changing different parameters without using any surfactant. In addition to pure CuO and Cu_2O, composite materials of Cu_2O—Cu_2O-Cu and Cu_2O-CuO—with different morphologies were also synthesized. Then catalytic properties of Cu_2O with different morphologies were investigated, and effects of morphologies were studied. The nanocomposites of MgO, an insulator, and TiO_2, a semiconductor, were also synthesized by two methods: flame synthesis and aerogel. The nanocomposite materials with various mole ratios of MgO and TiO_2 were employed for the photocatalytic degradation of acetaldehyde under UV light and interesting results were found. Moreover, SiO_2, an insulator, was synthesized by two methods: detonation and flame synthesis. The properties of these nanomaterials were investigated.

References

1. Gogotsi, Y. 'Nanomaterials Handbook' *CRC Press*, Taylor and Francis Group, Boca Raton, Florida, **2006**.

2. Cao, G. 'Nastrstructures and Nanomaterials: Synthesis, Properties, and Applications' *Imperial College Press*, London, **2004**.

3. Koch, C. C. 'Nanostructrured Materials: Processing, Properties, and Application' *Noyes Publication,* Norwich, NY, **2002**.

4. M. A. El-Sayed, *Acc. Chem. Res*. **2004**, 37, 326.

5. (a) B. O. Dabbousi, J. Rodriguez-Viejo, F. V. Mikulec, J. R. Heine, H. Mattoussi, R. Ober, K. F. Jensen and M. G. Bawendi, J. Phys. Chem. B, 1997, 101, 9463.

   (b) Li, L.S.; Hu, J.; Yang, W.; Alivisatos, A. P. *Nano Lett*. **2001**, 1, 349.

6. Klabunde, K. J. *Wiley-Interscience* Nanoscale Materials in Chemistry, **2001**.

7. (a) Link, S.; El-Sayed, M. A. *J. Phys. Chem. B* **1999,** *103,* 4212.

   (b) S. Eustis, M. A. El-Sayed, Chem. Soc. Rev., 2006, 35, 209.

8. A. Moores, F. Goettmann *New J. Chem*. 2006, 30, 1121.

9. Liu, H.; Feng, L.; Zhang, X.; Xue, O. *J. Phys. Chem*. 1995, 99, 332.

10. Utiyama, M.; Hattori, H.; Tanabe, K. J. Catal. 1978, 53, 237.

11. Sun, N.; Klabunde, K. J. *J. Am. Chem. Soc*. 1999, 121, 5587.

12. Khaleel, A.; Kapoor, P. N.; Klabunde, K. J. *Nanostruct. Mater*. **1999**, 11, 459.

13. Klabunde, K. J.; Stark, J. V.; Koper, O.; Mohsm C.; Park, D. G.; Decker, S.; Jiang, Y.; Lagadic, I.; Zhang, D.; *J. Phys. Chem*., **1996**, 100, 12142.

14. Avedisian, C. T.; Cavicchi; McEuen, P. L.; Zhou, X. *Ann. N. Y. Acad. Sci*. **2009**, 1161, 62.

15. Merisko-Liversidge, E. M.; Liversidge, G. G. *Toxicol. Pathol.* **2008**, 36, 43-48.

16. Suganuma, Y.; Trudeau, P. E.; Dhirani, A. A. *Nanotechnol* **2005**, 16, 1196.

17. Li, Y. X.; Klabunde, K. J. *Langmuir* **1991**, 7, 1388.

18. Lucas, E.; Klabunde, K. J. *Nanostruct. Mater*. **1999**, 12, 179.

19. Fan, J.; Yates, J. T., *J. Phys. Chem*. **1994**, 98, 952.

20. Zhang, D.; Qian, A.; Chen, J.; Wen, J.; Wang, L.; Chen, C. *Ionics* **2012**, 18, 591.

21. Kiwi, J.; Gratzel, M.; *Angew. Chemie: Int. Ed. Engl*., **1979**, 18, 624.

22. Riegel, G.; Bolton, R. *J. Phys. Chem*.**1995**, 280, 1716

23. Sathish, M.; Viswanathan, B.; Viswanath,R. P. *Int. J. Hydrogen Energy* **2006**, 31,891.

24. Roy, S. C.; Varghese, O. K.; Paulose, M.; Grimes, C. A. *ACSNano* **2010**, 4, 1259

25. Ruivo, A.; Gomes, C.; Lima, A.; Botelho, M. L.; Melo, R.; Belchior, A.;Matos, A. P. *Journal of Cultural Heritage* **2008**, 9, 134.

26. Buining, P. A.; Humbel, B. M.; Philipse, A. P.;Verkleij, A. J. *Langmuir* **1997,** *13,* 3921-3926.

27. Trudeau, M. L.; Ying, J. *Nanostruct. Mater*., **1996**, 7, 245.

28. Rosenweigh, F. E. *Ferrohydrodynamics, Cambridge University Press*, Newyork, **1985**.

29. Heath, J. R.; Kuekes, P. J.; Snider, G. S.; Williams, R. S. *Science* **1998**, 280, 1716.

30. Moniruzzaman, M.; Winey, K. I. *Macromolecules* **2006,** *39,* 5194.

31. Ghosh, T.; Leonard, B.M.; Zhou, Q.; Disalvo, F. J. *Chem. Mater*. **2010**, 22, 2190.

32. Chen, F.; Zhao, J.; Hidaka, H. *Int. J. Photoenergy* **2003**, 5, 209.

33. Hu, Y.; Li, C.; Gu, F.; Zhao, Y. *J. Alloys Compd*. **2007**, 432, 5.

34. Fang, J.; Bi, X.; Si, D.; Jiang, Z.; Huang, W. *Appl. Surf. Sci*. **2007**, 253, 8952.

35. Bandara, J.; Pradeep, U. W. *Thin Solid Films* **2008**, 517, 952.

36. K. T. Ranjit, K. T.; Martyanov, I.; Demydov, D.; Uma, S.; Rodrigues, S.; Klabunde, K. J. *J. Sol-Gel Sci. Techn.* **2006**, 40, 335.

37. Wei, W.; Li, H.; Chen, S.; Yuan, C.; Yuan, Q. *Cryst. Res. Technol*. **2009**, 44, 86.

38. Hamal, D. B.; Klabunde, K. J. *J. Colloid Interface Sci*. **2007**, 311, 514.

Chapter 2 - Synthesis of CuO Nanorods, Reduction of CuO into Cu Nanorods, and Diffuse Reflectance Measurements of CuO and Cu Nanomaterials in Near Infrared Region*

*It has been published in Journal of Physical Chemistry C (2010, 114, 14368-14376.)

2.1 Introduction

Transitional metal oxides and metals are extensively used in various applications because of their specific catalytic, optical, electrical, magnetic properties.[1,2] Among them, copper oxide (CuO) and copper metal are important materials; CuO is a p-type semiconductor, anti-ferromagnetic material, and high temperature superconductor with a narrow band gap of 1.2eV. It is used in batteries, gas sensing, magnetic storage media, solar energy conversion.[3] On the other hand, copper metal is extensively used as a conductor in modern electronic circuits due to its excellent electrical conductivity, and lower cost.[4]

It has been shown that nanomaterials have different optical, electrical, and magnetic, and structural properties depending upon size and morphology which are not fully explained by current theories.[5-6] There have been considerable efforts toward fabrication of CuO and Cu nanomaterials to enhance their existing applications. There are several reports on the synthesis of CuO nanomaterials with different morphologies—CuO nanoparticles,[7,8] nanocrystals,[9,10] nanowires,[11,12] and nanorods.[13,14] Nanoribbons and nanorings,[15] and nanoflowers[16,17] have also been reported. Similarly, there are several reports about copper nanomaterials—nanowires,[18-20] nanorods,[21-23] and nanoparticles.[24-29]

The extinction of light by matter is a common phenomenon. The extent of extinction of light depends upon the nature of the material and radiation. The extinction of infrared (IR) has a

significant role in military applications as this is the basis of IR obscurants. IR wavelengths (0.5 to 15 μm, tactical IR wave band) are important in military applications because most observation technologies rely on sensors that are operated in this wave band.[30] IR obscurants play an important role in military operations because they provide protection of military personnel, equipment, and installations from IR guided weapons.[31-33] In this context, certain nanomaterials might be excellent IR obscurants because they have potential to enhance the IR extinction. Nanomaterials of some metal oxides give more diffuse reflectance (ratio of scattering coefficient to scattering coefficient plus absorption coefficient) than bulk materials at the near infrared region (NIR).[34]

Herein, we report the synthesis of CuO nanorods by novel routes. Moreover, we also synthesized spheroidal CuO nanoparticles. Then we reduced these CuO nanorods to Cu nanorods and CuO nanonoparticles to Cu nanoparticles with hydrogen. It is important to note that we were able to preserve the morphology of these CuO nanomaterials after reduction. To the best of our knowledge, this is the first report of reduction of CuO nanomaterials to form Cu nanomaterials while preserving the morphology.

The ultimate objective of preparing CuO and Cu nanomaterials (nanorods and nanoparticles) was to compare their diffuse reflectance properties in the NIR region. The motivation behind the investigation of this optical property is to find out whether these materials with specific shape might have potential applications in military applications for NIR obscuration. Experimentally, we found that CuO nanorods are better NIR diffuse reflectors, and Cu nanorods are better NIR absorbers than other CuO and Cu samples. The investigation showed that an optical property is dependent on morphology and nature of materials. This indicates that these nanorods might have potential as an IR obscurant.

2.2 Experimental Section

2.2.1 Materials

a. Copper (II) nitrate (Fisher Chemical)

b. Ethanol (Decon Labs, Inc.)

c. Lactic acid (Arcos Organic)

d. Sodium hydroxide (Fisher Chemical)

e. Sodium lactate (Fluka)

f. Copper (II) sulfate (Fisher Chemical)

g.4% H_2 hydrogen gas diluted with helium (Linweld)

h. Copper (II) chloride (Sigma Aldrich)

i. Copper (II) acetate (Alfa-Aesar)

j. Oxalic acid (Fisher Chemical)

k. Copper(II) oxide(Fisher Chemical)

2.2.2 Synthesis of CuO nanorods. All chemical reagents were of analytical grade and used without further purification. We synthesized CuO nanorods by three different chemical combinations.

(i) In the first case, CuO nanorods were synthesized using copper(II) nitrate solution in ethanol, aq. solutions of NaOH, and lactic acid. In a particular experiment, 6 mL 8.5% lactic acid in water and 3 mL of 0.5 M $Cu(NO_3)_2$ in ethanol were placed in a beaker and stirred vigorously; the solution was transferred to 100 mL Teflon-lined autoclave. Then 10 mL 5 M NaOH was added; the reaction mixture was sealed in the stainless pressure container and kept for 24 hours at 140 ^oC. Then it was cooled to room temperature. The product was washed with distilled water three times followed by ethanol and dried at 80 ^oC for three hours. The maximum yield of the product recovered was 78 %.

(ii) In the second case, CuO nanorods were synthesized using $CuSO_4$, sodium lactate and NaOH. During the synthesis, 0.5 g copper(II) sulfate, and 0.45 g sodium lactate were taken in a

beaker containing 40 mL water and stirred for 15 minutes. Then 0.24 g NaOH was added and stirred for 1 hour. Then the reaction mixture was transferred to a Teflon-lined stainless steel autoclave and sealed. The reaction mixture was kept for 24 h at 140 ^{o}C. The product was cooled to the room temperature and washed with distilled water three times followed by ethanol. It was dried at 80 ^{o}C for three hours. The product was recovered and the yield was 81 %.

(iii) In the third case, 0.5 M $Cu(NO_3)_2$ solution in ethanol and 10 M aq. solution of NaOH were prepared as stock solutions. In a particular experiment, a mixture of 1 mL of 0.5 M $Cu(NO_3)_2$ and 10 mL of 5 M NaOH was placed in a 100 mL Teflon-lined stainless steel autoclave and sealed. The reaction mixture was kept at different reaction conditions; the effects of NaOH concentration, aging times, and temperatures were studied. In all cases, the reactor was allowed to cool at room temperature. The product was washed with distilled water three times and with ethanol two times; it was dried at 80 ^{o}C for three hours. The yield of CuO product was up to 84 % when measured for many experiments.

2.2.3 Reduction of CuO nanomaterials into Cu metal nanorods and nanoparticles.

CuO nanomaterials (nanorods and nanoparticles) were reduced to corresponding Cu nanomaterials. In this process, CuO was placed into a small glass boat of 10 cm in length, 0.8 cm internal diameter, and 1 cm external diameter. The boat was inserted in the middle of a long glass tube (length=30cm and internal diameter = 1.2cm) and supported with glass wool. The glass tube containing the sample boat equipped with a temperature monitor (sensor) was inserted in the cylindrical hole (diameter=1.5cm) of a rectangular furnace (l= 20 cm, b= 6 cm, h=7cm). The temperature sensor was inserted between the cylindrical hole of the furnace and the glass tube near the sample. One end of the glass tube was connected with a plastic tube for incoming dilute H_2 gas and the other end was connected with another tube for outgoing waste gas after

reaction. Then 4 % hydrogen gas diluted in helium was passed across the sample to drive out air for 10 minutes in the beginning. Then the furnace was heated electrically until the reduction temperature was attained with a continuous supply of the dilute H_2 gas and the temperature was held for 1 h; the temperature was monitored with thermocouple. After the reduction of CuO into Cu, the product was cooled to room temperature with the continuous flow of the mixture of gases. Furthermore, CuO nanoparticles (two different sizes) were synthesized by two reported methods and they were reduced to Cu nanoparticles.

2.2.4 Characterization. (i) Powder X-ray Diffraction (pXRD): The prepared CuO and Cu nanomaterials were investigated by powder X-ray diffraction. The instrument was a Scintag XDS 2000 spectrometer. The light source was CuKα radiation with applied voltage of 40 kV and current of 40 mA.

(ii) Scanning Electron Microscopy (SEM) and Transmission Electron Microscopy (TEM): The morphologies of the synthesized nanomaterials were observed by Scanning Electron Microscopy (SEM) and Transmission Electron Microscopy (TEM). SEM experiments were carried out by using a Scanning Electron Microscope-S3500N, Hitachi Science System, Ltd. at the Entomology Department of Kansas State University (KSU), microscopy and imaging facility. Some CuO and Cu nanomaterials were imaged with a transmission electron microscope, CM 100, Phillips at the biology department of KSU.

(iii) Brunauer-Emmet-Teller (BET) measurements: Surface area, pore volume and pore diameter of CuO and Cu nanomaterials were measured by using BET methods. The measurements were carried out using Microsorb II 2300 and Quantachrome NOVA 1200 instrumentation. The samples were cooled to 77 K using liquid nitrogen during the measurement.

(iv) Measurement of Diffuse Reflectance at NIR by CuO and Cu Nanomaterials: The synthesized CuO and Cu nanomaterials (nanorods and nanoparticles) were used for NIR diffuse reflectance; it was determined with measuring diffuse reflectance as the function of wavelength. A Cary 500 UV-vis-NIR spectrometer with diffuse reflectance accessories (DRA) was used in the range of 900-1800 nm. The sample cell was made of two transparent CaF_2 discs, a Teflon O-ring and screw-type combination in which nanomaterials were packed between two discs and an O-ring. Polytetrafluoroethylene (PTFE) powder of 1 μm particle size was taken as a reference material.

2.3 Results and Discussion

CuO nanorods were synthesized by three chemical combinations. In the first case, we used copper nitrate, lactic acid, and sodium hydroxide. The reaction mixture appeared deep blue due to formation of copper lactate; Copper hydroxide was formed by the reaction between the copper lactate and sodium hydroxide, and CuO nanorods were obtained upon decomposition of the copper hydroxide. Fig. 2.1a shows the pXRD pattern and Fig. 2.2 shows the SEM-EDS elemental analysis of the product; the pXRD pattern confirm the formation of CuO and the elemental analysis shows 1:1 molar ratio of copper and oxygen. SEM images (Fig. 2.3a-c) show spherical assemblies of the nanorods synthesized at 140 ^{o}C; the diameter of a spherical assembly is up to 11 micrometers. The spherical assembly consists of rectangular rods with thickness 20 nm to 150 nm and breath 100 nm to 200 nm. There was no separation of individual rods since they firmly assembled in the spherical structure. However, the nanorods synthesized at 150 ^{o}C (Fig. 2.3d) were assembled loosely in an elliptical fashions. There were also separate individual rods, and the length was found to be up to 11μm and thickness 50 nm to 200 nm. When synthesized at 150 ^{o}C, thickness and breath of the rods were found to be shortened. The end sides

of the rods were tapered with a little curvature that helped to form the spherical assemblies of nanorods. In some cases, hundreds of nanorods combined together to give a dense array. The proposed scheme for the spherical assembly is described by Fig. 2.4. It is supposed that there should be self-assembly process of CuO nanorods so as to get spherical collection; the viscous medium of lactic acid and small diameter/breath of nanorods at the end side might be the guiding factors for the assembly.

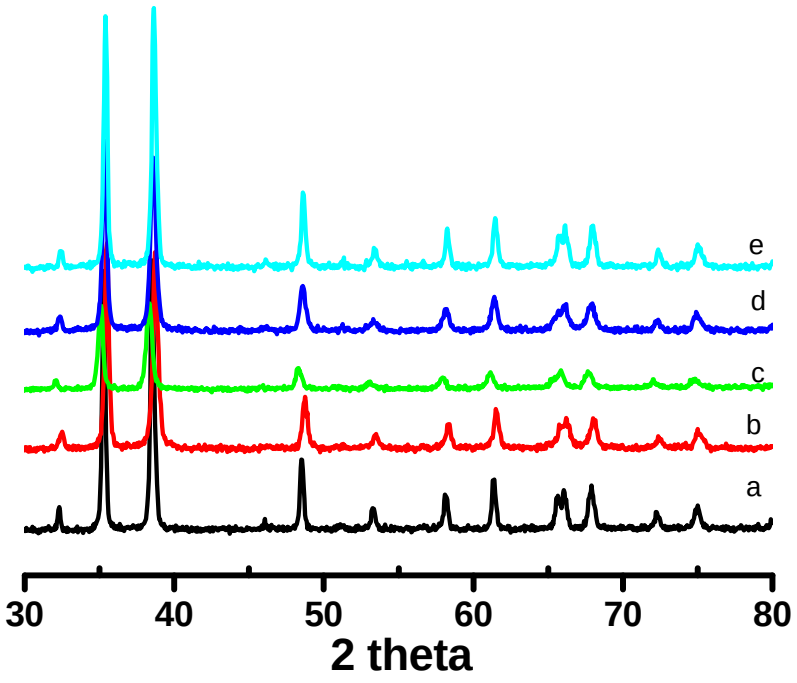

Figure 2.1 pXRD patterns of (a) spherical assemblies of CuO nanorods synthesized using $Cu(NO_3)_2$, lactic acid, and NaOH (b) CuO nanorods synthesized using $Cu(NO_3)_2$, sodium lactate, and NaOH (c) CuO nanoribbons and nanowires synthesized at room temperature in 24 h using 0.5 M $Cu(NO_3)_2$ and 5 M NaOH (d) CuO nanorods synthesized at 140 ^oC in 24 h using 0.5 M $Cu(NO_3)_2$ and 5 M NaOH (e) CuO nanorods synthesized at 140 ^oC in 24 h using 0.5 M $Cu(NO_3)_2$ and 7.5 M NaOH.

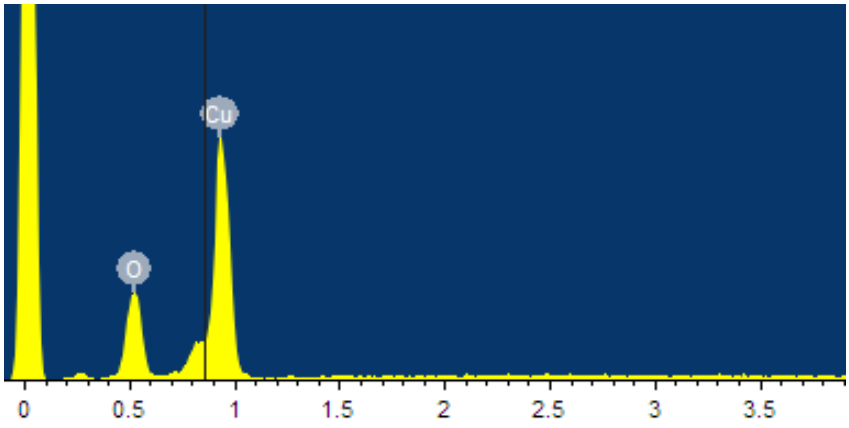

Figure 2.2 SEM-EDS element analysis for CuO nanorods synthesized at 140 ^{o}C in 24 h using 0.5 M $Cu(NO_3)_2$ and 5 M NaOH

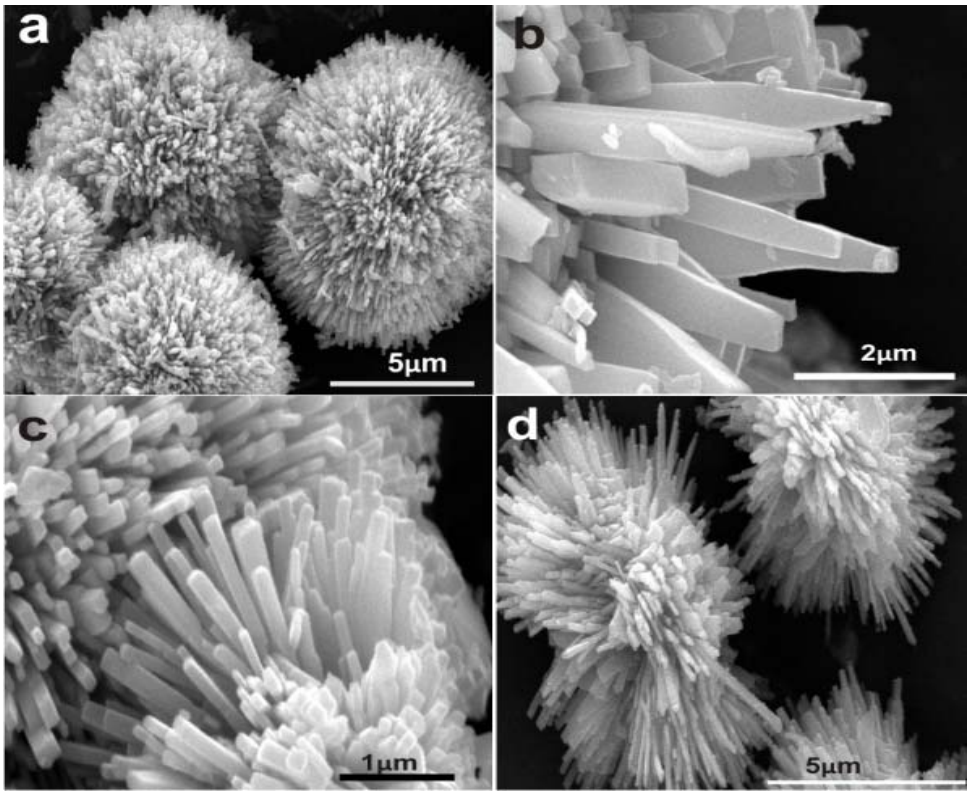

Figure 2.3 Spherical assemblies of CuO nanorods synthesized using copper nitrate, lactic acid, and sodium hydroxide in 24 h (a-b) at 140 ^{o}C (c-d) at 150 ^{o}C.

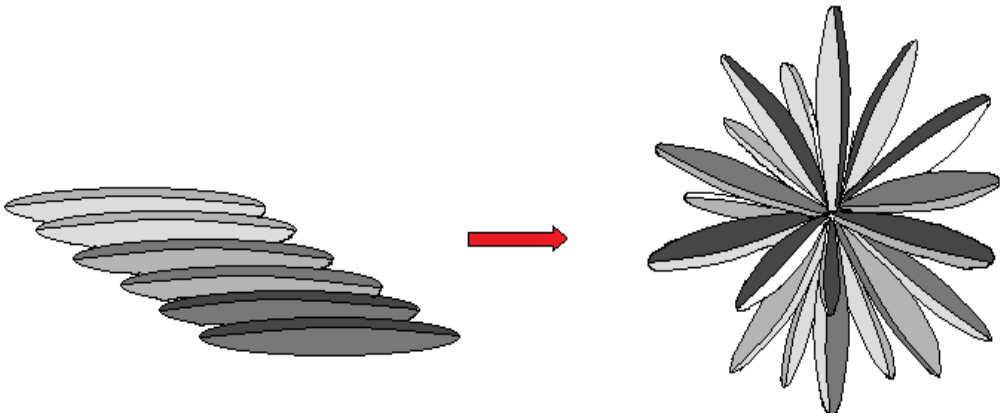

Figure 2.4 Proposed mechanism for spherical assemblies of CuO

In the second case, we synthesized the copper nanorods by using Copper(II) sulfate, sodium lactate, and sodium hydroxide. Copper sulfate and sodium lactate react to give copper lactate. Copper lactate reacts with sodium hydroxide to give copper hydroxide which under decomposition gives CuO nanorods; the formation of CuO was confirmed by pXRD (Fig.2.1b). Fig. 2.5a and 2.5b show SEM images of the CuO nanorods synthesized at 140 ^{o}C and 150 ^{o}C respectively. There was no significant difference on the morphology when they were synthesized at two different temperatures. Figure 5c show electron diffraction pattern the CuO nanorods (Fig. 2.5a). During the reaction, the formation of CuO can be illustrated by the following steps.

$$Cu^{2+} + \text{lactate} \rightarrow [Cu^{2+}\text{-lactate}]$$
$$[Cu^{2+}\text{-lactate}] + OH^{-} \rightarrow Cu(OH)_2$$
$$Cu(OH)_2 \rightarrow CuO + H_2O \qquad (2.1)$$

In the third case, CuO nanorods were synthesized using aq. solution of sodium hydroxide and ethanol solution of copper(II) nitrate; we carried out various sets of experiments changing temperature, concentration, aging time, and precursors so as to get optimum conditions for CuO nanorod synthesis, and studied the effects of these parameters on the morphology.

2.3.1 Effect of Temperature. First, we mixed the copper nitrate solution with 5 M NaOH and experiments were carried out for 24 h at various temperatures. The formation of CuO at room temperature was confirmed by pXRD (Fig. 2.1c) in the form of nanoribbons and nanowires (Fig. 2.6a). When the same reaction was carried out for 96 h, there were transitions of nanoribbons to nanoplates, and nanowires to nanorods (Fig. 2.6b). When the reaction was carried for 24 h at 100 ^{o}C, most CuO nanomaterials were thin rectangular nanoplates with a small number of nanorods (Fig. 2.6c). As the temperature was increased to 120 ^{o}C, most of the nanoplates were converted to nanorods with rectangular cross-section (thickness 40 nm to 150 nm). The length of the nanorods was found up to 2.8 micron (Fig. 2.6d). When the same experiment was carried out at 140 ^{o}C, we found all nanorods with similar structure (Fig. 2.6e). Figure 1d shows the pXRD pattern of CuO synthesized at this condition. These nanorods had both rectangular and square cross-sections, with length, breath, and thickness in the range of 1.5- 3.2 μm, 230- 500 nm, and 80- 200 nm respectively. When the experiment was carried out at 150^{o}C, all the nanorods were made of nearly square cross-section with sides of 250 - 650 nm and length up to 2.5 μm (Fig. 2.6f). In general, when the temperature was increased, the nanorods were found to be shortened and thickened. When the experiment was at 160 ^{o}C, nanorods were found to be broken down. On the basis of these experiments, the proper temperatures for the synthesis of CuO nanorods were between 140 ^{o}C and 150 ^{o}C.

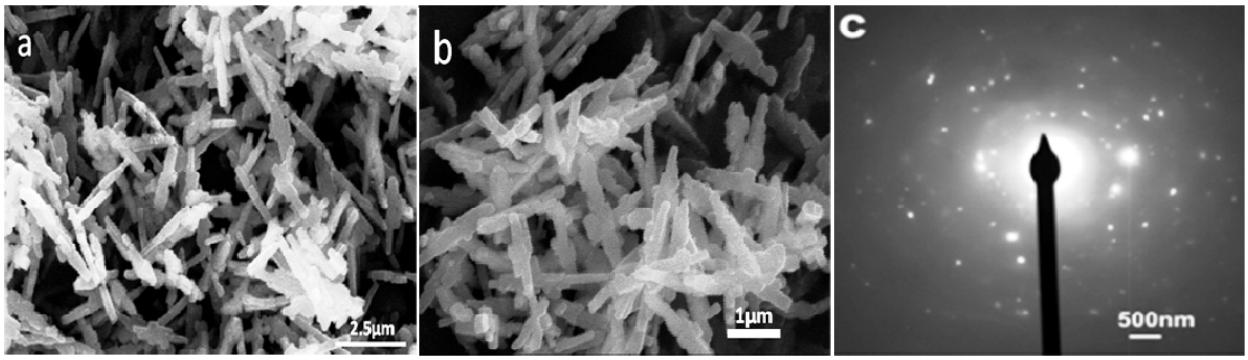

Figure 2.5 CuO nanorods synthesized using copper nitrate, sodium lactate, and sodium hydroxide for 24 h at (a) 140 ^{o}C (b) 150 ^{o}C (c) electron diffraction pattern of CuO nanorods.

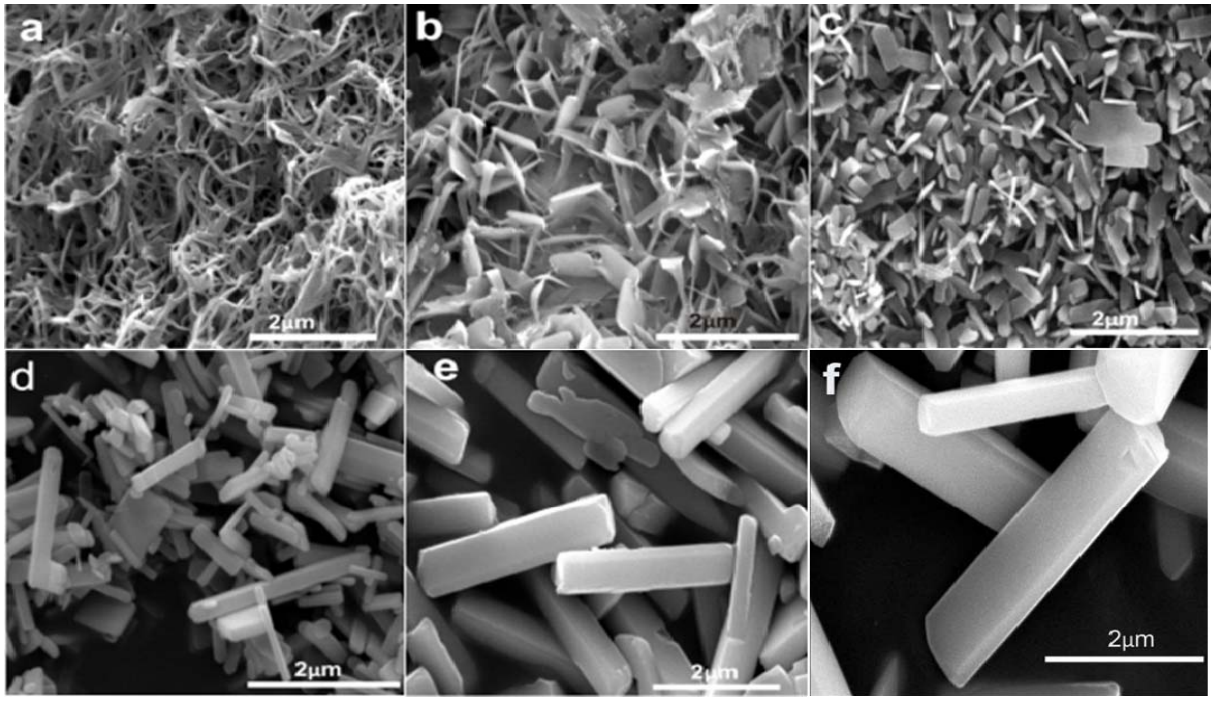

Figure 2.6 SEM images of CuO nanomaterials synthesized using copper nitrate and sodium hydroxide. (a) CuO nanoribbons and nanowires at room temperature in 24 h (b) conversion of CuO nanoribbons to nanoplates, and nanowires to nanorods in 96 h at room temperature (c) CuO nanorods and rectangular nanoplates at 100 ^{o}C in 24 h (d) CuO nanorods at 120 ^{o}C in 24 h (e) CuO nanorods at 140 ^{o}C in 24 h (f) CuO nanorods at 150 ^{o}C in 24 h.

2.3.2 Effect of NaOH Concentration. We also studied the effects of concentration of NaOH on the morphologies of CuO nanomaterials at 140 ^{o}C keeping other parameters the same. We used 2.5 M, 5.0 M, 6.5M, 7.5 M and 10.0 M sodium hydroxide solutions. At lower concentration of NaOH (2.5 M), most CuO nanomaterials were in the rectangular form and only a few were in the form of nanorods. When the concentration of NaOH was increased, the thickness of the nanorods was found to be increased. CuO nanorods with rectangular and square cross-section were found by using 5 M NaOH (Fig. 2.6e). When 6.5 M and 7.5 M NaOH were used, CuO nanorods with square and almost circular cross-section were formed (Fig.2.7a-b). The formation of CuO using 7.5 M NaOH was confirmed by pXRD (Fig. 2.1e). However, when 10 M NaOH was used, we observed a composite of Cu_2O and CuO with octahedral structure (Fig. 2.7c) instead of CuO nanorods. The formation of the composite was confirmed by pXRD (Fig. 2.7d). Some nanorods were distributed over the surface of the octahedral structure (Fig. 2.7c). The XRD pattern (Fig. 2.7d) shows that the main constituent of the octahedral structure was Cu_2O with a small amount of CuO. The major axis of the octahedron was found to be 6.7 μm to 10 μm. Apparently CuO was reduced to Cu_2O with ethanol used in the experiment.

2.3.3 Effects of different precursors. In addition to $Cu(NO_3)_2$, we used $CuCl_2$, and $(CH_3COO)_2Cu$ at 140^{o}C for 24 h. We obtained CuO nanorods in all cases and there were no significant changes in the morphology of the nanorods (Fig. 2.8a and 2.8b). However, we observed relatively shorter nanorods from $CuCl_2$ and $(CH_3COO)_2Cu$.

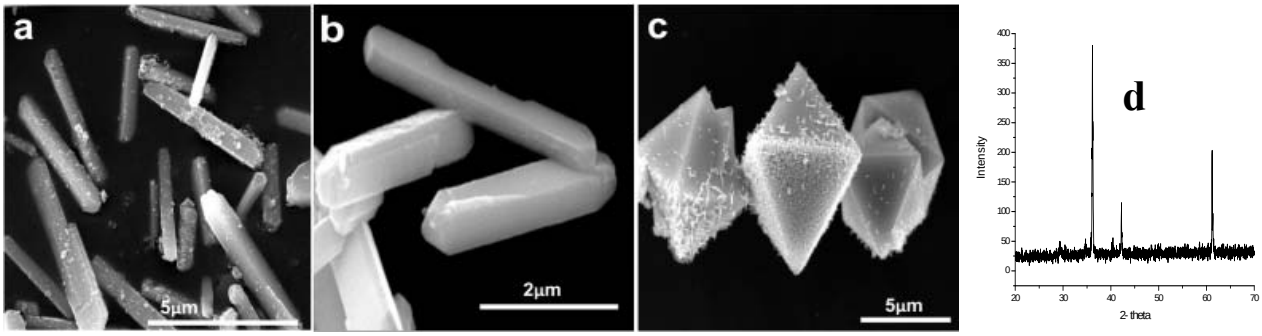

Figure 2.7 (a) CuO nanorods synthesized using 7.5 M NaOH and 0.5M $Cu(NO_3)_2$ at 140 ^oC for 24 h (b) CuO nanorods synthesized using 6.5 M NaOH and 0.5 M $Cu(NO_3)_2$ at 140 ^oC for 24 h (c) Octahedrons of CuO and Cu_2O composite synthesized using 10 M NaOH and 0.5 M $Cu(NO_3)_2$ at 140 ^oC for 24 h (d) XRD pattern of the octahedrons of CuO and Cu_2O composite.

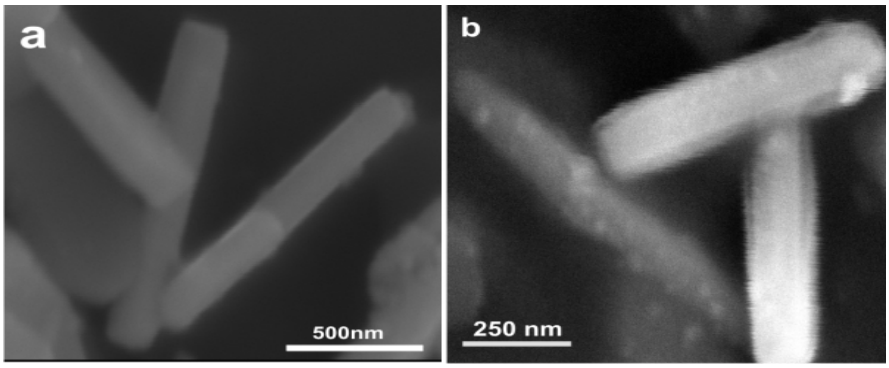

Figure 2.8 CuO nanorods synthesized using (a) $CuCl_2$ and (b) $(CH_3COO)_2Cu$ as Cu precursors.

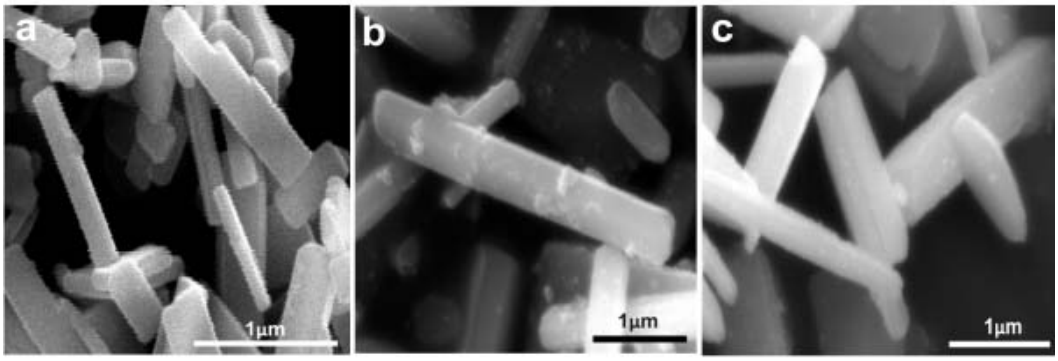

Figure 2.9 CuO nanorods synthesized at 140 ^oC using NaOH and $Cu(NO_3)_2$ at (a) 12 h (b) 48h (c) 96 h.

2.3.4 Effects of Aging Periods. We also studied the effects of aging times while keeping the other parameters the same. In this set of experiments, we used 1 mL 0.5 M $Cu(NO_3)_2$ and 10mL of 5 M NaOH at 140^oC. We carried out experiments for 12 h, 24 h, 48 h, and 72 h. As we increased the aging time, thickness of the nanorods was found to be increased continuously; we can clearly observe the effects comparing Figure 2.9a, 2.9b, 2.9c, and 2.6e. From the different sets of experiments, we found the following optimum conditions for the synthesis of CuO nanorods using Cu-precursors in ethanol and aqueous solution of NaOH— (a) Temperature: (140-150) ^oC (b) NaOH concentration: (5.0 -7.5) M (c) Aging Time: 24 h (d) Cupper Precursor: $Cu(NO_3)_2$.

When the $Cu(NO_3)_2$ solution was treated with concentrated sodium hydroxide, a blue precipitate was formed immediately. The blue precipitate turned into black after a couple of minutes. The SEM image of the black product formed at 24 h by the reaction between 10 mL of 5.0 M NaOH and 1 mL of 0.5 M $Cu(NO_3)_2$ at room temperature, shows long CuO chains (nanoribbons and nanowires) with width (30 – 160) nm (Fig. 2.6a). As the aging time was increased up to 96 h at room temperature with the same composition, these long chains of CuO were thickened and shortened, and a few started to break (Fig. 2.6b). The long chains (nanoribbons or nanowires) on treating at 100 ^oC were converted to CuO nanoplates or nanorods completely (Fig. 2.6c). On further treatment above 100 ^oC, rectangular nanoplates were converted into nanorods with various dimensions.

We optimized temperature, concentration of NaOH, aging period, and Cu-precursor for the synthesis of CuO nanorods with high aspect ratio and round-like cross section (Fig.2.7a-b) instead of rectangular cross section as these nanorods could diffuse more NIR (Fig 2.15a).

2.3.5 Reduction of CuO nanomaterials to Cu nanomaterials. Literature teaches that there are many methods for the synthesis of CuO nanomaterials but there are limited methods for the preparation of Cu nanomaterials. We investigated methods to reduce CuO nanomaterials to Cu nanomaterials while preserving the morphology. Among the methods, we tried hydrogen gas under specific conditions to reduce CuO to Cu.[35] During our experiments, we used 4 % H_2 gas diluted in helium at 285 ^oC for the reduction. Before raising the temperature, air was driven out using a mixture of helium and hydrogen gas. Then the temperature was raised by passing current electricity at the rate of 6 $^oC\ min^{-1}$ until 285 ^oC was attained with a continuous supply of hydrogen/helium gas at a flow rate 240 mL min^{-1}. We passed the gas mixture for one hour at 285 ^oC and then turned off the heat. The hot product was allowed to cool with a continuous supply of the dilute hydrogen gas until room temperature was attained so that copper product could be prevented from aerial oxidation above room temperature. The pXRD patterns of Cu products are shown in Fig. 2.10(a-d), which confirmed the reduction of all the CuO materials to copper metal; Cu_2O as a transient intermediate may or may not be formed that depends upon experimental conditions during the reduction.[35,44] SEM images (Fig. 2.11a-e) showed the reduction of CuO nanorods to Cu nanorods with preserving the morphology.

$$CuO + H_2 \rightarrow Cu + H_2O \qquad (2.2)$$

Panels a and b of Fig. 2.11 are SEM images of Cu nanorods obtained by reduction of the spherical assembly of CuO as described for Fig. 3(a-b); the reduction is confirmed by the pXRD pattern (Fig. 2.10b). Fig. 2.11c shows the SEM images of Cu nanorods obtained on reduction of CuO nanorods as described for Fig. 2.5a; and Fig. 2.11(d-e) are SEM images of Cu nanorods obtained on reduction of CuO nanorod samples as described for Fig.7b; the reduction was confirmed by XRD pattern (Fig.2.10c). Fig. 2.11f is a SEM image of Cu nanorods obtained

when the reduction was carried out at 295 ^{o}C by passing the dilute H_2 gas with the flow rate of 280 mL min^{-1} for CuO nanorods sample as described in Fig. 7b. Moreover, CuO porous particles with diameter of 2-3.8 μm were prepared by a reported method[36] (Fig.2.12a-b). They were reduced to porous Cu particles (Fig. 2.12c-d) under the same conditions of the reduction of CuO nanorods (pXRD pattern Fig.2.10a). Smaller nanoparticles with diameter 8-10 nm were also synthesized by another reported method[37] (Fig. 2.13a). Then the CuO nanoparticles were reduced to corresponding Cu nanoparticles (Fig. 13b) under the same condition as previously described (pXRD pattern Fig.2.10d).

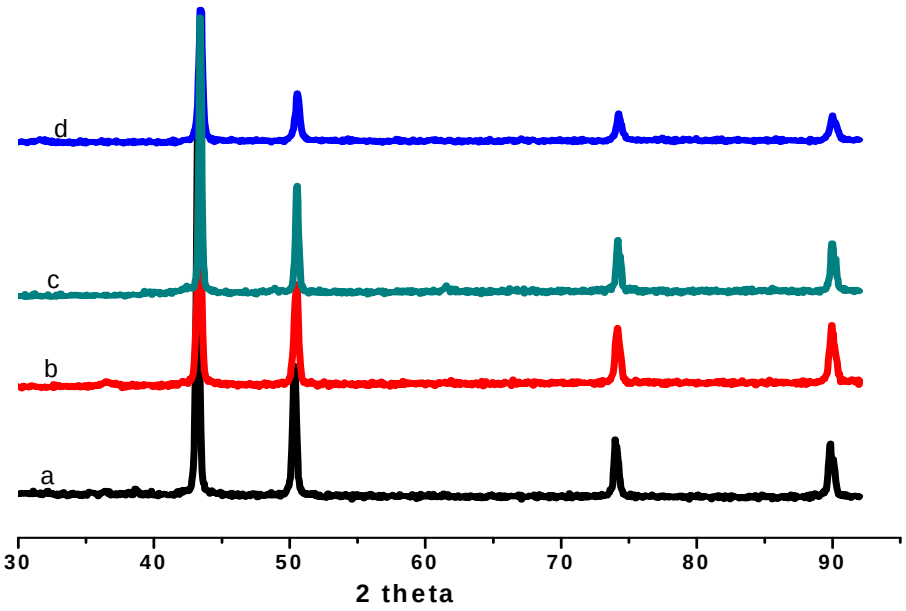

Figure 2.10 pXRD pattern for (a) Cu porous particles (fig. 12c,d) (b) Cu nanorods assembled spherically (fig. 11a) (c) Cu nanorods (fig. 11d) (d) Cu nanoparticles (fig. 13b)

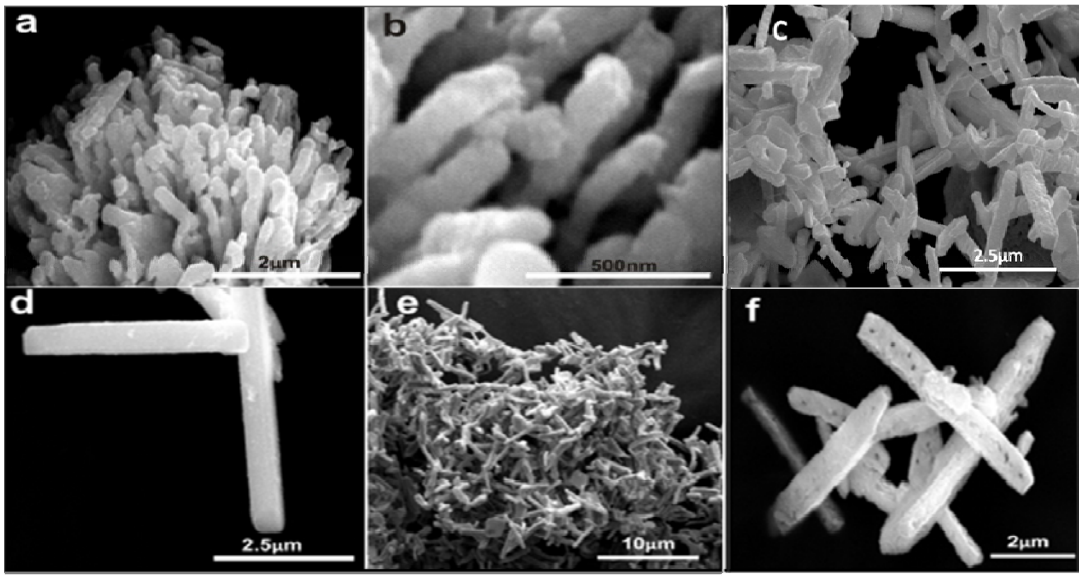

Figure 2.11 SEM images of (a-b) Spherical assemblies of Cu nanorods obtained by reducing CuO nanorods as described for figures 3a-b (c) Cu nanorods obtained reducing CuO nanorods as described for figures 5a (d) Cu nanorods obtained by reducing CuO nanorods as described for figure 7b at 285 ^{o}C at a flow rate 240 mL min^{-1}(e) Cu nanorods at lower magnifications obtained by reducing CuO nanorods as described for figure7a (f) Cu nanorods obtained by reducing CuO nanorods as described for figure 7a at 295 ^{o}C at a rate flow of 260 mL min^{-1}.

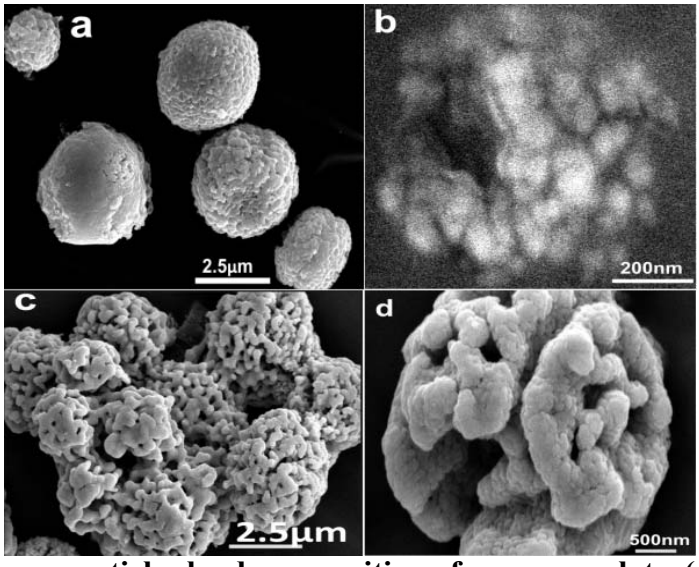

Figure 2.12 (a-b) CuO porous particles by decomposition of copper oxalate, (c-d) Cu porous particles by reducing the porous CuO particles (Fig.12a-b).

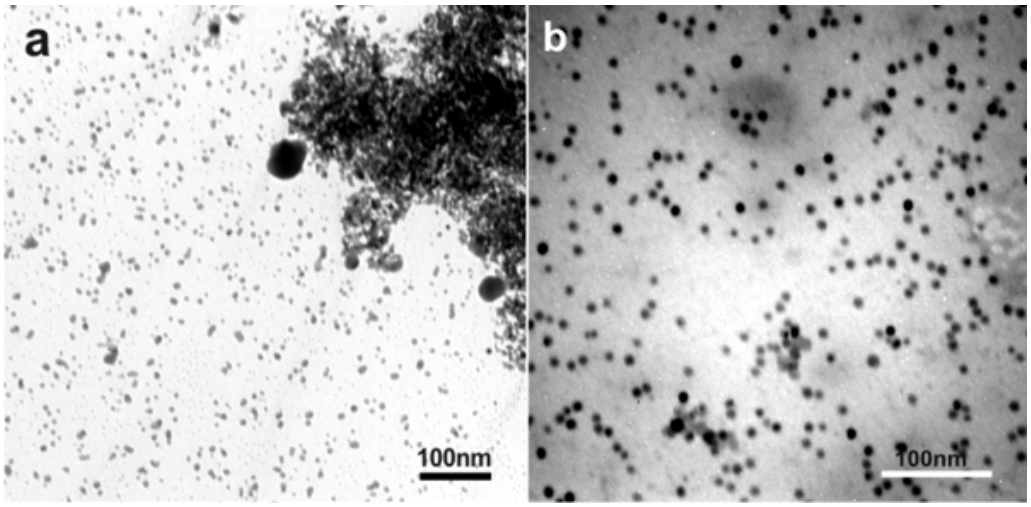

Figure 2.13. **(a) CuO nanopariticles by the reaction between copper acetate and ethanol (b) Cu nanoparticles obtained by reducing the CuO nanoparticles.**

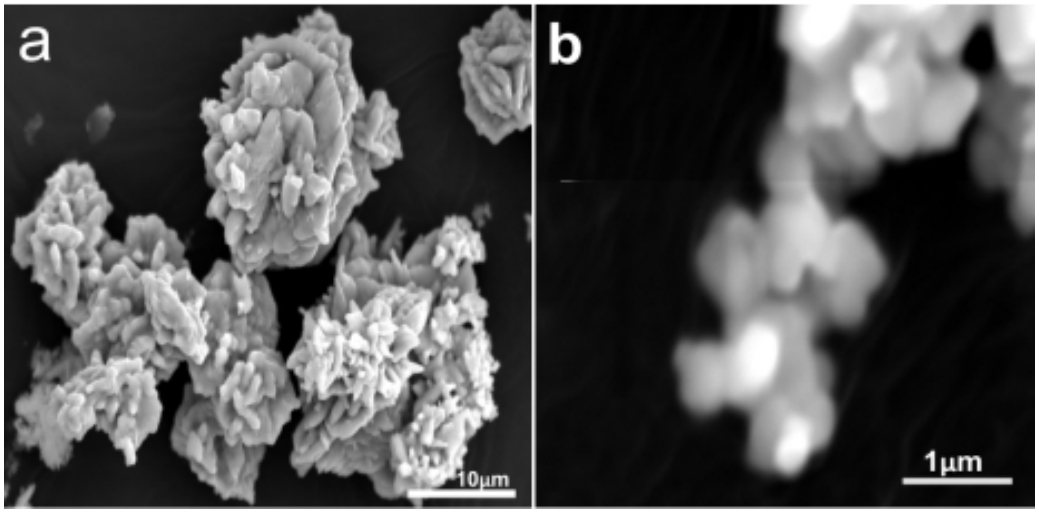

Figure 2.14 SEM images of commercial CuO bulk particles.

The important aspect of this reduction method was the absence of solvent and the reduction was carried out in a one step gas-solid phase reaction. The main achievement was to preserve the morphology of nanomaterials after reduction. However, we observed a slight decrease in the thickness of the nanorods and creation of a rough surface after reduction; the distortion was further enhanced when reduction was carried out at a higher rate flow (280 mL min^{-1}) of the

H_2/He mixture at 295 ^oC. The decrease in the thickness of nanorods is probably due to the lattice transition from monoclinic CuO nanorods to the more conpact face-centered cubic Cu nanorods. Mostly the thickness of the CuO nanorods or diameter of particles was decreased by 10-15 % during the reduction at 285 ^oC and 240 mL rate flow of H_2. The lattice change would induce the strain, and slower reduction was found to be more favorable to preserve the morphology. The rough surface of the Cu nanorods might be given by expulsion of water from the inner part of the nanorods especially at relatively higher temperature and continuous flow of H_2.

2.3.6 BET Measurement. Some CuO and Cu nanoparticles and nanorods were examined by BET measurements. During BET measurement, we took 150 ± 10 mg CuO and Cu nanomaterials. As expected, the surface area of the small nanoparticles (9-10 nm) was found to be relatively greater (58 ± 6 m^2/g) and lower (5 ± 2 m^2/g) for the bigger porous particles. Similarly the surface area of a sample of CuO nanorods, which are bigger in size than the smaller nanoparticles as described above, has lower suface area (5.2 ± 0.5 m^2/g, 9.2 ± 0.5 m^2/g). In general, surface area of all CuO nanomaterials were found to be relatively small since they were prepared by a hydrothermal process; in this method, solvents from the nanomaterials are removed without supercritical drying. So we cannot reduce the surface tension and pore network would be decreased. After reduction, the corresponding surface areas for each Cu nanomaterials were found to be lower. The decrease in surface area after reduction is possibly due to sintering when CuO is reduced at high temperature. The surface areas, pore volumes and pore diameters of various CuO and Cu samples with error data are shown in table 2.1.

Table 2.1 Surface area, pore volume and pore diameter of different CuO and Cu nanomaterials

Sample No.	Samples	BET surface area (m^2/g)	Pore volume (cc/g)	Pore Diameter (nm)
1	CuO nanorods (Fig. 2.7b)	5.2 ± 0.5	0.020 ± 0.010	2.4 ±0.5
2	CuO nanorods (Fig. 2.5b)	9.3 ± 0.5	0.030 ± 0.010	2.1 ± 0.2
3	CuO NPs (Fig. 2.12a)	5 ± 2	0.023 ± 0.007	2.9 ± 0.9
4	CuO NPs (Fig. 2.13a)	58 ± 6	0.128 ± 0.001	5.6± 0.0
5	Cu NRs (Fig. 2.11c)	1.3 ± 0.3	0.006 ± 0.002	2.9 ± 0.8
6	Cu NRs (Fig. 2.11d)	1.9 ± 0.3	0.007 ± 0.002	2.4± 0.4
7	Cu NPs (Fig. 2.13b)	5.2 ± 0.3	0.033 ± 0.001	3.8 ±0.0

(1) Sample 1: the CuO nanorods as described for figure 2.7b. (2) Sample 2: the CuO nanorods as described for figure 2.5b. (3) Sample 3: the porous nanoparticles as described for figure 2.12a. (4) Sample 4: the CuO nanoparticles as described for figure 2.13a. (5) Sample 5: Cu nanorods obtained by reduction of sample 1. (6) Sample 6: the Cu nanorods obtained reduction of sample 2. (7) Sample7: Cu nanoparticles obtained by reduction of sample 4.

2.3.7 Comparative Study of Diffuse Reflection at NIR by CuO and Cu nanomaterials. The CuO and Cu nanomaterials can be used in different applications; in particular, CuO can used as a catalyst[43-46] and Cu as a sensor based on its metallic plasmon

resonance properties.[47-49] However, our main interest was to investigate their NIR diffuse reflectance properties based on their morphologies.

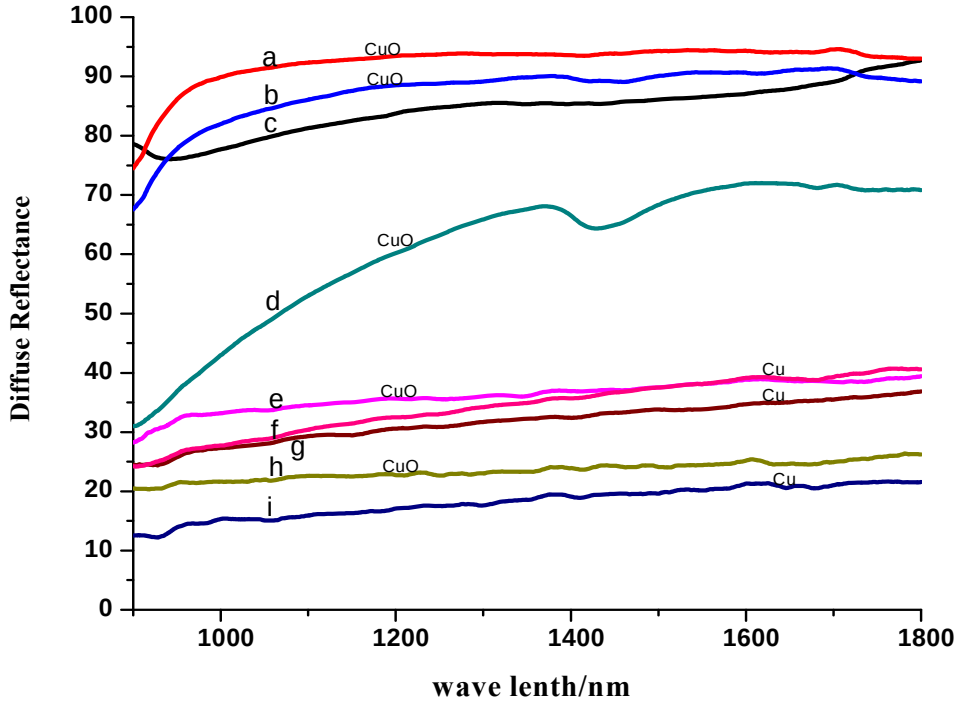

Figure 2.15. **Diffuse reflectance curves at NIR given by (a) CuO nanorods as described for figure 2.7b (b) CuO nanorods as described for figure 2.6e (c) PTFE as reference material (d) CuO nanoparticles as described for figure 2.13a (e) CuO porous particles as described for 2.12a-b (f) Cu porous particles as described for figure 2.12c-d (g) Cu nanoparticles as described for 2.13b (h) CuO commercial bulk particles (i) Cu nanorods as described for 2.11d-e.**

When a beam of radiation strikes an object, absorption, reflection and transmission take place. Light is extinguished either by absorption or scattering.[38] The extent of these phenomena depends upon the nature of material, particle size, morphology, surface, and wave length of radiation. If a sample is optically thick enough, no transmitted light is possible, so light is either absorbed or reflected by the sample. If a sample weakly absorbs, most of the light is reflected. So

when a NIR beam strikes a weakly absorbing media without transmission, the radiation penetrates the medium up to a certain thickness. The beam changes its direction due to reflection, refraction, and random diffraction at surfaces of various particles. The combination of all these effects is called diffuse light scattering.[39]

Previously, the diffuse reflectance of NIR from various metal oxide nanoparticles and corresponding bulk material has been compared in our laboratory; metal oxide nanoparticles have the ability to diffusely reflect more NIR (~15-20 %) than the corresponding bulk material.[34] Then our interest was to study how the change of morphology of the same nanomaterial affects NIR diffuse reflectance.

The diffuse reflectance of NIR by samples of CuO and Cu as described above were measured; powdered CuO and Cu nanorods (length= 2.7-5.4 μm, sides = 250-600 nm) and CuO nanoparticles of two different sizes (porous particles with diameter = 2-3.8 micron; smaller particles with diameter = 8-10 nm) were employed during measurements. About (300±10 mg) of each sample was taken in a sample holder so as to get a sufficient optical thickness to prevent transmission of the NIR. The measurement was carried out using a Cary 500 UV-vis-NIR spectrophotometer along the diffuse reflectance accessory (DRA). The measurement was carried out in a NIR region (wavelength range 900-1800 nm) in diffuse reflectance mode. Polytetrafluroethylene (PTFE) powder (Aldrich, particle size ~ 1 μm) was taken as a reference sample for the normalization of diffuse reflectance of CuO and Cu materials. The reproducibility limit was within ±5 %. Considering that there might be some adsorbate on the surface of the CuO and Cu samples that might affect the diffuse reflectance of NIR, all these samples were heated at 130^{o}C so as to remove volatile adsorbates, such as water. After cooling,

diffuse reflectance of NIR were measured immediately, and showed no significant differences for corresponding samples before and after heating; the differences were within the range of ±4. Figure 15 shows NIR diffuse reflectance curves (diffuse reflectance vs wave length) for different samples. CuO nanorods have the highest diffuse reflectance (Fig. 2.15a) and, relatively shorter and thinner CuO nanorods (Fig. 2.15b) gave slightly less diffuse reflectance. The diffuse reflectance of smaller nanoparticles (8-10 nm) is less than the diffuse reflectance given by both types of nanorods but greater than diffuse reflectance (Fig. 2.15e) given by bigger porous nanoparticles (diameter = 2-3.8 μm). The commercial CuO particles (Fig. 2.14) diffused the least amount of NIR (Fig. 2.15h). CuO nanorods are good diffuse reflectors among other CuO materials (nanoparticles and commercial CuO bulk powders), however, Cu nanomaterials are poor diffuse reflectors (Fig.2.15 f, g, i). The sample which reflects less NIR absorbs more so that Cu nanomaterials are good NIR absorbers. To understand and compare clearly, the diffuse reflectance given by all CuO and Cu materials with error data at three particular wave lengths has been presented in the table 2.2.

Table 2.2 **Diffuse reflectance of various CuO and Cu materials at 1000 nm, 1400 nm and 1800 nm**

Samples	R^a at 1000nm	R^a at 1400nm	R^a at 1800nm
CuO NRs- figure 2.15a	92	94	94
CuO NRs-figure 2.15b	83	91	90
CuO NPs(nm)- figure 2.15d	44	67	72
CuO NPs (μm)-figure 2.15e	34	37	40
CuO (CM)-figure 2.15h	22	24	27
Cu NRs-figure 2.15i	15	20	21
Cu NPs(nm)- figure 2.15g	27	33	37
Cu NPs(μm)-figure 2.15f	28	37	39

R^a: Diffuse Reflectance

Diffuse reflectance of light by complex systems such as powder nanorods and nanoparticles can be explained by Kubelka-Munk (KM) theory.[40-41] KM theory is expressed by following equation.

$$(1-R_\infty)^2/2R_\infty = F(R) = K/S \qquad (2.3)$$

K is the absorption coefficient, S is the scattering coefficient, R_∞ is the reflectance of the sample at infinite thickness, and F(R) is the KM function. Kubelka-Monk theory shows that diffuse reflectance from a thick powder starts at unity when the absorption is zero and then falls monotonically with an increase in the ratio of absorption to scattering, K/S, and the rate of fall decreases with increasing K/S. To lowest order scattering, S, increases with increasing real part, and absorption, K, increases with increasing imaginary part of the complex refractive index of the material; the complex refractive index is shown by equation (2.4).[42]

$$m = n + ik \qquad (2.4)$$

where ‘n’ and ‘k’ are real and imaginary parts of complex refractive index(m) respectively, ‘i’ is an imaginary number.

Fig. 2.15 shows reflectance measurements for a variety of the samples described herein. Plots (a) and (b) show results for CuO rods with dimension on the order of a couple of microns, shown in Fig. 2.7b and 6e, respectively. Reflectances are uniformly large above a wavelength λ ~960 nm but show a rapid drop for shorter λ. CuO is a semiconductor with a band gap of 1.2eV which correspond to λ_{gap} = 1030 nm. Thus we expect for $\lambda > \lambda_{gap}$ the CuO is an insulator with negligible imaginary part of the refractive index, hence small K leading to large reflectance; whereas for $\lambda < \lambda_{gap}$ CuO is a conductor with large imaginary part of the refractive index, hence large K leading to small reflectance, and plot (a) and (b) in Fig. 2.15 can be explained on this basis. However, it is remarkable that the known band gap value is 7% larger in λ than observed here, a discrepancy that we cannot explain. Plot (d) in Figure 2.15 is for CuO nanoparticles on the order of 8-10 nm in diameter, shown in Fig. 13a. The reflectance is significantly different than for the same composition, CuO, in plots (a) and (b) to imply the particle morphology is the cause of the difference. Small particles can provide a textured surface with many reflectance leading to large effect on K (equation 2.1). Overall the reflectance is smaller with smaller λ, consistent with the semiconductor interpretation given for (a) and (b). However, the implied band gap is diffuse, possibly due to a particle size distribution. Moreover, small semiconductor particles typically have higher energy, blue shifted band gaps relative to the bulk. Plot (d) in Fig. 2.15, if anything, tends to show a redder, lower energy band gap, which is not clear to explain.

Plot (e) in Fig. 2.15 is for CuO porous particles shown in Figure 2.12(a,b). The reflectance is uniformly low with the band gap onset at around 970 nm. The overall size of particles is ca. 3 microns but the porosity makes the spheres rough. To explain the low reflectance we propose

that the surface roughness causes an enhanced absorption K even though the refractive index for $\lambda > \lambda_{gap}$ is mostly real. This roughness enhanced K causes the reduced diffuse reflectance. This is similar to the texture argument for small particles given above. In the same way, we explain the diffused reflectance curve, plot (h) in Fig. 2.15, for commercial bulk CuO as shown Fig. 2.14(a,b); commercial CuO has more surface roughness with particle size from a couple of microns to several micrometers. Plot (f) in Fig. 2.15 is for Cu porous spherical particles as shown in Fig. 2.12(c, d). Copper is a metal with a large imaginary part to the complex refractive index, hence large K leading to small reflectance, as observed. It is interesting that plot (f) is very similar to plot (e) for CuO which was explained by surface roughness enhanced K. The similarity implies that surface roughness is more important than the imaginary refractive index in this case. Plot (g) in Fig. 2.15 is for Cu nanoparticles on the order of 8-10 nm in diameter, shown in Figure 2.13b. The reflectance is low consistent with a large K due to the metallic, imaginary refractive index, Cu. Plot (i) in Fig. 2.15 is for Cu rods with dimension on the order of a few microns, shown in Fig. 2.11(d,e). Once again, the reflectance is low, consistent with a large K due to the metallic imaginary refractive index.

Furthermore, nanorods were randomly oriented; in addition to morphology, size, refractive indices, and surface texture, diffuse reflectance of CuO/Cu nanorods might possibly depend on their orientation. In randomly oriented samples, there will be more inner space so that NIR will penetrate the layer of the samples, and the direction of the radiation will be changed each time when it strikes a boundary within the sample, possibly leading to more interaction (scattering or absorption).[34,39,41] From the experimental data (Table 2.2 and Fig. 2.15), CuO nanorods showed more diffuse reflectance, whereas Cu nanorods showed less diffuse reflectance (more absorption), and this result could possibly be related to orientation of these nanorods.

These data improve our empirical knowledge of diffuse reflectance properties of various CuO and Cu nanomaterials with different shapes and sizes. At this point, we are not able to theoretically model these materials, but hope to delve into this area in the future.

2.4. Conclusions

CuO nanorods were synthesized by hydrothermal synthetic routes under novel physical and chemical conditions. The size, morphology, and dimensions of nanorods were significantly affected by concentration, temperature and aging time. These CuO nanorods were reduced to Cu nanorods by 4% hydrogen diluted in helium at elevated temperature. Furthermore, CuO porous particles (2-3.7μm) and CuO nanoparticles (8-10 nm) were also reduced by the 4% dilute H_2 to metallic copper particles at the same conditions. The morphology of the CuO nanomaterials after reduction was preserved in the form of metallic Cu. The CuO and Cu nanomaterials were employed for diffuse reflections at NIR region. From the comparative study, we found that CuO nanorods exhibited high NIR diffuse reflectance due to the large real (mathematical) part of the complex refractive index. However, normal micron scale CuO particles, and Cu nanomaterials with different morphologies demonstrated low NIR diffuse reflectance. The low NIR diffuse reflectance by relatively large CuO particles is attributed to their rough surface so as to absorb NIR; the low diffuse reflectance of Cu nanomaterials is attributed to the large imaginary (mathematical) part of the complex refractive index of copper metal. The high diffuse reflectance of NIR by CuO nanorods suggests that it could have applications as an NIR obscurant.

Acknowledgement

This work was partially funded through the award of a contract from the United States Marine Corps Systems Command To M2 Technologies Inc, KY, and the Army Research Office.

2.5 References

(1) Nickolov, R. N.; Donkova, B.V.; Milenova, K.I.; Mehandjiev, D.R. *Adsorpt. Sci. Technol.* **2006**, 24, 2006.

(2) Khanna, P.K.; Gaikwad, S.; Adhyapak, P.V.; Singh, N.; Marimuthu R., *Mater. Lett.* **2007**, 61, 4711–4714.

(3) Yang, Z.; Xu, J.; Zhang, W.; Liu, A.; Tang, S. *J. Solid State Chem.* **2007**, 180, 1390-1396.

(4) Wen, X.; Xie, Y.; Choi, C.L.; Wan, K.C.; Li, X.; Yang; S. *Langmuir* **2005,** *21,* 4729-4737.

(5) Klabunde, K.J. *Nanoscale Materials in Chemistry*, *1st Edition*, Wiley Inter-Science, 2001.

(6) Liz-Marzán, L.M.; Kamat, P.V. *Nanoscale Materials*, Kluwer Academic Publisher, Massachusetts, **2003.**

(7) Qi, J. Q, ; Tian, H.Y.; Li, L.T.; Chan, H.L.W. *Nanoscale Res. Lett.* **2007**, 2, 107–111.

(8) Son, D.I.; Ho.,Y.C.; Kim T.W. *Appl. Surf. Sci.* **2009**, 255, 8794–8797.

(9) Chen, L.J.; Li, G.S.; Li, L.P. *J. Therm. Anal. Calorim.* **2008**, 91, 581–587.

(10) Zhou, K.; Wan, R.; Xu, B.; Li, Y. *Nanotechnology* **2006,** 17, 3939-3943.

(11) Jiang, X.; Herricks, T.; Xia, Y. *Nano Lett.* **2002**, 2, 1333-1338.

(12) Wang, W.; Zhan, Y.; Wang, G. *Chem. Commun.* **2001**, 8,727–728.

(13) Xiao, H.; Zhu, L.; Liu, X.; Fu, S. *Solid State Commun.* **2007**, 141, 431–435.

(14) Kumar, A.; Srivastava, A.K.; Tiwari, P.; Nandedkar, R.V. *J. Phys. Condens. Matter.* **2004,** 16, 8531–8543.

(15) Wang, X.; Xi, G.; Xiong, S.; Liu, Y.; Xi, B.; Yu, W.; Qian, Y. *Cryst. Growth Des.* **2007**, 7, 930-934.

(16**)** Zhu, J.; Bi, H.; Wang, Y.; Wang, X.; Yang, X.; Lu, L. *Mater. Lett.* **2007**, 61, 5236–5238.

(17) Zhang, X.; Guo, Y.; Liu, W.; Hao, J. *J .Appl. Phys.* **2008**, 103, 114304.

(18) Monson, C.F.; Woolley, A.T. *Nano Lett.* **2003**, 3, 359-363.

(19) Chang, Y.; Lye, M.L.; Zeng, H.C. *Langmuir* **2005,** *21,* 3746-3748.

(20) Tung, H.; Song, J.; Dong, T.; Hwang, W.; Chen, I. *Cryst. Growth Des.* **2008**, 8, 3415-3419.

(21) Panigrahi, S.; Kundu, S.; Ghosh, S.K.; Nath, S.; Praharaj, S.; Basu, S.; and Pal, T. *Polyhedron* **2006***,* 25, 1263-1269.

(22) Yang, G. X.; Chen, S.; Zhao, S.; Li, D.; Houyim, D. *J. Serb. Chem. Soc.* **2003,** 68, 843–847.

(23) Liu, Z.; Bando, Y. *Adv. Mater*. **2003**, 5, 303-305.

(24) Qi, L.; Ma, J.; Shen J. *J. Colloid Interface Sci.* **1997**, 186, 498-500.

(25) Zhu, H.; Zhang, C.; Yin Y. *Nanotechnology* **2005**,16, 3079–3083.

(26) Dhas, N.A.; Raj, C.P.; Gedanken, A. *Chem. Mater.* **1998,** *10,* 1446-1452

(27) Lee,Y.; Choi, J.; Lee, K.J.; Stott, N.E.; Kim, D. *Nanotechnology* **2008**, 19, 415604(1-7).

(28) Mamun, M.A.; Kusumoto,Y.; Muruganandham, M. *Mater. Lett.* **2009**, 63, 2007–2009

(29) Grouchko, M.; Kamyshny, A.; Ben-Ami, K.; Magdassi; S. *J. Nanopart. Res.* **2009**, 11, 713–716.

(30) Appleyard, P.G. *J. Opt. A: Pure Appl. Opt*. 2007, 9, 278-300.

(31) Singh, A.; Avachat, S.G.; Singh, H. *J. Sci. Ind. Res.***1994**, 53, 667-673.

(32) Shi, J.M. ; Chen, L.L. ; Ling, Y. S. ; Lu Y. *Int. J. Infrared Millimeter Waves* **1998**, 19, 1671-1679.

(33) Shi, J.M.; Wang, J.Y.; Xu, B.; Wang, J. C.; Yuan, Z.C. *Int. J. Infrared Millimeter Waves* **2003**, 24, 2007-2013.

(34) Jeevanandam, P.; Mulukutla, R.S.; Philips, M.; Chaudhari, S.; Erickson, L.E.; Klabunde, K.J. *J. Phys. Chem. C* **2007**, 111, 1912-1918.

(35) Kim, J.Y.; Hanson, J.C.; Frenkel, A.I.; Lee, P.L.; Rodriguez, J.A. *J. Phys. Condens. Matter* 2004, 16, 3479-3484.

(36) Zhang, X.; Zhang, D.; Ni, X.; Song, J.; Zheng, H. *J. Nanopart. Res.* 2008, 10, 839-844.

(37) Hong, Z.; CaO, Y.; Deng, J. *Mater. Lett.* **2002**, 52, 34-38.

(38) K.L.; Coronado, E.; Zhao, L.L.; Schatz, G. C., *J. Phys. Chem. B* **2003,** 107, 668-677

(39) Pasikatan, M.C.; Steele, J.L.; Spillman, C.K.; Haque, E. *J. Near Infrared Spectrosc.* **2001**, 9, 153-164.

(40) Körtum, G. *Reflectance Spectroscopy*: *Principle, Methods, and Application*; Springer-Verlag: New York, 1969.

(41) Lagorio, M.G. *J. Chem. Edu.* **2004**, 8, 1607-1611.

(42) Appleyard, P.G.; Davies, N. *Opt. Eng.* **2004**, 43, 376-386.

(43) GuO, X.; Mao, D.; Lu, G.; Wang, S.; Wu, G. J. Cat. ,2010, 271, 178-185.

(44) Rodriguez, J.A.; Kim, J.Y.; Hanson, J.C.; Perez, M.; Frenkel, A.I. *Catal. lett*. 2003,85, 247-254.

(45) Wan, L.; Cui, X.; Chen, X.; Shi, J. *Mater. Lette*. 2010, 64, 1379-1382.

(46) Horns, A.; Hungria, A.B.; Bera, P.; Camara, A.L.; Fernandez-Garcia, M. Martinez-Arias, A.; Barrio, L.; Estrella, M.; Zhou, G.; Fonseca, J.J.; Hanson, J.C., Rodriguez, J.A. *J. Am. Chem. Soc.* 2010, 132, 34-35.

(47) Pedersen, D.B.; Wang S. *J. Phys. Chem. C* 2007, 111, 17493-17499.

(48) Duan, J.L.; Cornelius, T.W.; Liu, J.; Karim, S.; Yaho, H.J.; Picht, O.; Rauber, M.; Muller, S.; Neumann, R. *J. Phys. Chem. C* 2009,113, 13583-13587.

(49) Willets, K.A.; Duyne, R.P.V, *Annu. Rev. Phys. Chem*. 2007, 58, 267-297.

Chapter 3 - Surfactantless Morphology-controlled Synthesis of Cu_2O Microstructures, and Investigation of Catalytic Properties

3.1 Introduction

Metal oxides are widely used in various applications due to their special physical and chemical properties.[1] Among them, cuprous oxide, Cu_2O, is a semiconductor with some important electrical, magnetic, and optical properties.[2] The material is naturally abundant, non-toxic, and low in cost.[3-5] It is a p-type semiconductor due to the Cu vacancies forming an acceptor level 0.4 eV above the valence band;[6-7] its direct band gap is ~ 2.2 eV.[8] It is one of the materials with higher negative band edge potential so as to produce more energetic electrons for reduction when used as a semiconductor catalyst.[9]

With specific morphologies, Cu_2O hollow nanostructures are more desirable for their numerous potential applications in drug delivery, as a biomedical diagnosis agent, and cell imaging.[19-20] It has been also examined as the negative electrode, anode, in lithium ion batteries[21], and as a basic material for superconducting materials.[22] Excitons formed in Cu_2O samples have shown to be a suitable material for Bose Einstein condensate because of large binding energy, 150 meV.[23-25] It has been reported that excitons could conduct through the Cu_2O crystal. Photons are converted to excitons that travel through small aperture with small loss of diffraction and scattering, and then the excitons converted into photons again.[26]

In addition to intrinsic properties, size and shape are also important.[27-28] Semiconductor nanomaterials have unique physical properties—electrical, magnetic, and optical properties—compared to that of bulk materials.[29] Cu_2O nanomaterials have also shown unique properties from its bulk form. The quantum-confinement threshold for Cu_2O is deduced to be ~ 4 nm and optical absorption showed a blue-shift due to quantum size effect as particle size decreased.[30]

There are different methods—electrodeposition, sonochemical, thermal relaxation, liquid-phase reduction, complex precursor surfactant-assisted, vacuum evaporation method—for the synthesis of Cu_2O micro and nanostructures.[31-38] Furthermore, there are several reports about the synthesis of Cu_2O with various morphologies and symmetrical structures—nanoparticles, nanowires, nanorods, nanotubes, octahedra, nanowhiskers, cubes, multipodes, nanocages, nanoplates, spheres, whiskers, hollow nanostructures, star-like and flower-like structures.[39-51]

In chapter 2, we discussed the synthesis of CuO and Cu nanomaterials with different shape and size, and investigated the variation of an optical property—the diffuse reflectance at NIR region—by CuO and Cu nanomaterials with different morphology. In this chaper, our objective is to synthesize Cu_2O samples with different morphologies by changing various parameters. The main motivation of preparing these Cu_2O samples is the visible active semiconconductor nature of Cu_2O, and it is one of the materials with highest negative band edge potential so as to investigate the effects of morphology in catalytic properties. Herein we report the synthesis of Cu_2O microstructures with different morphologies by simple solution phase reactions without use of surfactants. Indeed, identical reaction mixtures of copper(II) actetate and D-glucose were allowed to react under three different physical conditions; interestingly, different morphologies were obtained. In addition to the change of physical conditions, the reductant, D-glucose, was also replaced with ethylene glycol. Then, another new morphology was obtained. When the precursor was changed, again an entirely different morphology was obtained; some of the morphologies described herein have not been reported yet, to the best of our knowledge. Furthermore, these Cu_2O materials were used as the dark catalyst for the decomposition of hydrogen peroxide under identical conditions so as to investigate the effect of morphology on the rate of decomposition. Different decomposition rates were found. Since Cu_2O is a

semiconductor, these Cu_2O samples were employed for the photochemical degradation of methyl violet 2B, a dye commonly used in textile industries, using UV-vis light under identical conditions so as to investigate the effect of morphology on the degradation of the dye solution; we found different degradation rates from these samples.

3.2 Experimental Section

3.2.1 Materials

a. Copper (II) acetate (Alfa Aesar)
b. Acetic acid (Fisher Chemical)
c. D-glucose (Sigma Aldrich)
d. Ethylene glycol (Fisher Chemical)
e. Copper sulfate (Fisher Chemical)
f. Sodium citrate (Fisher Chemical)
g. Sodium carbonate (Fisher Chemical)
h. Polytetrafluoroethylene (PTFE) (Sigma Aldrich)
j. Methyl violet 2B (Sigma-Aldrich)
k. Oxygen gas (Linweld)
j. Hydrogen Peroxide (Fisher Chemical)
k. Cuprous (I) oxide (Fisher Chemical)

3.2.2 Synthesis Cu_2O microstructures with various morphologies were prepared under different conditions. During the experiment, a saturated aq. solution of copper (II) acetate (Alfa Aesar) was prepared by dissolving 2-3 drops of acetic acid (Fisher Chemical) in 100 mL water; the saturated solution at room temperature was separated from undissolved copper precursor by filtration. The copper acetate solution was reduced with aq. D-glucose (Sigma Aldrich) solution at three different physical conditions by (a) heating at 60 ^oC and 80 ^oC for one hour (ii) refluxing in an argon environment for one hour (iii) by hydrothermal treatment at 100 ^oC in air

Teflon-lined autoclave for 24 h. In each case, 10 mL of the precursor solution and 10 mL of 10 % D-glucose were mixed and stirred. After treatment at different conditions, precipitates were obtained. In the first, second, and third cases, around 61 %, 68 %, and 75% yields were obtained. In another experiment, copper acetate solution was reduced with ethylene glycol (Fisher Chemical) instead of D-glucose by hydrothermal treatment at different temperatures. In a particular experiment, 10 mL of copper acetate solution was taken in a Teflon-lined autoclave and 4 mL of ethylene glycol was added and stirred thoroughly; then hydrothermal treatment was carried out for 24 h at three different temperatures—120 ^{o}C, 130 ^{o}C and 140 ^{o}C—so as to get black precipitates. Lastly, the copper precursor was changed; copper sulfate (Fisher Chemical) was used as a precursor in the form of Benedict's solution. 100 mL Benedict's solution was prepared by mixing two solutions; the first solution was prepared by dissolving 6.8 mmol copper (II) sulfate in distilled water and the second solution was prepared by dissolving 58 mmol sodium citrate (Fisher Chemical) and 94 mmol sodium carbonate (Fisher Chemical) in distilled water.

In a particular experiment, 10 mL of the copper sulfate solution was taken in an Erlinmeyer flask and 10 mL of 5% of D-gluclose was added and stirred with a magnetic stirrer. The solution was warmed up to 55 ^{o}C for an hour; the red precipitate was obtained. All the precipitates were washed with water followed by ethanol. Then they were dried at 80 ^{o}C in air keeping in the dry dissicator, the yield was found up to 81%. All the samples prepared at different conditions are represented by symbols (table 3.1)

Table3.1 Symbolic representation of Cu_2O and it composite samples prepared at different conditions.

S. N.	Reaction Mixtures	Synthesis Conditions	Symbolic Representation of products
1	Copper(II) acetate + D-glucose	Warmed in air at 60 ^oC and 80 ^oC	C1
2	Copper(II) acetate + D-glucose	Refluxed in Argon at 100 ^oC	C2
3	Copper(II) acetate + D-glucose	Hydrothermal treatment at 100 ^oC	C3
4	Copper(II) acetate + Ethylene Glycol	Hydrothermal treatment at 140 ^oC, 130 ^oC, 120 ^oC,	C4
5	Copper(II) sulfate + Sodium Citrate + D-glucose	Warmed at 55 ^oC and 80 ^oC in air at 80 ^oC	C5

3.2.3 Characterization. (i) Powder X-ray Diffraction (pXRD): All as-synthesized copper oxides were characterized by powder X-ray diffraction. The instrument was Bruker AXS Diffractometer D8. The light source was CuKα radiation with applied the voltage of 40 kV and current of 40 mA.

(ii) Scanning Electron Microscopy (SEM): The morphologies of the synthesized materials were observed by Scanning Electron Microscopy (SEM). SEM experiments were carried out by using a Scanning Electron Microscope-S3500N, Hitachi Science System, Ltd. at the Entomology Department of Kansas State University (KSU), microscopy and imaging facility.

(iii) Brunauer-Emmet-Teller (BET) method: Surface area, pore volume and pore diameter of these materials were measured by using BET N_2 adsorption and desorption experiments. The

measurements were carried out using Microsorb II 2300 and Quantachrome NOVA 1200 instrumentation. The samples were cooled to 77 K using liquid nitrogen during the measurement.

(iv) UV-vis spectra: A Cary 500 UV-vis spectrometer with diffuse reflectance accessory (DRA) was used in the range of 200-800 nm. The sample cell was made of two transparent CaF_2 discs, a Teflon O-ring and screw-type combination in which nanomaterials were packed between two discs and an O-ring. Polytetrafluoroethylene (PTFE) (sigma Aldrich) powder of ~100 μm particle size was taken as a reference material.

(v) The Cu_2O samples with four different morphologies were employed for photocalytic degradation of methyl violet 2B dye using UV-vis light generated from 1000 W high-pressure Xenon lamp (Oriel Instrument, Model 66921). Furthermore, the pure Cu_2O samples were also employed as dark catalysts for the decomposition of hydrogen peroxide so as to get water and oxygen as products; the oxygen was measured to determine the decomposition rate.

3.3 Results and Discussion

3.3.1 pXRD Analysis. All the samples obtained by reducing copper precursors—copper (II) acetate and copper (II) sufate—reduced with D-glucose and ethylene glycol were analyzed with pXRD. Before pXRD analysis, these samples were prepared at different conditions. When copper acetate (II) was reduced with D-glucose at 60 ^oC in air, Cu_2O (C1) was found to be formed by the pXRD analysis (Fig.3.1a). Similarly, a mixture of copper acetate (II) and glucose subjected to reflux condition under argon environment yielded a red precipitate (C2). The product was also found to be Cu_2O from pXRD analysis (Fig. 3.1b). In another experiment, a reaction mixture was subjected to hydrothermal treatment for 24 h; a red-black sample (C3) was obtained. From pXRD analysis (Fig. 3.1d), the pattern of Cu_2O and Cu was obtained, indicating that Cu_2O was partially reduced to copper. When the copper precursor was reduced with

ethylene glycol under hydrothermal treatment at 140 ^{o}C for 24 h, a black product (C4) was formed; the pXRD analysis of this sample showed that the sample was a composite of CuO and Cu_2O (Fig. 3.2), indicating copper(II) was not completely reduced to Cu_2O. Furthermore, another copper oxide sample, C5, was also prepared by reducing Benedict's solution with glucose. This is the example of change of Cu-precursor. Copper(II) acetate used in previous cases was replaced with copper(II) sulfate; in this case, not only the precursor was changed, but also an additional reagent, sodium citrate, was also added. The sample obtained by this process was also characterized with pXRD. The pXRD pattern showed the formation of pure Cu_2O ((Fig. 3.1c).

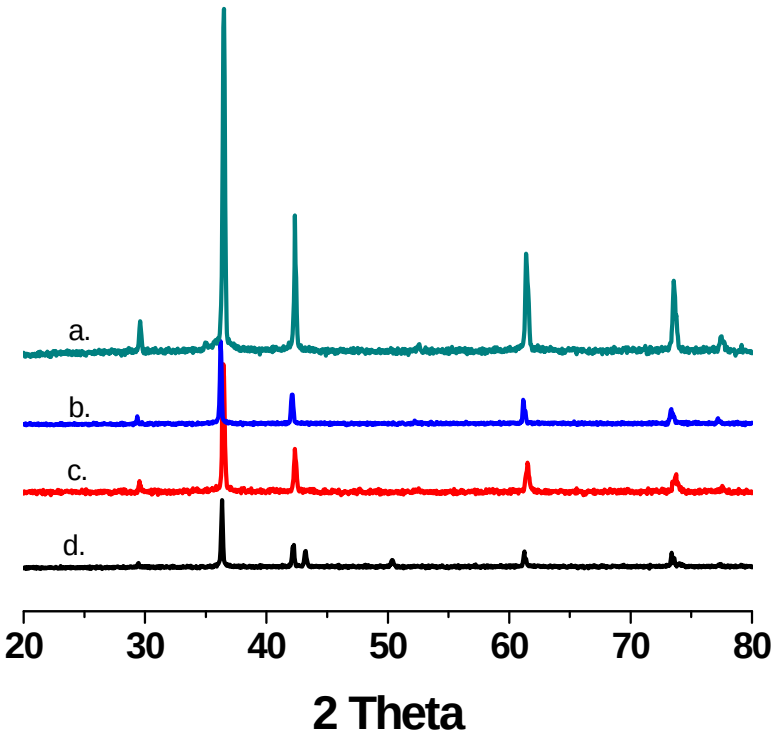

Figure3.1 pXRD patterns of samples (a) C1, (b) C2, (c) C5, and (d) C3 .

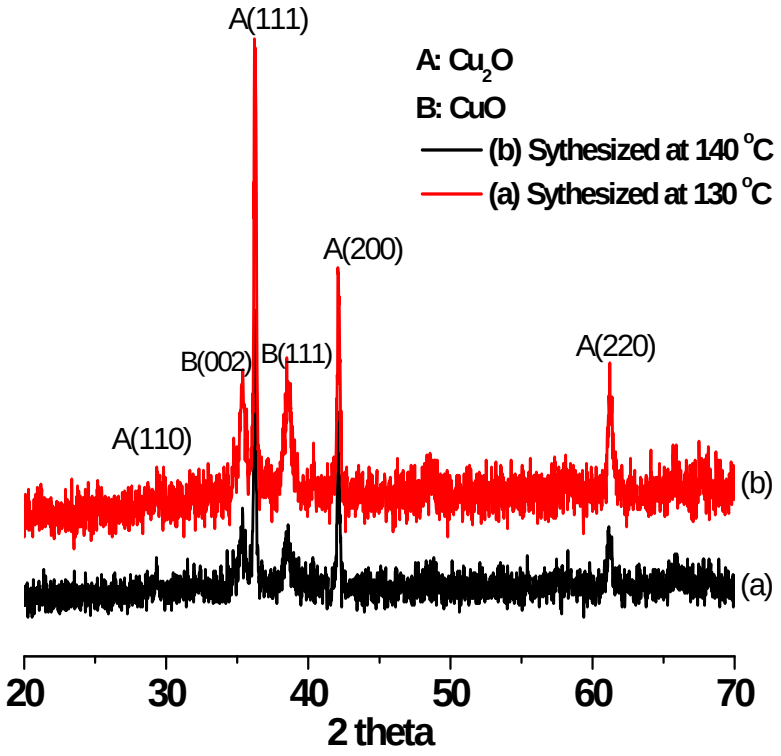

Figure3.2 p**XRD patterns of hollow sphere particles, C4, obtained by reducing saturated copper(II) acetate solution with ethylene glycol under hydrothermal treament at (a) 140 °C (b) 130 °C.**

3.3.2 Scanning Electron Microscopy Analysis. Morphologies of the copper oxide samples were investigated by SEM. The SEM images of the Cu_2O sample, C1, showed assemblies of hexapods with symmetrical morphology directed along the six octahedral directions (Fig. 3.3a-b). Interestingly, each pod consisted of many crystals as the branches; the individual crystals were found to be assembled on the axis of each pod along four sides of an axis; relatively larger crystals were observed towards the junction and small crystals outwards forming a peak at the end. The length of a pod was found to be up to 16 μm. Similar morphology of Cu_2O was found

when prepared at 80^{o}C (Fig. 3.3c); however, the assembly was found to be partially disintegrated at this temperature (Fig. 3.S1)

When a Cu_2O sample was prepared by hydrothermal treatment, the morphology of the sample was found to be different although the assembly of pods had similar orientation. Most pods have four grooves and ridges along the axial direction with a tip in the end (Fig. 3.4); however, some pods have been broadened outwards and formed a structure like a half part of octahedral structure with four facets (Fig. 3.4c) in pods. The length of a pod was found to be up to 30 μm. The self-assembled hexapods were held together weakly; the pods in the assemblies were often found to be broken at the junction.

When the Cu_2O sample was prepared by refluxing in the presence of D-glucose, Cu_2O with an entirely new morphology, the octahedral structure, was obtained (Fig.3.5). In the octahedral structures, the distance between two vertices along an axis was found to be 6.4 μm or less. Since the sample was prepared at the boiling point of the reaction mixture with continuous stirring under argon, it is likely that the morphology of Cu_2O product prepared by this process is thermodynamically more stable than the assemblies of the hexapods in previous case.

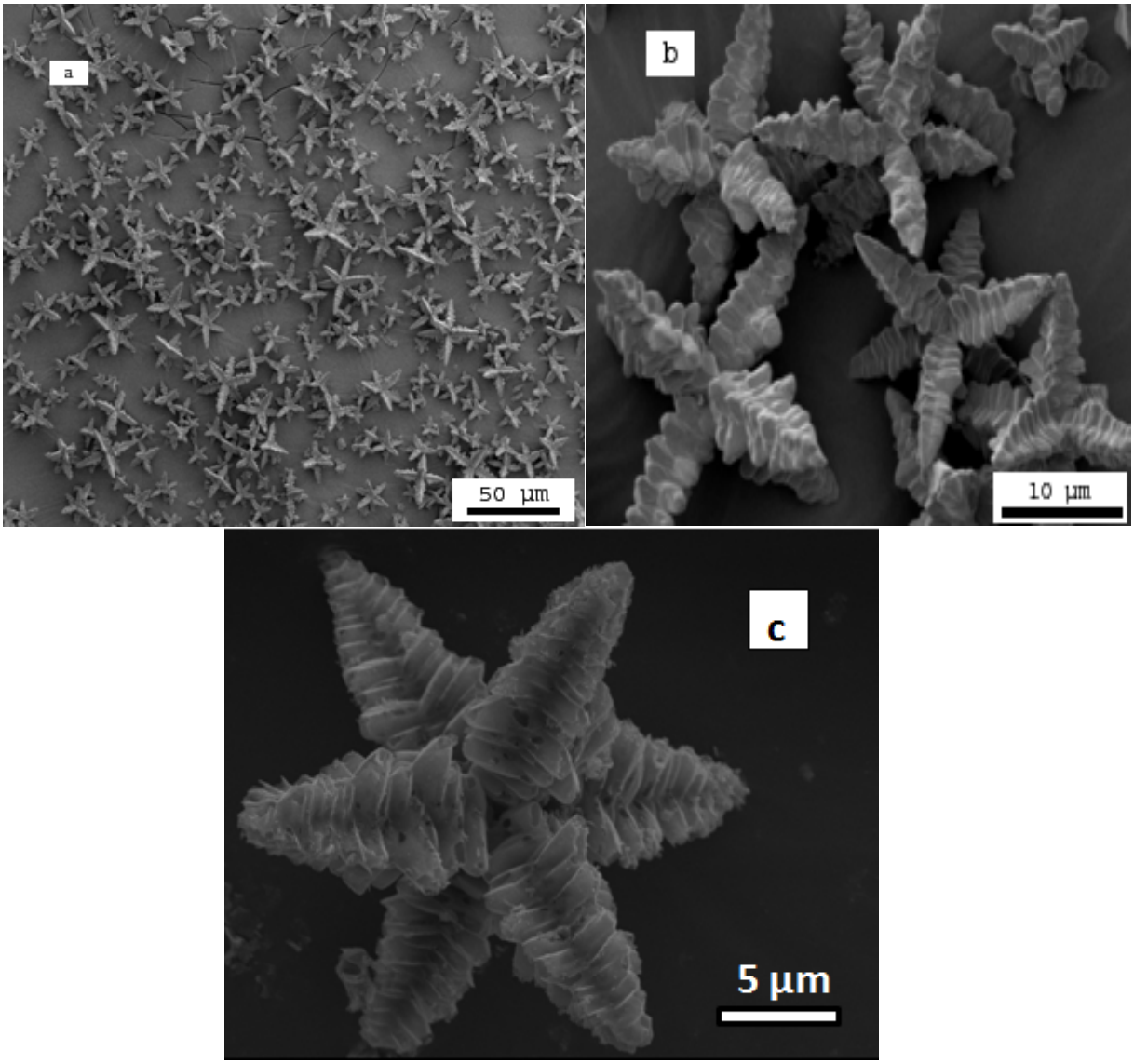

Figure3.3 Cu_2O samples, C1, prepared by reducing saturated copper(II) acetate solution with D-glucose under air (a, b) at 60 ^oC and (c) at 80 ^oC

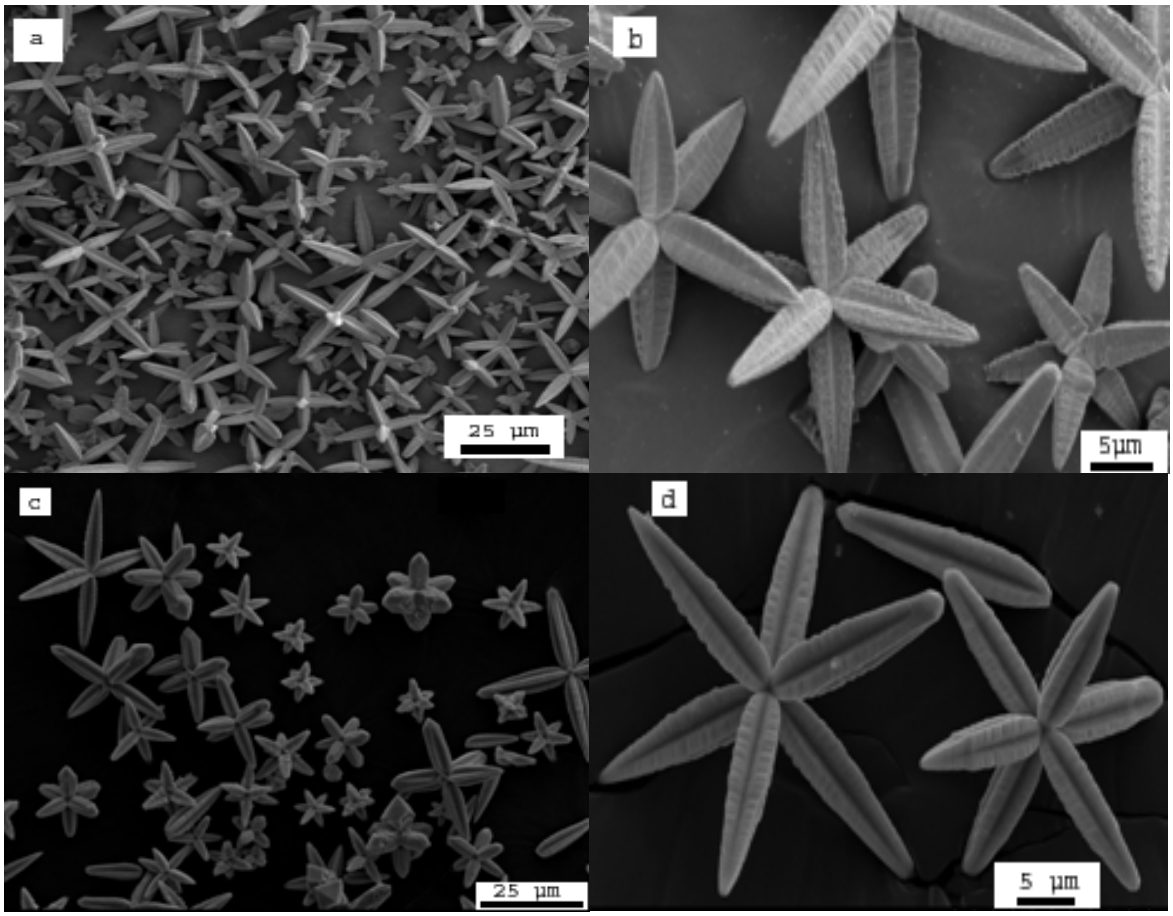

Figure3.4 Cu_2O sample, C3, prepared by reducing saturated copper(II) acetate solution with D-glucose under under hydrothermal treatment at 100 ^oC.

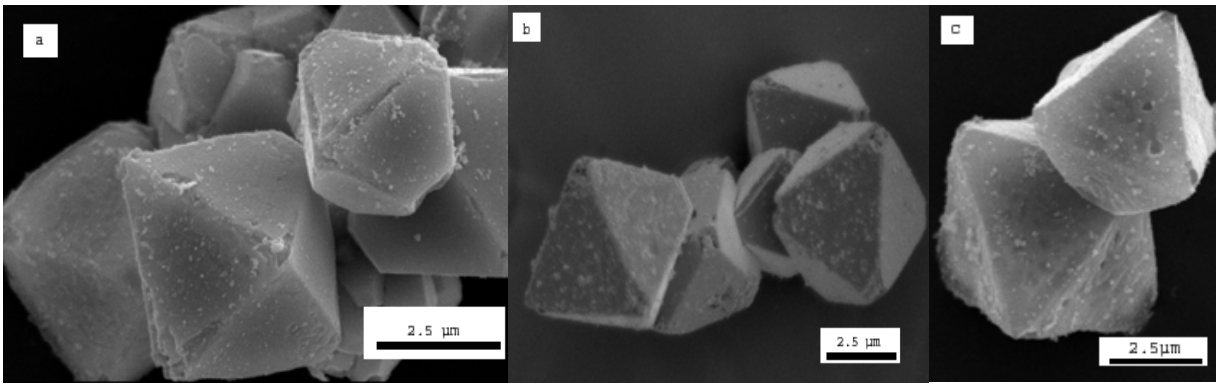

Figure3.5 Cu_2O sample, C2, prepared by reducing saturated copper(II) acetate solution with D-glucose under reflux and stirring.

The sample obtained by the hydrothermal treatment of copper(II) acetate solution with ethylene glycol (EG) was also characterized with SEM imaging; the images showed the formation of hollow spheres when prepared at 140 ^{o}C (Fig. 3.6); the maximum length of the external diameter of a hollow sphere was found to be 5.7 μm, and most of the hollow spheres were found to be broken into smaller fragments (Fig.3.6a and Fig. 3.S1). When the samples were synthesized at lower temperature, 130 ^{o}C, there were less fragmented hollow spheres (Fig.3.7a). So temperature played a crucial role in the stability of the hollow spheres. When synthesized even at lower temperature, 120 ^{o}C, there were almost no broken hollow spheres (Fig.3.7b).

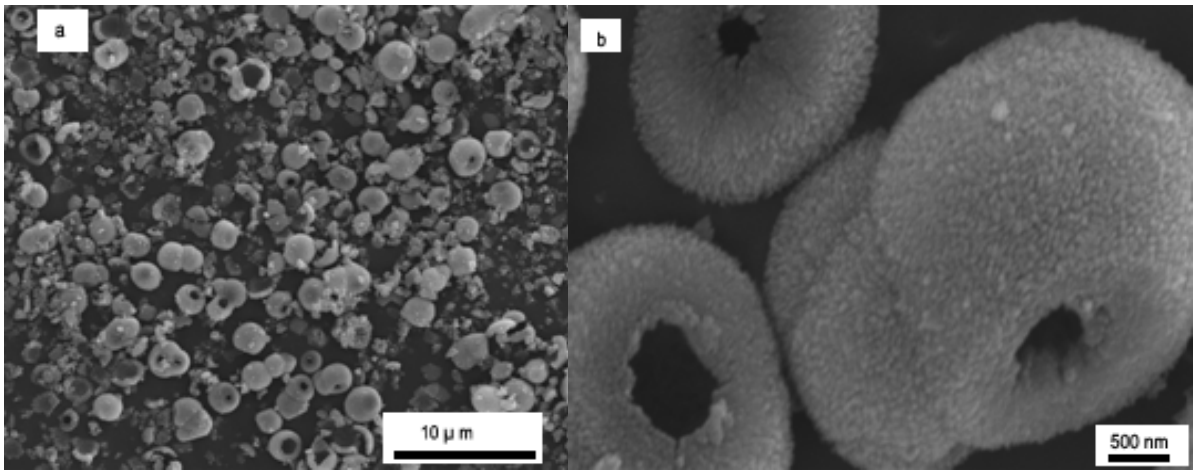

Figure3.6 Cu_2O sample, C4, prepared by reducing saturated copper(II) acetate solution with ethylene glycol under hydrothermal treatment at 140 ^{o}C.

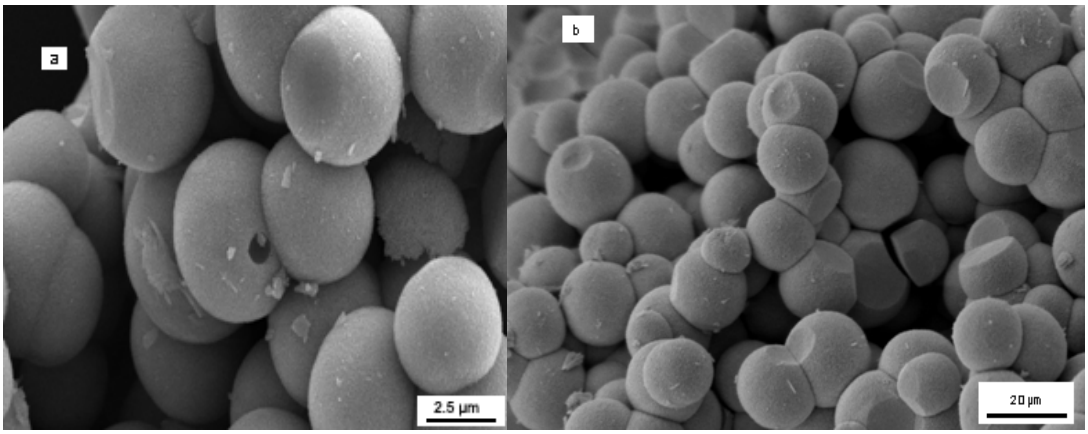

Figure3.7 Cu_2O sample, C4, prepared by reducing saturated copper(II) acetate solution with ethylene glycol under hydrothermal treatment at (a) 130 ^oC (b) 120 ^oC.

The Cu_2O sample (C5) was also characterized with SEM. The SEM images showed a unique morphology with a symmetrical structure with eight corners, almost equivalent to eight corners of a cube with six faces; a face was like a flower like structure (Fig. 3.8). There was almost a concave-like structure, deep space at the middle of the face, with greater mound at the corner and less at the middle of each edge. The six faces of the symmetrical structure appeared as a flower-like structure. When prepared at 55 ^oC, there were different sizes of the individual units. A side of a structure was found to be up to 5.4 µm. A single unit was made of four blocks; these blocks were observed when a single structure was found to be disintegrated as the Cu_2O sample was prepared at relatively higher temperature, 80 ^oC (Fig.3.S3), indicating that the structure is unstable at higher temperature. The thickness of a block was higher towards the corner and lowest at the center. During the synthesis, when the reaction mixture of Benedict's solution and D-glucose was heated, the blue solution was converted to green; the color is supposed to be given by the formation of a copper citrate complex.

$$2CuSO_4 + Na_3C_6H_5O_7 \longrightarrow Cu_2C_{12}H_{10}O_{14} + Na_2SO_4 \qquad (3.1)$$

The citrate ion worked as a chelating agent, and played an important role as a modifier for the growth of Cu_2O with a new morphology after formation of Cu_2O seed particles by the reduction of Cu^{2+} to Cu^{1+} oxide.

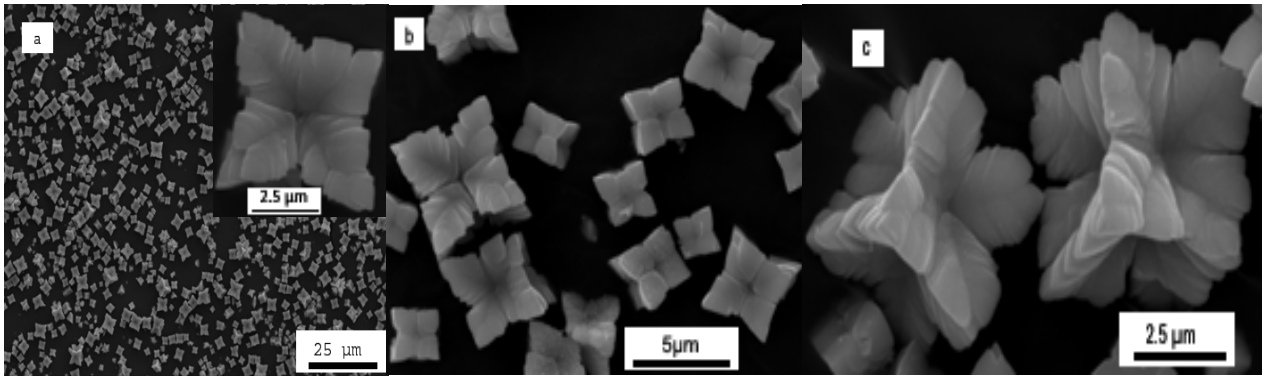

Figure3.8 Cu_2O sample, C5, prepared by reducing Benedict's solution with D-glucose at 55 ^oC under ambient condition.

The growth of crystals with various morphologies depends upon various factors. Some morphologies were obtained using directing agents such as alumina membrane and micelles in template method. Furthermore, chemical agents, capping agents, and other physical conditions can play an important role.[52] The crystal growth is thermodynamically and kinetically controlled at subsequent steps so as to produce different complicated structures.[53] The crystal growth process might complete by multiple steps. In the beginning of the crystal growth process, there might be the formation of small solid seeds from the supersaturated solution. It is also accepted that there might be preferential adsorption of molecules/ions in the solution to different crystal faces so that rates of crystal growth might be different at different crystal axes.[54]

When the Cu_2O sample was prepared by reduction of copper acetate solution with glucose in air by increasing temperature at a slow rate, 1 ^oC per minute, the precipitation took place relatively slowly. Before the precipitation, the blue color of the reaction mixture was converted into deep

blue probably due to the formation of a co-ordination complex between copper ion and glucose.[55] During the synthesis, temperature (55 ^{o}C) and pressure (atmospheric) were relatively low. At this condition, comparatively bigger crystal particles were formed. In this mild condition, each pod of a hexapod assembly has extra growth of crystals as branches along four sides; the mild environment seemed to be favorable for such growth of Cu_2O crystals. The assembly of hexapods prepared at lower temperature, 55 ^{o}C, was found to be stable; however, when prepared at relatively higher temperature, 80 ^{o}C, the assemblies were partially broken (Fig. 3.S1). So we found relatively more stable assemblies when synthesized at lower temperature. Speculation about the mechanism of formation could be taken from the disintegrated parts of hexapods.

In the beginning, there should be the formation of small Cu_2O crystal entity from the supersaturated solution of Cu_2O by the nucleation process; the nucleation is an atomic or molecular process in which atoms or molecules are rearranged into a cluster which would be large enough with an irreversible growth. The supersaturation is supposed to be the driving force for the nucleation and growth of crystals; it is defined as the difference between chemical potentials of a molecule in a solution and in the bulk of the crystal phase. According to nucleation theory, the cluster of a number of molecules is formed by performing the work which is the difference of free energy of final and initial states of the system and by forming an interface between nucleus and solution. During the crystal growth, atom/molecule is incorporated on the surface of the crystal so as to increase the size.[56]

It is supposed that small seed particles are formed at first that combine by Ostwald ripening to give bigger particles at a central position. Then, there could be preferential adsorption of ions/molecules along six faces of the central crystal so as to direct the growth of crystals along

six octhedrally oriented directions, and each pod grew up to a certain length. Furthermore, there might be the growth of new crystals of different sizes along four sides of a pod. There might be adsorption and desorption of molecules/ions. Obviously, the environment for the growth of a crystal plays an important role for the growth of a particular morphology. The slow rate of precipitation, low temperature, and appropriate pressure are supposed to be major reasons for the development of more branches on a pod. When the reaction was carried at high pressure by hydrothermal treatment at 100 ^{o}C for 24 h, more pointed pods were grown. There was no proper growth of Cu_2O crystals as the branch of each pod although we could see the tendency to grow the crystals as the branches. Each pod could be seen with four grooves and ridges, and a tip at the end. Relatively high pressure and temperature, and longer time might have hindered the growth of the crystal structure as the branches.

When the Cu_2O was prepared by reflux of an identical reaction mixture under argon environment for two hours with continuous stirring, the octahedral structure was obtained. This indicates that there must be different preferential adsorption of Cu_2O seed particles so as to develop the crystal as the octahedral structure. These observations clearly indicate that identical reaction mixtures at three different physical conditions could produce different morphologies.

From the fragmented hollow spheres, the composite of Cu_2O and CuO, prepared by reducing copper acetate with ethylene glycol, we can also speculate about the mechanism of formation of hollow spheres. In the beginning of the reaction, there must be formation of small seed particles from super saturated solution of copper oxide solution. After the formation of seed particles, they should be aggregated by Ostwald digestive ripening so as to form bigger particles; the bigger particles should have united to form the asymmetric rectangular rod-like structure with small size in one end and big size in other end; the inward portion of the structures could be seen as

smaller, and outward portion was found to be greater in the fragmented parts of a hollow spheres (Fig.3.S2). These asymmetric rod-like structures must be assembled to give the hollow structures.

3.4.3 BET Data Analysis. All these Cu_2O and Cu_2O composite materials were also characterized by BET nitrogen adsorption and desorption measurements; the specific surface area, pore volume, and pore diameter are given in table 4.2. The surface area values were found to be relatively low. The specific surface area value of Cu_2O samples prepared by the reducing copper(II) acetate solution with glucose under hydrothermal treatment was found to be comparatively greater, and the specific surface areas for the remaining samples were found to be low. The pore diameters of the samples were in the range of 17-30 A^o, and pore volume was in the range of 0.009 - 0.01 cc/g.

Table 3.2 BET data of Cu_2O samples

Method of Synthesis	Surface Area (m^2/g)	Pore Volume (cc/g)	Pore Diameter (A^o)
C1	1.3	0.089	30
C2	8	0.089	17
C5	44	0.07	17

3.4.4. UV-Vis Absorption Spectra. These Cu_2O samples with different morphologies were employed for UV-vis absorption, and compared with the UV-vis absorption of commercial Cu_2O (Fig.3.9). The as-synthesized Cu_2O samples could absorb significantly more photons at wavelength $\lambda < 575$ nm than commercial Cu_2O. The absorptions by various as-synthesized Cu_2O samples were found to be different from each other. The absorption by one of the as-synthesized Cu_2O samples, C5, was found to be blue shifted, and the absorption of another as-synthesized

Cu_2O sample (C1) at wavelength rage of 240 – 580 nm was found to be highest among all Cu_2O samples. This change in optical properties may be due to the change in morphology and textural properties of these Cu_2O samples.

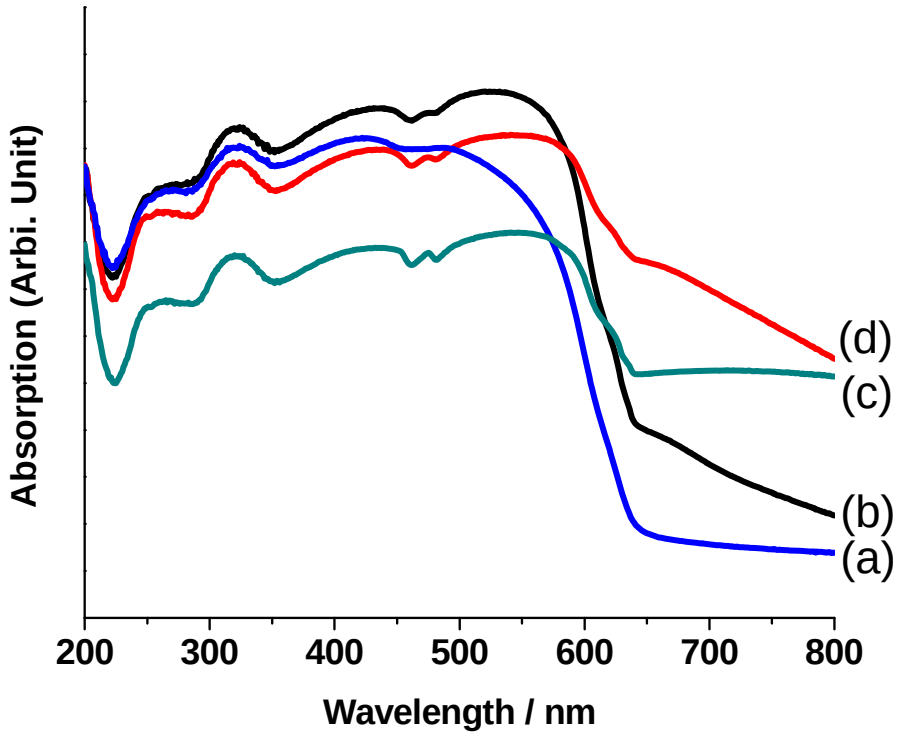

Figure3.9 UV-vis absorption spectra of samples (a) C5, (b) C1 (c) CM, Commercial Cu_2O (d) C2

3.4.5 Investigation of Photocatalytic Activities. The pure Cu_2O samples with different morphologies were employed as photocatalysts for the degradation of methyl violet 2B, a dye commonly used in textile industries under UV-visible light. Our objective was to investigate the effect of morphology for the photocatalytic degradation of the dye solution; the dye solution was prepared by dissolving 4 mg methyl violet 2B (Sigma-Aldrich) in 1 liter water. During an experiment, 70 mL of the dye solution was taken in a 305 mL static cylindrical glass reactor

having the water jacket through which cold water at 25 ^{o}C could be circulated, and then 50 mg of Cu_2O sample was placed in the reactor. The contents of the reactor was stirred with a small magnetic bar for 30 min for the equilibrium, and then UV-vis light ($\lambda > 320$ nm) was introduced from a 1000 W high-pressure Xenon lamp (Oriel Instrument, Model 66921) at a height of 20 cm above the solution. Then the photocatalytic degradation of the dye solution was measured at different time intervals by measuring UV-vis absorption with the maximum absorption peak for the dye at $\lambda_{max} = 584$ nm. The absorptions of degrading dye solution were taken at 0, 1, 2, 3, 4, and 5 h. Each as-synthesized Cu_2O sample was investigated as the photocatalyst, and the dye was found to be degraded in the course of time; the degradation under the light and catalyst was confirmed by the decreasing trend of the 584 nm peak. Without Cu_2O samples, no dye was found to be degraded; similarly no dye was degraded in the absence of UV-vis light, confirming the photocatalytic degradation of the dye. The rates of dye degradation by four pure Cu_2O samples were compared (Fig. 3.10). The rate of degradation was found to be different for different Cu_2O samples. The largest rate was observed by Cu_2O, C1, as the photocatalyst and the lowest rate was observed by commercial copper(I) oxide (I), Cu_2O (CM). The rates closely correspond to the trend of UV-vis absorption spectra of the Diffuse Reflectance UV-vis absorption spectra for the Cu_2O samples (Fig. 4.9 and Fig. 4.10); the greater UV-absorption, the greater was the dye degradation.

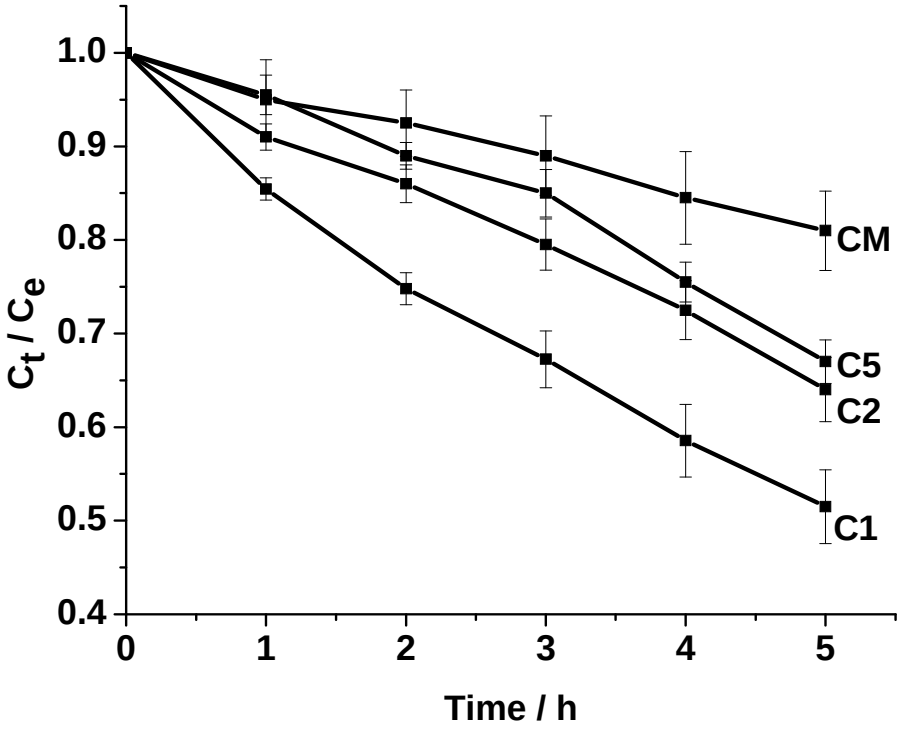

Figure3.10 The rate of photocatalytic degradation of methyl violent 2B using pure Cu_2O samples— C1, C2, C5, and CM— under UV-vis light (C_e: concentration of the dye at equilibrium before introduction of light, C_t: concentration of dye at a time 't')

3.4.6 Investigation of Dark Catalytic Activities. As-synthesized pure Cu_2O samples with various morphologies were also employed as dark catalyst for the decomposition of H_2O_2 so as to produce O_2 and H_2O. The total amount of oxygen produced from the beginning of the reaction was calculated at every hour by an online GC system (GOMAC model) employing a Supelco molecular 80/90 sieve 5A column with Ar as the carrier gas, and using a thermal conductivity detector. During the experiment, 340 mL of 1 % H_2O_2 solution in water was placed in a reactor in which 20 mg Cu_2O sample was dispersed with continuous stirring using a small bar magnet. The total amounts of oxygen produced from the beginning of the reaction in every additional

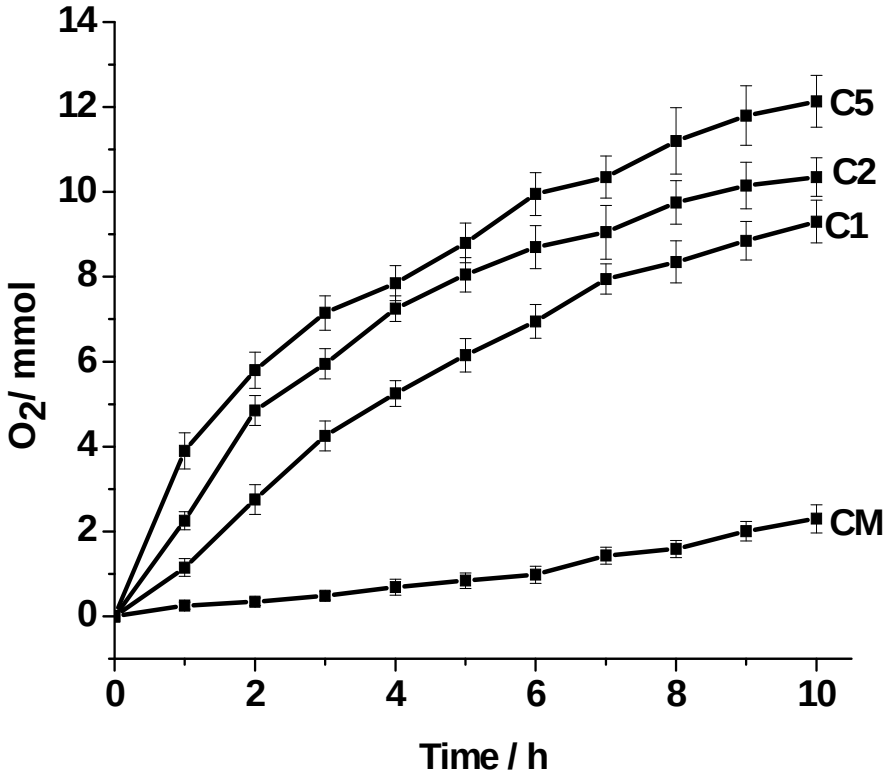

Figure3.11 Amount of O_2 produced from the decomposition of H_2O_2 at different time in presence using Cu_2O samples of different morphologies as the dark catalyst.

hour have been shown in Fig. 4.11. During the control reaction, no O_2 gas was produced in the absence of Cu_2O in 1% H_2O_2 solution indicating Cu_2O as a true dark catalyst. The catalytic activities of Cu_2O samples were found to decrease with decrease in surface areas. The amounts of oxygen were found to be 9.3, 10.5, 12.1 mmol from the decomposition of H_2O_2 using pure Cu_2O samples—C1, C2, and C5— as dark catalysts whose surface area values were 2, 8, and 44 m^2/g respectively. The Cu_2O sample, C5, with the highest specific surface area among them gave the highest amount of O_2. So the surface area of an as-synthezed Cu_2O sample does have the effect on the decomposition of H_2O_2. Although the decomposition was found to increase with increase in surface area, the amount of oxygen was not proportional to the surface areas. This

indicates that surface area is not the only the determining factor. For example, Cu_2O (CM) as a dark catalyst, whose surface area value was close to 0 m^2/g, could give 2.6 mmol under the same reaction conditions. So we speculate that morphology also might be another important factor for the different rates. From the p-XRD pattern, we did not see oxidation of Cu_2O to CuO during the experiment up to 24 h, and there was no change in morphology of Cu_2O. However, when an experiment was carried out a long time, 48 h, Cu_2O was found to be slightly oxidized to CuO as indicated by pXRD pattern (Fig.3.S4). Furthermore, morphology of the Cu_2O sample was also found to be slightly changed; some particles were found to be disintegrated from the surface, and more roughness was observed (Fig.3.S5). This change might be due to the oxidation of Cu_2O to CuO. It is speculated that Cu_2O acts as a dark catalyst for the decomposition of H_2O_2 to produce oxygen and water, and the nascent oxygen would oxidize Cu_2O to give CuO.

3.4. Conclusions

Cu_2O samples were synthesized by reducing two copper precursors with D-glucose and ethylene glycol at different conditions. A copper precursor, copper(II) acetate, was reduced with D-glucose under three different physical conditions, and three different morphologies were obtained. In one of the experiments, when the copper precursor was reduced under hydrothermal treatment, the Cu_2O sample was partially reduced to Cu so as to obtain the composite of Cu_2O and Cu. Copper(I) acetate was also reduced with ethylene glycol instead of D-glucose under hydrothermal treatment. In this case, Cu^{2+} was not completely reduced to Cu^{1+} so as to form a composite of CuO and Cu_2O with hollow spherical structure. Furthermore, the previous copper precursor, copper acetate, was also replaced with copper(II) sulfate in the form of Benedict's solution, and reduced with D-glucose. In this case, a Cu_2O sample with another unique morphology was obtained. As-synthesized Cu_2O samples were investigated as dark catalysts and

photocatalysts to observe the effect of morphology. As-synthesized Cu_2O samples were used as photocatalyst in UV-vis region for the photo degradation of methyl violet B. The degradation was found to be dependent on the morphology to some extent; the Cu_2O sample which absorbed UV-vis light more strongly could degrade the dye solution at a relatively higher rate. As-synthesized pure Cu_2O samples with different morphologies were also employed for the decomposition of 1% H_2O_2 solution in water. Surface area and morphology were both important for the photocatalytic activity. Table 3.3 summaries the catalytic findings.

Table3.3 Summary of catalytic data

Cu_2O Sample	Morphology	Surface Area (m^2/g)	Relative rate		Relative rate per unit surface area	
			Cu_2O as dark catalyst[a] (mmol h^{-1})	Cu_2O as photo-catalyst[b] ($mgL^{-1}h^{-1}$)	Cu_2O as dark catalyst (mmo h^{-1} m^2g^{-1})	Cu_2O as photo-catalyst ($mgL^{-1}h^{-1}$ m^2g^{-1})
C1	Hexapod-like structure	1.3	0.93	9.6 $C_e \times 10^{-2}$	0.71	7.4 $C_e \times 10^{-2}$
C2	Octahedral structure	8	1.05	7.2 $C_e \times 10^{-2}$	0.13	0.9 $C_e \times 10^{-2}$
C5	Star-like structure	44	1.22	6.6 $C_e \times 10^{-2}$	0.03	0.15 $C_e \times 10^{-2}$
CM	-	0	0.23	4.2 $C_e \times 10^{-2}$	-	-

[a]20 mg Cu_2O was used as the dark catalyst for the decomposition of 340 mL of 1 % H_2O_2 and O_2, a product, was measured to determine the decomposition rate.

[b]50 mg Cu_2O was used as the photocatalyst for dedgradation of methyl violet 2B; intial concentration of the dye (C_o) was 4 mg/ L ; concentration at equilibrium (C_e) when stirred for 30 min before introduction of light was 3.7 mgL^{-1}; concentration of dye was measured in the course of time to determine the rate.

4.5 References

(1) Nickolov, R. N.; Donkova, B.V.; Milenova, K.I.; Mehandjiev, D.R. *Adsorpt. Sci. Technol.* **2006***,* 24, 2006.

(2) Khanna, P.K.; Gaikwad, S.; Adhyapak, P.V.; Singh, N.; Marimuthu R., *Mater. Lett.* **2007***,* 61, 4711.

(3) Fernando, C. A. N.; De Silva, L. A. A.; Mehra, R. M.; Takahashi, K. *Semicond. Sci. Technol*. **2001**, 26, 433.

(4) Chen, Z. Z.; Shi, E. W.; Zheng, Y.; Li, W. J.; Xiao, B.; Zhuang, J. Y. J. *Cryst. Growth* **2003**, 249, 294.

(5) Mathew, X.; Mathew, N. R.; Sebastian, D. J. *Sol. Energy Mater. Sol. Cells* **2001**, *70*, 277.

(6) Shin, H. S.; Song, J. Y.; Yu, J. *Mater. Lett*. **2009**, 63, 397.

Briskman, R. N. *Sol. Energy Mater. Sol. Cells* **1992**, 27, 361.

(7) Olsen, L. C.; Addis, F. W.; Miller, W. *Sol. Cells* **1992**, 7, 247.

(8) Ng, C. H. B.; Fan, W. Y. *J. Phys. Chem. B.* **2006**, 110, 20801-20807.

(9) Caballero-Briones, F.; Arte´s, J. M. ; Dı´ez-Pe´rez, I.; Gorostiza, P.; Sanz, F. *J. Phys. Chem. C* **2009,** *113,* 1028–1036.

(10) R.N. Briskman, *Sol. Energy Mater. Sol. Cells* 1992, 27, 361.

(11) D. Snoke, *Science* **2002**, 298, 1368.

(12) T. Takata, S. Ikeda, A. Tanaks, S. Hara, J.N. Kondo, K. Domen, *Appl. Catal., A* **2000**, 200, 255.

[13] Ramírez-Ortiz, J.; Ogura, T.; Medina-Valtierra, J.; Acosta-Ortiz, S. E.; Bosch,P.; Reyes, J. A.; Lara,V. H. *Appl. Surf. Sci*. **2001**, 174, 177-184.

[14] Yang, H.M.; Ouyang, J.; Tang, A.D. *Mater. Res. Bull*. **2006**, 41, 1310-1318.

(15) White, B.; Yin, M.; Hall, A.; Le, D.; Stolbov, S.; Rahman, T.; Turro, N.; O'Birien, S. *Nano Lett*. **2006**, 6, 2095.

(16) Zhang, H.; Zhou, D.F. ; Zhang, L.; GuO, L.; He, C. P.; Chen, J. *Nanosci. Nanotechnol*.**2009**, 9, 1321.

(17) Jayatissa, A. H.; Samarasekera, P.; Kun. G. *Phys. Status Solidi A* **2009**, 206, 332.

(18) Samarasekera, P.; Yapa, N. U. S.; Kumara, N.T.R.N.; Perera, M.V.K. *Bull. Mater. Sci.* **2007**, 30, 113.

(19) Pei. A. H.; Shen, Z. W.; Yang, G. S. *Mater. Lett*. **2007**, 61, 2757.

(20) Chen, J.; Saeki. F.; Wiley, B.; Cang, H.; Cobb, M. J.; Li, Z.; Au, L.; Zhang, H.; Xia. Y.; Li, X. *Nano Lett*. **2007**, 7, 1318.

(21) Poizot, P.; Laruelle, S.; Grugeon, S.; Dupont, L.; Taracon, J. M. *Nature* **2000**, *407*, 496.

(22) Singh, D.P.; Neti, N. R.; Sinha, A. S. K.; Srivastawa, O. N. *J. Phys. Chem. C* **2007,** *111,* 1638.

(23) Snoke, D. *Science* **1996**, *273*, 1351.

(24) Merizzi, A.; Masse, M.; Fortin, E. *Solid State Commun.* **2001**, *120*,419.

(25) Johnson, K.; Kavoulakis, G. M. *Phys. Rev. Lett.* **2001**, *86*, 858.

(26) Jongh, P. E.; Vanmaekelbergh, D.; Kelly, J. J. *Chem. Mater*. **1999**, 11, 3512-3517.

(27) Klabunde, K.J. *Nanoscale Materials in Chemistry, 1st Edition*, *Wiley Inter-Science*, **2001**.

(28) Liz-Marzán, L.M.; Kamat, P.V. *Nanoscale Materials*, *Kluwer Academic Publisher, Massachusetts*, **2003.**

(29) Cingarapu, S.; Yang, Z.; Sorensen, C. M.; Klabunde, K. J. *Chem. Mater*. **2009**, 21, 1248.

(30) Hentze, H-P.; Raghavan, S. R.; McKelvey, C. A.; Kaler, E. W. *Langmuir* **2003***,* 19, 1069.

(31) Barton, J. K.; Vertegal, A. A.; Bohannan, E. W.; Switzer, J. A. *Chem. Mater*. **2001**, *13*, 952.

(32) Jongh, P. E.; Vanmaekelbergh, D.; Kelly, J. J. *Chem. Mater*. **1999**, *11*, 3512.

(33) Kumar, R. V.; Mastai, Y.; Diamant, Y.; Gedanken, A. J. *Mater. Chem*. **2001**, *11*, 1209.

(34) Deki, S.; Akamatsu, K.; Yano, T.; Mizuhata, M.; Kajinami, A. J. *Mater. Chem*. **1998**, *8* 1865.

(35) Wang, W.; Wang, G.; Wang, X.; Zhan, Y.; Liu, Y.; Zhang, C. *Adv. Mater*. **2002**, *14*, 67.

(36) Wang, W.; Zhan, Y.; Wang, G. *Chem Commun*. **2001**, 727.

(37) Xiong, Y.; Li, Z.; Zhang, R.; Xie, Y.; Yang, J.; Wu, C. J. *Phys. Chem. B* **2003**, *107*, 3697.

(38) Yanagimoto, H.; Akamatsu, K.; Gotoh, K.; Deki, S. J. *Mater. Chem*. **2001**, *11*, 2387.

(39) Wang, W.Z.; Wang, G.H.; Wang, X.S.; Zhan, Y.J. ; Liu, Y.K.; Zheng, C.L. *Adv. Mater*. **2002**, 14, 67.

(40) Xiong, Y.J.; Li, Z.Q. ; Zhang, R. ; Xie, Y.; Yang, J.; Wu, C.Z. ; *J. Phys. Chem.,* B **2003**, 107, 3697.

(41) Cao, M.H.; Hu, C.W. ; Wang, Y.H. ; Guo, Y.H. ; Guo, C.X. ; Wang, E.B. *Chem. Commun*. **2003**, 3, 1884.

(42) Yu, Y. ; Du, F.P.; Yu, J.C. ; Zhuang, Y.Y. ; Wong, P.K. *J. Solid State Chem.* **2004**, 177, 4640.

(43) Zhang, H.R. ; Shen, C.M.; Chen, S.T.; Xu, Z.C.; Liu, F.S. ; Li, J.Q.; Gao, H.J. *Nanotechnology* **2005**, 16, 267.

(44) Yin, M.; Wu, C.K.; Lou, Y.B.; Burda, C.; Koberstein, J.T.; Zhu, Y.M.; O'Brien, S. *J. Am. Chem. Soc.* **2005**, 127, 9506.

(45) Luo,F.; Wu,D.; Gao, L.; Lian, S.Y.; Wang, E.B.; Kang, Z. H.; Lan, Y.; Xu, L. *J. Cryst. Growth* **2005**, 285, 534.

(46) Wang, D.B.; Mo, M.S.; Yu, D.B.; Xu, L.Q.; Li, F.Q.; Qian, Y.T. *Cryst. Growth Des*. **2003**, 3, 717.

(47) Zhang, J.T.; Liu, J.F.; Peng, Q.; Wang, X.; Li, Y.D. *Chem. Mater*. **2006**, 18, 867.

(48) Xu, L.S.; Chen, X.H.; Wu, Y.R.; Chen, C.S.; Li, W. H.; Pan, W.Y.; Wang, Y.G. *Nanotechnology* **2006**, 17, 1501.

(49) Liang, Z.H.; Zhu, Y.J. *Mater. Lett*. **2005**, 59, 2423.

(50) Lu, C.H.; Qi, L.M.; Yang, J.H.; Wang, X.Y.; Zhang, D.Y.; Xie, J.L.; Ma, J.M. *Adv. Mater*. **2005**, 17, 2562.

(51) Jing, S.Y.; Xing, S.X.; Wu, Y.; Wang, Y.F.; Zhao, B.; Zhao, C. *Mater. Lett*. **2007**, 61, 2281.

(52) Murphy, C. J. *Science*, 2002, 298, 2138.

(53) Zhang, W.; Shi, L.; Tang, K.; Dou, S. Eur. J. Inorg. Chem. **2010**, 1103-1109.

(54) Ping, H.; Shen, X.; Cao, H. *J. Colloid Interface Sci.* **2005**, 284, 510.

(55) Cerchiaro, G.; Sant'Ana, A. C.; Temperini, M. L. A.; Ferreira, A. M. C. *Carbohydr. Res.* **2005**, 340, 2352.

(56) Cubillas, P.; Anderson, M. W. '*Zeolites and Catalysis, Synthesis, Reactions, and Applications, Vol. 1*' **2010**, Wiley-VCH Verlag GmbH & Co. KGaA, Weinheim, Germany.

3.6 Supporting Information

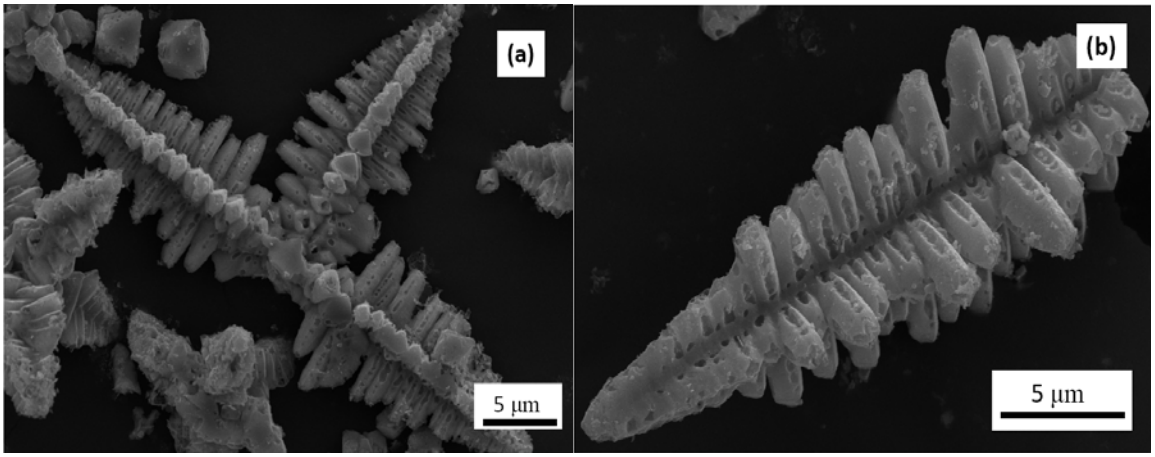

Fig. 3.S1. Cu_2O sample prepared at 80 ^oC in air using copper (II) acetate and D-glucose

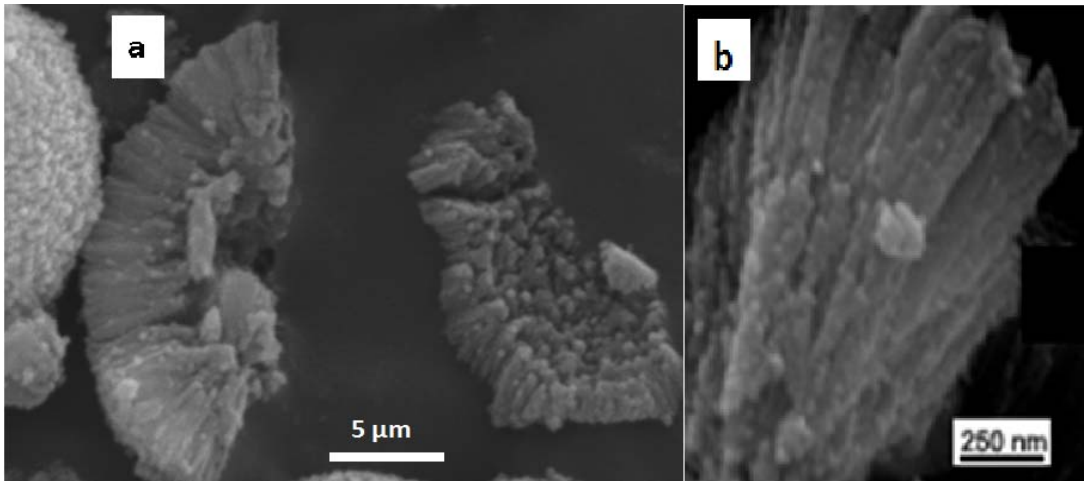

Fig. 3.S2. Disintegrated Cu_2O-CuO hollow sphere samples prepared by reducing saturated copper(II) acetate solution with ethylene glycol under hydrothermal treatment at 140 ^oC.

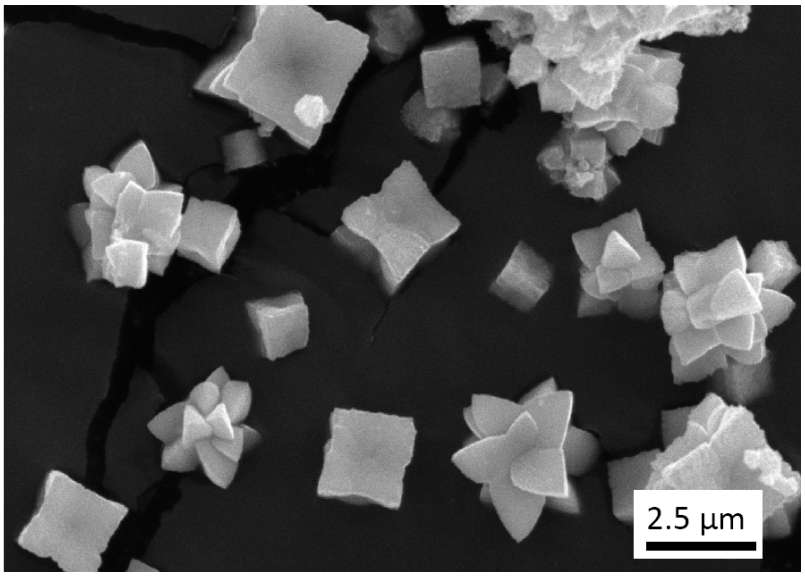

Fig. 3.S3. Cu_2O samples prepared by reducing Benedict's solution with α-D-glucose at 60 ^oC under ambient condition.

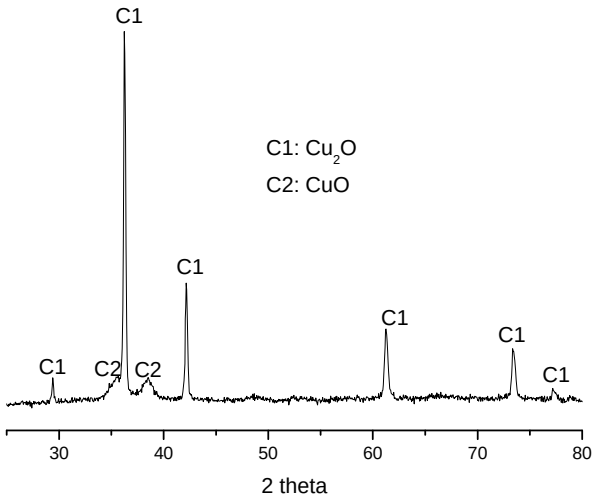

Fig. 3.S4. pXRD Pattern of Cu_2O, C5, after treatment in 1 % H_2O_2 in water as a photocatalyst under UV-vis for 48 h.

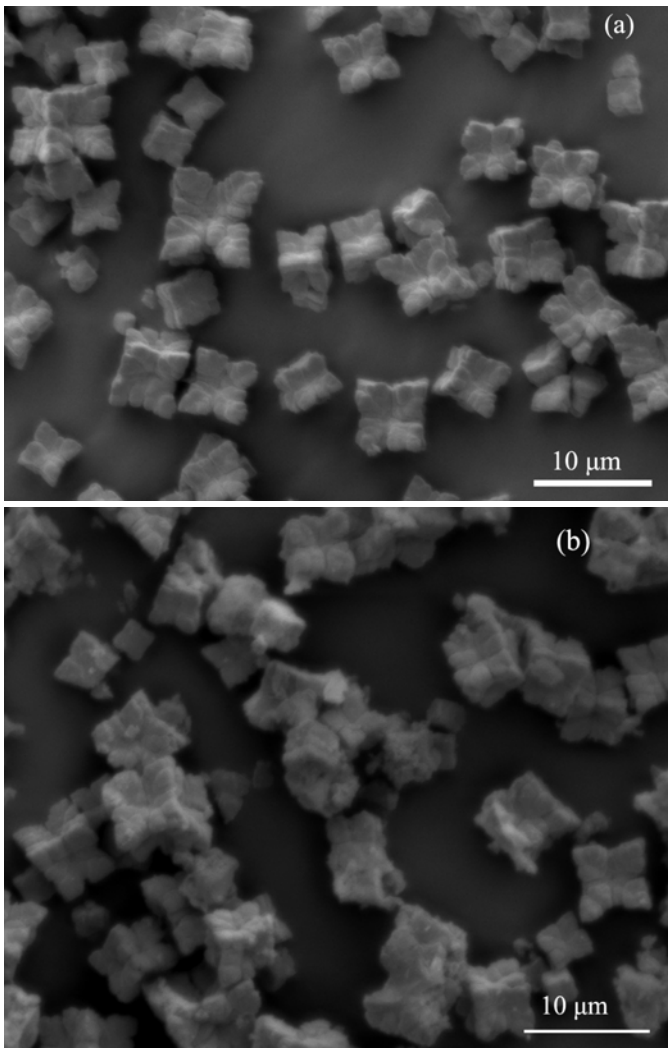

Fig. 3.S5. SEM images of Cu_2O, C5, (a) before (b) after treatment in 1 % H_2O_2 in water as a photocatalyst under UV-vis for 48 h.

Chapter 4 - MgO-TiO_2 Mixed Oxide Nanoparticles: Comparison of Aerogel Vs Flame Synthesis; Characterization and Photocatalytic Activities*

*This is currently in press, Journal of Materials Research

4.1 Introduction

TiO_2, a semiconductor, is traditionally used in pigments, as photocatalysts, as a supporter of catalysts, and for water purification.[1-3] In the last two decades, TiO_2 nanomaterials with various morphologies—nanoparticles, nanotubes, nanorods—have been synthesized by various methods.[4-11] As the material is UV active, the TiO_2 nanomaterials have been widely investigated as photocatalysts in the UV region;[12-14] the photocatalytic activities have been enhanced in visible and UV regions by doping with various metal and non-metal based materials.[15-19]

MgO, an insulator, is traditionally used for the preparation of cement, medicines, insulators, desiccants, and optical materials.[20] In recent decades, people have given attention to the synthesis of MgO nanomaterials with different morphologies—nanoparticles, nanotubes, and nanorods—which have been investigated for different purposes;[21-27] MgO nanomaterials have been investigated as catalysts, adsorbents, and destructive adsorbents for toxins, including chemical warfare agents.[28-30]

There are many reports about the synthesis and properties of composite materials of TiO_2 with other oxides —TiO_2-SiO_2, TiO_2-CeO_2, TiO_2-SnO_2, TiO_2-ZrO_2, TiO_2-Al_2O_3, TiO_2-Fe_2O_3, TiO_2-RuO_2, and TiO_2-IrO_2— in the form of nanomaterials.[31-43] Similarly, there are many reports about the mixed oxides of MgO with other oxides— MgO-Al_2O_3, MgO-SnO_2, MgO-ZrO_2, MgO-CeO_2, MgO-SiO_2 and MgO-Sm_2O_3—and their properties.[44-56]

There are some salient features of MgO and TiO_2; they are environmentally friendly and economically low in cost. These nanomaterials have been widely investigated for many purposes. There are many reports about synthesis, characterization, and applications of these nanomaterials; our group has widely investigated the properties of MgO and TiO_2 based materials nanomaterials.[18,24,50] Most of these materials are usually prepared by the sol-gel method in organic media; they are usually prepared by hydrolysis of corresponding metal alkoxides in organic solvents. The the sol-gel synthesis process is time consuming and low mass production. Although their properties appear significant and interesting, the samples prepared by sol-gel method are commercially less viable. Furthermore, the mixed oxides of MgO-TiO_2, the mixed oxides of an insulator and semiconductor, might have new properties which might be interesting and important; there are relatively few reports about the synthesis, characterization, and application of MgO-TiO_2 mixed oxides;[57-61] most of these materials were prepared by the sol-gel method. Since this method has some limitations as already discussed, we were interested for the synthesis of MgO-TiO_2 mixed oxides by an alternative method, flame synthesis, as there are no reports about the flame synthesis of MgO-TiO_2 mixed oxides to the best of our knowledge. Moreover, the method is continuous and seems economically more viable. The mixed oxide system has rarely been investigated in photocatalytic or non-photocatalytic applications.[62-65] However, it is necessary to determine whether the samples prepared by flame synthesis have similar properties or not in comparison of the properties of similar samples prepared by sol-gel method. Therefore, we synthesized the mixed oxide nanomaterials of MgO and TiO_2 with different ratios by both aerogel[66] and flame synthesis,[67] and our primary goal was to compare the properties of these mixed oxides obtained by aerogel vs flame synthesis (low

temperature vs high temperature methods). To the best of our knowledge, this is the first time such a comparison has been.

We characterized the physical properties by different techniques and employed them as photocatalysts for the mineralization of acetaldehyde, a common outdoor and indoor pollutant, using both UV and visible light. We found that these samples demonstrated enhanced photocatalytic activities over pure TiO_2 in UV light with low content of MgO; particularly the mixed oxides of MgO-TiO_2 (1:50 molar ratio) prepared by both methods were found to be a superior composition for the mineralization of CH_3CHO in UV light. Moreover, the photocatalytic activity of the MgO-TiO_2 prepared by the aerogel method was found to be better than that of the samples prepared by flame synthesis with equal ratio of MgO and TiO_2.

4.2 Experimental Section

4.2.1 Materials

a. Titanium (IV) isopropoxide (Sigma-Aldrich)
b. Methanol (Fisher Chemical)
c. Acetylacetone (Fisher Chemical)
d. Hydrated magnesium acetate (Alfa-Aesar)
e. Nitrogen (Linweld)
f. Oxygen gas (Linweld)
g. Methane gas (Linweld)
h. Magnesium ribbon (Sigma-Aldrich)
j. Toluene (Fisher Chemical)
k. Hydrochloric acid (Fisher Chemical)

4.2.2 Flame synthesis of TiO_2, and MgO-TiO_2 nanoparticles

TiO_2 nanoparticles were prepared by using titanium(IV) isopropoxide (Sigma-Aldrich) as a Ti-precursor; the precursor was dissolved in methanol (Fisher Chemical) in the presence of

acetylacetone (Fisher Chemical). In a particular experiment, 3 mL of titanium(IV) isopropoxide was dissolved in a mixture of 5 mL methanol and 3 mL acetylacetone and stirred. Then the solution was used for the synthesis of TiO_2 during the flame synthesis.

The magnesium and titanium precursors were used to prepare MgO-TiO_2 mixed oxides with molar ratios of 2:1, 1:1, 1:2, 1:20, 1:50, and 1:100. For the synthesis of mixed oxides, titanium(IV) isopropoxide was dissolved in methanol in the presence of acetyl acetone; acetyl acetone slows the hydrolysis of the titanium precursor. Magnesium acetate was dissolved in methanol. In a particular experiment, 3 mL titanium (IV) isopropoxide was dissolved in 3 mL acetylacetone and 2.1 g of hydrated magnesium acetate (Alfa-Aesar) was dissolved in 5 mL methanol. These two solutions were mixed together and stirred from which 1:1 molar ratio of MgO and TiO_2 could be prepared. Then the mixed solution was injected into the glass tube and converted into mist with the help of an ultrasonic nebulizer fixed at the bottom of the tube which was extracted from an ultrasonic humidifier (Model V5100 NS; PN 32GB5100B09, Kaz, Inc.); the mist along with the flow of ultra high pure (UHP) nitrogen (rate = 2 L/min) was driven to the flame of a burner. The flame of the burner was prepared by passing industrial oxygen (10 L / min) and methane (4 L / min) gases (Linweld). We did not measure the flame temperature during the experiment. The reported flame temperature produced by a mixture of 80 % methane and 20 % oxygen is 1974 ^oC;[77] the temperature could be increased from 1601 ^oC to 2692 ^oC with increase in percentage of oxygen,[78] and the adiabatic flame temperature in the hottest region was about 2781 ^oC.[79] Since sufficient oxygen was passed during our experiment, to burn all combustible materials so as to produce metal oxide particles from metal precursors, possibly the flame temperature at the hottest zone was expected around 2700 ^oC. The outer cold surface of a steel bowl with a flat bottom containing ice water was set at the height of 10 cm above the nozzle

of the burner so as to collect a deposit of the oxide samples by the thermophoresis process. The precursor was passed through the burner for about 30 min. Then, the oxide sample was scrapped out and collected.

4.2.3 Synthesis of MgO-TiO_2 mixed oxide by aerogel method

Mixed oxides of MgO and TiO_2 were also prepared by the aerogel method with the same molar ratios as those prepared by the flame synthesis. For the synthesis of the mixed oxides, the desired amount of clean magnesium ribbon (Sigma-Aldrich) was allowed to react with methanol completely, to obtain a magnesium methoxide suspension in methanol.[66] Then the magnesium methoxide suspension and titanium(IV) isopropoxide in toluene were mixed together, and stirred with a magnetic stirrer. A stoichiometric amount of water was added to the mixed suspension for the complete hydrolysis of both metal alkoxides with continuous stirring so as to form a gel; the ratio of methanol and toluene was 2:3 as an appropriate mixture of methanol and toluene that could help to form the gel rapidly. The gel was treated for supercritical drying followed by calcination. In a particular experiment, 0.8 g of clean Mg ribbon was allowed to react with 40 mL methanol so as to form magnesium methoxide. 10 mL of titanium(IV) isopropoxide was dissolved in 60 mL toluene; both of them were mixed together and stirred to get a 1:1 molar ratio of MgO and TiO_2. Then 3.5 mL of water with 2 drops of 11.5 N HCl was added for the complete hydrolysis of both metal alkoxides, and a gel was formed. After 4 h aging, the gel was transferred to an autoclave and heated at 265 ^{o}C to attain a supercritical condition for subsequent venting of solvent. The solid aerogel obtained was then calcined at 500 ^{o}C in air for 1h with heating and cooling at the rate of 5 ^{o}C min^{-1}.

4.2.4 Characterization

(i) Powder X-ray diffraction (pXRD): The samples prepared by both flame synthesis and aerogel method were characterized by the pXRD patterns with 2 theta angle in the range of 20-80^{o} measured with a Scintag XDS 2000 spectrometer; the X-ray was CuKα radiation with applied voltage of 40 kV and the current 40 mA.

(ii) Transmission Electron Microscopy (TEM) and Scanning Electron Microscopy (SEM): The sizes and morphologies of these metal oxide nanomaterials were observed by TEM, and the elemental analyses were carried out by SEM. SEM experiments were carried out by using a Scanning Electron Microscope-S3500N, Hitachi Science System, Ltd. at the Entomology Department of Kansas State University (KSU), microscopy and imaging facility. TEM experiments were carried out by using a transmission electron microscopy, Phillips 100 at the biology department of KSU.

(iii) Brunauer-Emmet-Teller (BET) Method: Specific surface areas and pore diameters of TiO_2 and MgO-TiO_2 nanoparticles were measured by the BET method. The measurements were carried out using Microsorb II 2300 and Quantachrome NOVA 1200 instrumentation at 77 K employing liquid nitrogen.

(iv) UV-Vis and Fourier Transform Infrared (FTIR) Analysis: A Cary 500 UV-vis-NIR spectrometer with reflectance accessory was used in the range of 200-800 nm. The sample cell was made of two transparent calcium fluoride discs, a Teflon O-ring and screw type combination in which the oxide materials were packed between two discs and the O-ring. In this technique, absorption of a solid material was measured by using diffuse reflectance mode; the instrumental system calculates the absorption automatically measuring the diffuse reflectance.[76] Polytetrafluoroethylene (PTFE) powder of ~100 μm particle size (Sigma Aldrich) was taken as a reference material. After using the reference sample, absorption of each individual oxide sample

was measured. Furthermore, some samples were characterized by Fourier Transform Infrared (FTIR) using Thermo Necolet Nexus 670 FT-IR with Avatar Diffuse Reflectance accessory.

(v) Photocatalytic Study: The photocatalytic oxidation of acetaldehyde was carried out with aerial-oxygen in a 305 mL static cylindrical glass reactor with a water-jacketed base at room temperature. During the experiment, a catalyst was placed in a circular glass dish (radius = 7 mm) mounted in the reactor with a small magnetic stirrer underneath the dish. Then side tubes of the reactor were closed with rubber septa; 100 μL of liquid acetaldehyde (Sigma-Aldrich) was introduced and then the opening of the reactor was closed immediately with the quartz window. The acetaldehyde (boiling point = 25 ^{o}C) was converted to vapor at room temperature; the mixture of acetaldehyde and air was stirred for 40 min in the dark for achieving equilibrium of the reacting molecules prior to illumination. Then 35 μL of gas from the reactor was extracted periodically with a syringe through a septum and the gas was injected into the GC-MS port (Shimadzu GCMS-QP 5000); the temperatures of the injector, column, and detector were maintained at 40 ^{o}C, 200 ^{o}C, and 280 ^{o}C, respectively. After the injection of the third sample from the reactor at 40 min, UV light ($\lambda > 320$ nm) was introduced through the quartz glass from the 1000 W high-pressure Xenon lamp (Oriel Instrument, Model 66921) at the height of 20 cm.

4.3 Results and Discussion

4.3.1 pXRD Analysis

The pXRD patterns of MgO-TiO_2 mixed oxides with relatively high content of MgO—2:1, 1:1, and 1:2 molar ratios of MgO and TiO_2—demonstrated the formation of titanates of Mg with different chemical compositions: $MgTiO_3$, Mg_2TiO_4 and $MgTi_2O_5$. The pXRD patterns of the MgO-TiO_2 mixed oxides with 2:1 ratio prepared by both aerogel and flame synthesis demonstrated the formation of $MgTi_2O_4$ (Fig.4.S1a and Fig.4.S1b where ‘S’ stands for

supporting information); however, the mixed oxide prepared by the flame synthesis was found to be relatively more crystalline than that prepared by aerogel method. The pXRD pattern of the MgO-TiO_2 mixed oxides with 1:1 molar ratio prepared by the flame synthesis showed the formation of two compounds: $MgTi_2O_4$ as a major product and $MgTiO_3$ as the minor product (Fig.4.S2a). The pXRD patterns of the mixed oxides with molar ratio of 1:1 prepared by aerogel demonstrated the formation of $MgTi_2O_5$ (Fig.4.S2b). The pXRD pattern of the mixed oxides with ratio of 1:2 prepared by the flame synthesis demonstrated the formation of $MgTiO_3$ as the major product and TiO_2 (anatase and rutile) as the minor product (Fig.4.S3a). The pXRD patterns of mixed oxides with ratio 1:2 prepared by aerogel method demonstrated the formation of $MgTi_2O_5$ but with a nearly amorphous nature (Fig.4.S3b).

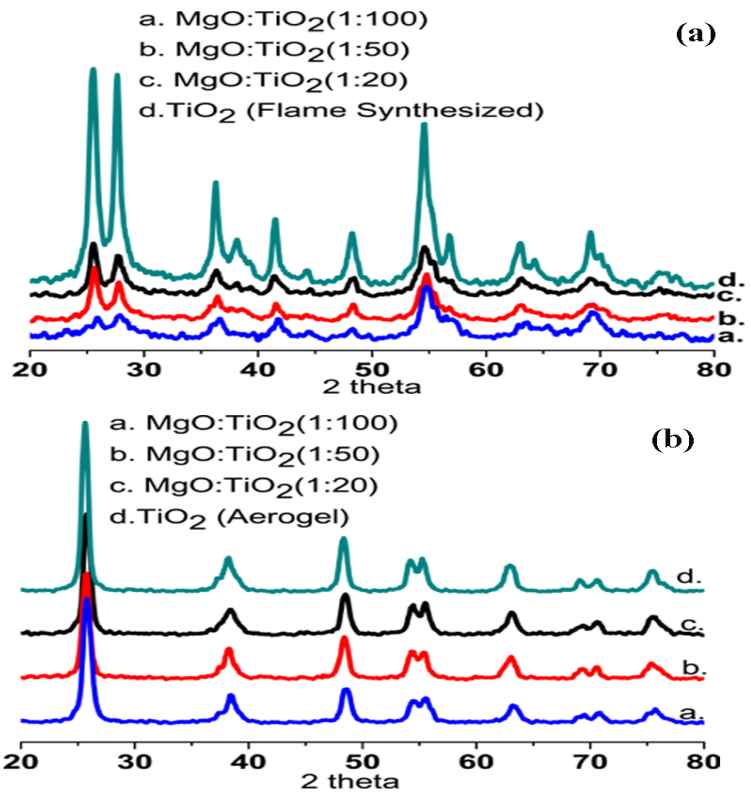

Figure 4.1 pXRD patterns of MgO-TiO_2 with mole ratios of 1:100, 1:50, 1:20, and TiO_2 prepared by (a) flame synthesis (b) aerogel method.

Fig.4.1(a) and 4.1(b) show the pXRD patterns for the TiO_2 and the MgO-TiO_2 mixed oxides with ratios 1:20, 1:50, and 1:100. TiO_2 prepared by flame synthesis process were found to be in both anatase and rutile phases [Fig.4.1(a.)]; the ratio of anatase and rutile was found to be about one. However, TiO_2 aerogel was found to be only in the anatase phase [Fig.4.1(b)]. This could be possible as the anatase phase usually forms at lower temperature (< 500 ^oC); the rutile phase and anatase phases form at relatively higher temperature (>500 ^oC).[72] Herein aerogel samples were calcined at relatively low temperature (500 ^oC) and the samples from the flame synthesis were prepared at higher temperature (> 500 ^oC). The MgO-TiO_2 mixed oxides with 1:20, 1:50, and 1:100 ratios prepared by flame synthesis showed the presence of both anatase and rutile TiO_2, and the aerogel samples with these ratios showed the presence of anatase only. However, the pXRD patterns of MgO-TiO_2 (1:20, 1:50, 1:100) mixed oxides prepared by both methods did not show the presence of MgO. The reason might be the low quantity of MgO and it could be well dispersed throughout the TiO_2. However, the presence of a small amount of Mg on the surface of mixed oxides was confirmed by EDX analysis (Fig.4.S4). In MgO-TiO_2 mixed oxides with mole ratios of 1:50 and 1:100, the mole percentages of Mg were found to be ~1.9 and ~1 respectively in total mole of Mg and Ti in the mixed oxides when prepared by aerogel method; similarly, the mole percentages of Mg were found to be ~1.1 and ~ 0.4 in total mole of Mg and Ti in MgO-TiO_2 mixed oxides with mole ratios of 1:50 and 1:100 respectively when prepared by flame synthesis.

4.3.2 Infrared Analysis

TiO_2 and some MgO-TiO_2 (1:1 and 1:50) mixed oxides prepared by both flame synthesis and aerogel method were characterized by FTIR spectra (Fig.4.S5 and Fig.4.S6). The spectra of MgO-TiO_2 (1:1) mixed oxides were found to be different from the spectra of TiO_2 and MgO-

TiO_2 (1:50); the spectra of MgO-TiO_2 (1:1) prepared by both flame and aerogel methods showed characteristic peaks below 500 cm^{-1} due to the rotational mode by IR absorption of Mg-O-Ti indicating the formation of titanates of Mg.[65] However, there were no characteristic peaks in this region for the pure TiO_2 and MgO-TiO_2 (1:50) mixed oxides.

4.3.3 BET Data Analysis

The samples were characterized with BET N_2 adsorption and desorption experiments; the specific surface area and pore diameter values of TiO_2 and the mixed oxides prepared by aerogel and flame synthesis are shown in table 4.1.

Table 4.1 BET data for TiO_2 and MgO-TiO_2 samples prepared by flame synthesis and aerogel method calcined at 500 ^oC.

Samples prepared by flame synthesis	Surface area (m^2/g)	Pore diameter (nm)	Samples prepared by aerogel	Surface area (m^2/g)	Pore diameter (nm)
TiO2	98	27	TiO_2	96	17
MgO-TiO_2 (2:1)	121	34	MgO-TiO_2 (2:1)	230	8
MgO-TiO_2 (1:1)	156	30	MgO-TiO_2 (1:1)	220	8
MgO-TiO_2 (1:2)	101	31	MgO-TiO_2 (1:2)	201	8
MgO-TiO_2 (1:20)	91	27	MgO-TiO_2 (1:20)	86	28
MgO-TiO_2 (1:50)	105	15	MgO-TiO_2 (1:50)	84	29
MgO-TiO_2 (1:100)	72	16	MgO-TiO_2 (1:100)	80	29

The surface area of TiO_2 nanoparticles prepared by the flame synthesis process was found to be 98 m^2/g and the value was found to be 96 m^2/g when prepared by the aerogel method. Different specific surface area values were found for the mixed oxides of MgO and TiO_2 with various ratios prepared by both aerogel and flame synthesis. The surface areas were found to be greater

for the MgO-TiO_2 mixed oxides in the form of titanates of Mg with ratios of 2:1, 1:1, and 1:2. The surface areas of the mixed oxides with these ratios prepared by aerogel were found to be relatively greater than those prepared by flame synthesis. Higher values of the surface areas may be possibly due to the lower temperature for the synthesis in the aerogel method which would minimize sintering. The surface areas of the mixed oxides with the low amount of MgO were found to be less than that of pure TiO_2 nanoparticles when prepared by both methods. These mixed oxides were found to be porous, especially mesoporous as pore diameters of the samples were in the range of 8-34 nm (Table 4.1).

4.3.4 Transmission Electron Microscopy Analysis

Some mixed oxides were characterized by TEM analysis. Fig.4.2(a) shows TEM image of MgO-TiO_2 mixed oxides with ratio of 1:50 prepared by the flame synthesis process; the size of individual particles was in the range of 11-15 nm; the particle size is close to crystallite size of 12 nm calculated from the Scherrer equation. The mixed oxide with 1:50 ratio prepared by aerogel method was also characterized by TEM [Fig.4.2(b)]; the figure shows the particle size of ~ 10-20 nm; the particle size is close the crystallite size of 13 nm calculated from Scherrer equation.

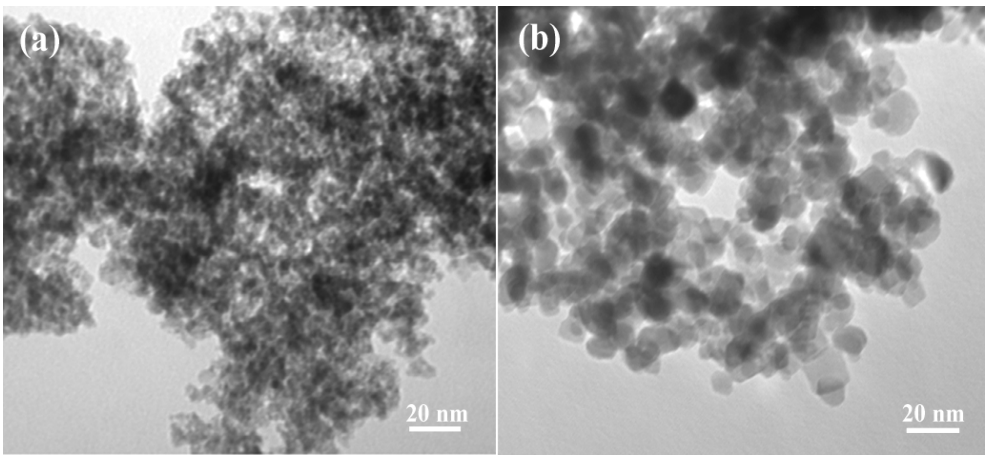

Figure 4.2 TEM images of MgO-TiO_2 (1:50) samples prepared by (a) flame synthesis (b) aerogel method.

4.3.5 UV-vis Absorption Spectra

Samples were also characterized by UV-vis absorption spectra, and compared with the spectrum of Degussa P25 [Fig.4.3(a) and 4.3(b)]. In the UV-vis spectra, the absorption by MgO-TiO_2 mixed oxides with high content of MgO (MgO : TiO_2 = 1:1 and 1:2) was found to be in the shorter wavelength region due to the formation of titanates of Mg with different compositions. The spectra of as-prepared TiO_2 and the mixed oxides with low content of MgO were found to be slightly red shifted. The band gap of pure TiO_2 and mixed oxides of MgO-TiO_2 (1:20, 1:50, 1:100) prepared by aerogel method, which showed anatase phase of TiO_2 only from pXRD analysis, was found to be ~ 3.1 eV; the band gap of those types of samples prepared by flame synthesis, which showed both anatase and rutile phases of TiO_2, was found to be 2.9 eV. The absorption at longer wavelength, red shift, possibly might be due to the various types of crystal defects. Furthermore, there was relatively stronger absorptions of UV light ($\lambda \geq 320$ nm) by the TiO_2 and mixed oxides prepared by the aerogel method, when compared with spectra of similar samples prepared by flame synthesis.

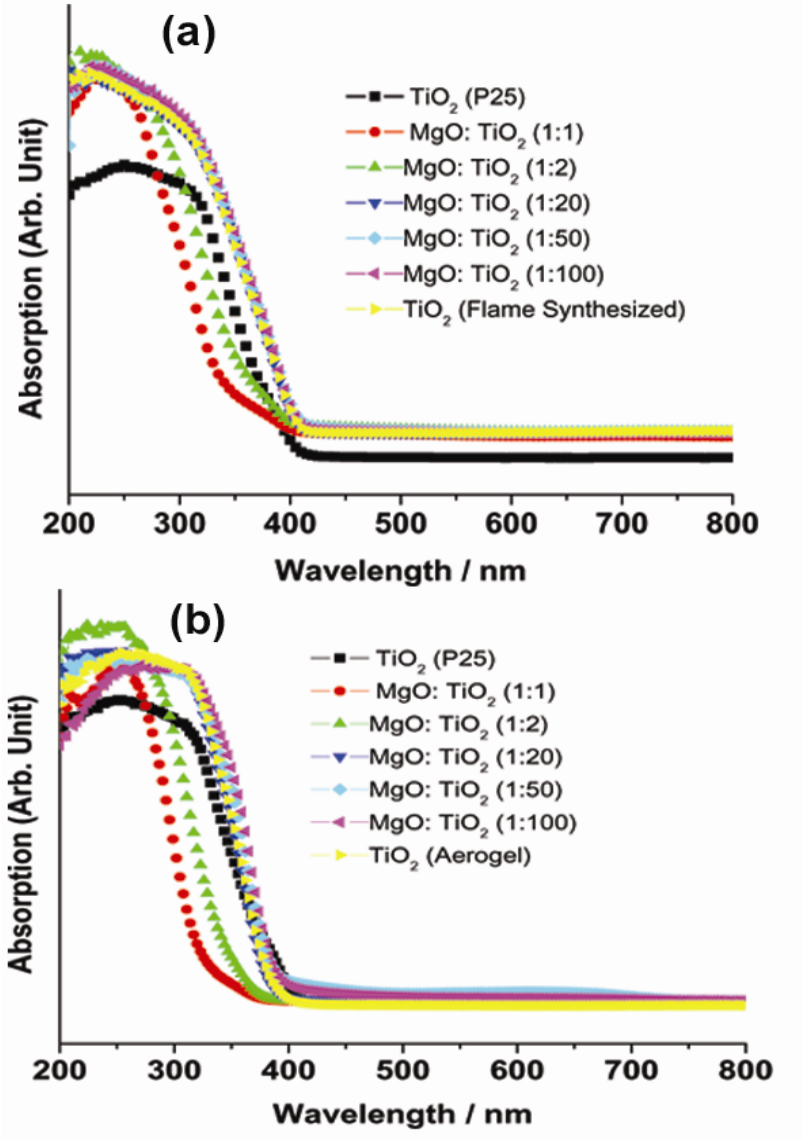

Figure 4.3 UV-vis absorption spectra of Degussa P25, TiO_2 (as-synthesized), and MgO-TiO_2 mixed oxides with mole ratios of 1:1, 1:2, 1:20, 1:50, and 1:100 synthesized by (a) flame synthesis (b) aerogel method.

4.3.6 Photocatalytic Studies

Samples prepared by both flame synthesis and aerogel method were employed as photocatalysts using UV light. The oxidation of acetaldehyde in presence of air was studied at room temperature, 25 ^{o}C, and CO_2 was measured as a final product by the following reaction.

$$2CH_3CHO + 5O_2 \rightarrow 4CO_2 + 4H_2O \qquad (4.1)$$

The CO_2 that accumulated inside the closed reactor was measured at different intervals [Fig. 4.4(a,b) and Fig.4.S7]. No CO_2 was found to be formed in the dark or under visible light. Furthermore, UV-light was also introduced to the reactor containing acetaldehyde without oxide samples; no CO_2 was found to be formed, indicating that oxide samples are indeed, photocatalysts.

The photocatalytic activities of the mixed oxides with different ratios and TiO_2 prepared by the same method were compared. The photocatalytic activities of MgO-TiO_2 (1:1) were found to be the lowest, and also note that these were the samples that absorbed only the shorter UV wavelength and therefore, would probably absorb fewer photons overall at longer wavelength of UV for the photocatalytic reaction.

When the amount of MgO was decreased in the mixed oxides, the catalytic activities were found to be enhanced. Interestingly, a maximum activity was obtained when MgO-TiO_2 with the ratio of 1:50 was used. Thus, small amount of MgO are beneficial, for both flame synthesized and aerogel samples. It should also be noted that aerogel samples were generally found to be better photocatalysts than produced by flame synthesis. The overall photocatalytic reactivity order for the oxide samples prepared by the flame synthesis process was found to be MgO-TiO_2 (1:50) > MgO-TiO_2 (1:100) > TiO_2 (Degussa P25) > TiO_2 (as-synthesized) > MgO-TiO_2 (1:20) > MgO-TiO_2 (1:1). The order for the aerogel samples was found to be MgO-TiO_2 (1:50) > MgO-TiO_2 (1:100) >

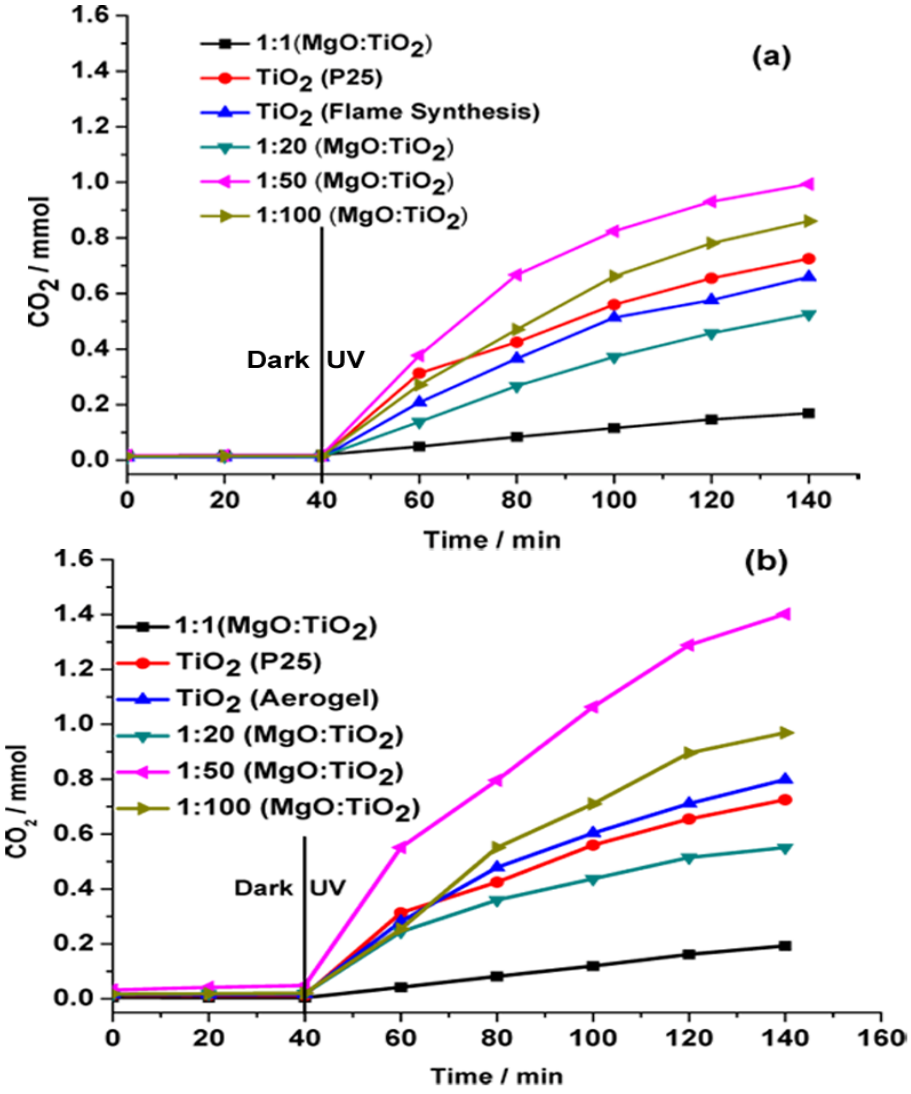

Figure 4.4 Measurement of CO_2 produced from photocatalytic oxidation of acetaldehyde under UV light by Degussa P25, TiO_2 (as-synthesized), and MgO-TiO_2 mixed oxides with ratios of 1:1, 1:20, 1:50, and 1:100 as photocatalysts prepared by (a) flame synthesis (b) aerogel method.

TiO_2 (as-synthesized) > TiO_2 (Degussa P25) > MgO-TiO_2 (1:20) > MgO-TiO_2 (1:1). Slightly higher surface area could partially explain these trends, but the 1:50 ratio samples appeared to be special, and in particular the aerogel system. Indeed, the photocatalytic activities in UV light were found to be greater by the samples prepared by aerogel in every case (table 4.2).

Table 4.2 Comparison of amount of CO_2 produced by TiO_2 and MgO-TiO_2 mixed oxides with similar composition prepared by flame and aerogel method at the end of 140 minutes.[a]

Sample Preparation Methods	CO_2 (mmol) produced by				
	TiO_2	MgO :TiO_2 (1:1)	MgO :TiO_2 (1:20)	MgO :TiO_2 (1:50)	MgO :TiO_2 (1:100)
Flame synthesis	0.64 ± 0.02	0.19 ± 0.02	0.53 ± 0.03	0.99 ± 0.01	0.86 ± 0.03
Aerogel	0.82 ± 0.04	0.19 ± 0.03	0.55 ± 0.02	1.30 ± 0.03	0.97 ± 0.02

[a]UV light was introduced after 40 minutes in dark.

When MgO is mixed with the TiO_2, there might be surface modification with change in surface energy. If a large amount of MgO, an insulator, is mixed, there would be more MgO on the surface, which would reduce TiO_2 surface. Furthermore, the mixed oxides with high content of MgO in the MgO-TiO_2 mixed oxides (2:1, 1:1, and 1:2) would form titanates of Mg which have high band gap; these compounds absorb at shorter wave length and are not favorable for the photocatalytic oxidation of acetaldehyde.

When a small amount of MgO is introduced to TiO_2, there must be good dispersion of MgO without formation of a separate crystalline phase of MgO. This might be the reason why there were no pXRD patterns of MgO in MgO-TiO_2 mixed oxides with ratios of 1:20, 1:50, and 1:100 although Mg was detected by EDX. The surface modification of the mixed oxide by the introduction of a small amount of MgO might produce different kinds of crystal defects on TiO_2.

The crystalline structure of MgO might be also an important factor to develop more defects. MgO is coordinated octahedrally with coordination number 6 and {100} facets are predominant in the MgO microcrystalline structure.[69,70,75] At the surface of the mixed oxide, there might be a greater number of unsaturated sites of MgO so as to produce more defects in the mixed oxide. Furthermore, some Mg^{2+} could substitute Ti^{4+} so as to produce crystal defects on TiO_2 crystals and cation vacancies (F-centers). Furthermore, there might be anion vacancies (V-centers) as the defects. These defects are probably important for the photocatalytic oxidation of acetaldehyde. F-centers could be both neutral or charged; the F-centers with charge have a tendency to trap electrons generated from photo-excitation, possibly leading to a separation of the electron-hole pair and suppress recombination; as a result, there would be an enhancement of the photocatalytic degradation of acetaldehyde.[71-72] Due to these defects, the MgO-TiO_2 with ratios of 1:50 and 1:100 absorbed at longer wavelength than Degussa P25. The small amount of doped MgO might have created intermediate energy levels between the valence band and conductance band of TiO_2 so as to absorb at longer wavelength. MgO-TiO_2 (1:50), ~ 2 mole % MgO, was found to be optimum for the photooxidation acetaldehyde; the result is close to the reported data for the maximum oxidation of chlorophenol by 3% MgO doped TiO_2 synthesized by the sol-gel method.[63] Larger (5%) or smaller (1%) loadings were not so effective.

As mentioned above, the aerogel samples were found to be superior to that of samples prepared by the flame synthesis when compared for equal ratio of mixed oxides. The Mg doped in the mixed oxide was found to be homogeneously distributed on the surface of mixed oxide particles when prepared by aerogel method, as indicated by EDX data, but this was not the case of mixed oxides prepared by flame synthesis. Furthermore, there were formations of both anatase and rutile phases of TiO_2 present in the mixed oxides with lower content of MgO on the surface of

nanoparticles when synthesized by the flame synthesis. However, only the anatase phase was found to be formed when synthesized by the aerogel method.

It has been reported that the anatase phase is superior for the photocatalytic oxidation of organic compounds especially by the small porous anatase particles; the anatase TiO_2 might adsorb relatively more water and form hydroxyl group so as to enhance the degradation of acetaldehyde;[63,74,79] Ohno *et al.* revealed that relatively bigger rutile particles (>1μm) with {110} and {110} faces were found to be active for the photocatalytic oxidation of water, an inorganic compound, using a suitable electron acceptor, whereas they found that smaller anatase particles were found to be very active for the oxidation of alcohols especially at low concentration. Smith and Ford demonstrated that more heat of oxygen adsorption was produced by anatase than produced by rutile;[75] in other words, more oxygen could be adsorbed on the surface of anatase leading to photocatalytic oxidation of acetaldehyde effectively. So the formation of anatase only in as-synthesized TiO_2 and in the MgO-TiO_2 mixed oxides of 1:20, 1:50, and 1:100 ratios prepared by aerogel played an important role for enhancing photocatalytic oxidation of acetaldehyde.

4.4 Conclusions

The mixed oxides of MgO and TiO_2 with various ratios were prepared by flame synthesis and aerogel methods. From the pXRD patterns, titanates of MgO with different compositions were found to be formed using a relatively high content of MgO in the mixed oxides. When MgO content was relatively low, only the patterns of TiO_2 were found, indicating well dispersed MgO; only the TiO_2 anatase phase was found in the aerogel samples, but both anatase and rutile were found in the mixed oxides prepared by flame synthesis. However, the presence of Mg could also be detected by EDX analysis. From the UV-vis spectra, it was found that the mixed oxide

samples with low content of MgO absorbed at slightly longer wavelength when compared the spectrum of Degussa P25. These mixed oxides with low content of MgO were found to be more UV active photocatalysts than TiO_2 for the mineralization of acetaldehyde. The MgO-TiO_2 mixed oxide with 1:50 ratio showed the highest photocatalytic degradation of acetaldehyde. When the photocatalytic activities of mixed oxides with equal ratio prepared by flame synthesis and aerogel method were compared, in each case an aerogel sample was found to be superior.

Acknowledgement. The partial financial support of the Department of Energy (DF-FGO2-10ER16202) and KSU Targeted Excellence are acknowledged with gratitude.

4.5 References

(1) Jacobsen, A. E. *Ind. Eng. Chem*. **1949**, 41, 523.

(2) Pramauro, E.; Vincenti, M.; Augugliaro, V.; Palmisano, L. *Environ. Sci. Technol*. **1993**, 27, 1790.

(3) Zhang, Y.; Crittenden, J. C.; Hand, D. W.; Perram, D. L. *Environ. Sci. Technol*. **1994**, 28, 435.

(4) Liu, J.; Hu, Y.; Gu, F.; Li, C. *Ind. Eng. Chem. Res*. **2009,** 48, 735.

(5) Lim, K.T.; Hwang, H. S. *Langmuir* **2004**, 20, 2466.

(6) Liu, S. M.; Gan, L. M.; Liu, L. H.; Zhang, W.D.; Zeng, H. C. *Chem. Mater*. **2002**, 14, 1391-1397.

(7) Zhang, M.; Bando, Y.; Wada, K. *J. Mater. Sci. Lett*. **2001**, 20, 167.

(8) Grimes, C. A. *J. Mater. Chem*. **2007**, 17, 1451.

(9) Yin, H.; Wada, Y.; Kitamura, T.; Kambe, S.; Murasawa, S; Mori, H.; Sakata, T.; Yanagida S. *J. Mater. Chem.* **2001**, 11, 1694.

(10) Murugan, A. V.; Samuel, V.; Ravi, V. *Mater. Lett*. **2006**, 60, 479.

(11) Gossens, A.; Maloney, E. L.; Schoonman, J. *J. Chem. Vap*. **1998**, 4, 109.

(12) Omno, T.; Takieda, K.; Higashida, S.; Matsumura, M. *Appl. Catal. A* **2003**, 244, 383.

(13) Kawahara, T. ; Konishi, Y.; Tada, H.; Tohge, N.; Nishii, J.; Ito, S. *Angew. Chem*. **2002**, 114, 2935.

(14) Ohno, T.; Surukawa, K.; Matsumura, M. *J.Phys. Chem. B* **2001**, 105, 2417.

(15) Sun, Q.; Xu, Y. *J. Phys. Chem. C* **2010**, 114, 18911.

(16) Ohno, T.; Surukawa, K.; Matsumura, M. *New J. Chem*. **2002**, 26, 1167.

(17) Varghese, O. K.; Paulose, M.; LaTempa, T. J.; Grimes, C. A. *Nano Lett*. **2009**, 9, 731.

(18) Hamal, D. B.; Klabunde, K. J. *J. Colloid Interface Sci*. **2007**, 311, 514.

(19) Paola, A. D.; Lopez, E. G.; Ikeda, S.; Marci, G.; Ohtani, B. Palmisano *Catal. Today* **2002**, 75, 87.

(20) Bailor, J. C.; Emeteus ,H. J.; Nyholm, R. ; Trotman-Dikenson, A.F. ; Comprehensive Inorganic Chemistry, Volume 1, *Compendium Publishers*, First Edition **1973**.

(21) Zhan, J.; Bando, Y.; Hu, J.; Golberg, D. Inorg. Chem. **2004**, 43, 2462.

(22) Richards, R.; Mulukutla, R.S.; Mishakov, I.; Chesnokov, V.; Volodin, A.; Zaikovski, V.; Sun, N.; Klabunde, K. J. *Scr. Mater*. **2001**, 44, 1663.

(23) Narske, R. M.; Klabunde, K.J.; Fultz, S. *Langmuir* **2002**, 18, 4819.

(24) Richards, R.; Li, W.; Decker, S.; Davidson, C.; Koper, O.; Zaikovski, V.; Volodin, A.; Rieker, T.; Klabunde, K. J. *J. Am. Chem. Soc*. **2000**, 122, 4921.

(25) Mohandes, F.; Davar, F.; Salavati-Niasari, M. *J. Phys. Chem. Solids* **2010**, 71, 1623.

(26) Sharma, M.; Jeevanandam, P. *J. Phys. Chem. Solids* **2011**, 509, 7881.

(27) Lopez, T.; Garcia-cruz, I.; Gomez, R. *J. Catal*. **1991**, 127, 75.

(28) Li, Y. X.; Klabunde, K. J. *Langmuir* **1991**, 7, 1388.

(29) Stark, J. V.; Park, D.G.; Lagadic, I.; Klabunde, K. J. *Chem. Mater*. **1996**, 8, 1904.

(30) Duan, G.; Yang, X.; Chen, J.; Huang, G.; Lu, L.; Wang, X. *Powder Technol*. **2007**, 172, 27.

(31) Chen, F.; Zhao, J.; Hidaka, H. *Int. J. Photoenergy* **2003**, 5, 209-217.

(32) Hu, Y.; Li, C.; Gu F. Zhao, Y. *J. Alloys Compd*. **2007**, 432, 5.

(33) Fang, J.; Bi, X.; Si, D.; Jiang, Z.; Huang, W. *Appl. Surf. Sci*. **2007**, 253, 8952.

(34) Das, D.; Mishra, H.K.; Parida, K.M.; Dalai, A.K. *J. Mol. Catal. A: Chem.* **2002**, 189, 271.

(35) Pal, B.; Sharon, S.; Nogami, G. *Mater. Chem. Phys*. **1999**, 59, 254.

(36) Lin, J.; Yu, J.C. *J. Photochem. Photobiol., A* **1998**, 116, 63.

(37) Osman, J.R.; Crayston, J.A.; Pratt, A.; Richens, D.T. *J. Sol-Gel Sci. Technol* **2008**, 46, 126.

(38) Jung, Y. S.; Kim, K.H.; Jang, T.U.; Tak, Y.; Baeck, S.H. *Curr. Appl. Phys*. **2011**, 11, 358.

(39) Barison, S.; Daolio, S.; Fabrizio, M.; Battisti, A. D. *Rapid Commun. Mass Spectrom*. **2004**, 18, 270.

(40) Reddy, B. M.; Ganesh, I.; Khan, A. *Appl. Catal., A* **2003**, 248,169.

(41) Julian-Lopez, B.; Martos, M.; Ulldemolins,N.; Odriozola, J. A.; Cordoncillo, E.; Escribano, P. *Chem. Eur. J*. **2009**, 15, 12426.

(42) Osman, J.R.; Crayston, J.A.; Pratt, A. ; Ritcher, D.T. *Mater. Chem. Phys*. **2008**, 110, 256.

(43) Hou, L. R.; Yuan, C. Z.; Peng, Y. *J. Hazard. Mater*. **2007**, 139, 310.

(44) Bandara, J.; Pradeep, U.W. *Thin Solid Films* **2008**, 517, 952.

(45) Aberuagba, F.; Kumar, M.; Gupta, J. K.; Muralidhar, G.; Sharma, L. D. *React. Kinet. Catal. Lett.* **2002**, 75, 245.

(46) Wei, X.; Li, H.; Chen, S.; Yuan, C.; Yuan, Q. *Cryst. Res. Technol*. **2009**, 44, 861.

(47) Aramendia, M.A.; Borau, V.; Jimenez,C.; Marinas, J.M.; Porras, A.; Urbano, F.J. *J. Mater. Chem*. **1999**, 9, 819.

(48) Reddy, B.M.; Kumar, M. V.; Ratnam, K. J. *Appl .Catal., A* **1999**, 181, 77.

(49) Qiujie, S.; Ning, L.; Yi, L. *Chin J. Catal* **2007**, 28, 57.

(50) Martin, M.E.; Narske, R. M.; Klabunde, K.J. *Microporous Mesoporous Mater*. **2005**, 83, 47.

(51) Gawande, M.B.; Branco, P. S.; Parghi, K.; Shrikhande, J. J.; Pandey, R. K.; Ghumman, C. A. A. Bundaleski, N.; Teodoro, O. M. N.D.; Jayaram, R. V. *Catal. Sci. Technol*. **2011**, 1, 1653.

(52) Ilian, E. V.; Mishakov, I.V.; Vedyagin, A. A.; Bedilo, A. F.; Klabunde *NSTI-Nanotech*. **2010**, 1, 452.

(53) Abimanyu, H.; Ahn, B. S.; Kim, C.S.; Yoo, K. S. *Ind. Eng. Chem. Res*. **2007**, 46, 7936.

(54) Llanos, M.E.; Topez, T.; Gomez, R. *Langmuir* **1997**, 13, 974.

(55) Carnes, C.L.; Kapoor, P. N.; Klabunde, K.J.; Bonevich, J. *Chem. Mater*. **2002**, 14, 29

(56) Sieger, H.; Suffner, J.; Hahn, H.; Raju, A. R.; Miehe, G. *J. Am. Ceram. Soc*. **2006**, 89, 979.

(57) Aramendia, M. A.; Borau, V.; Jimenez, C.; Marinas, A.; Marinas, J. M. ; Navio, J.A. ; Ruiz, J.R. ; Urbano, F. J. *Colloids Surf., A* **2004**, 234, 17.

(58) Sung, H. S.; Lee, J. K. ; Nastasi, M. *Langmuir* **2005**, 21, 10332.

(59) Stubicar, N.; Tonejc, A.; Stubicar, M. *J. Alloys Compd*. **2004**, 370, 296.

(60) Osabe, D.; Seyama, H.; Maki, K. *Appl. Opt*., **2001**, 41, 739.

(61) Bernard, J.; Belnou, F.; Houid, D. Haussonne, J. M.; *J. Mater. Process. Technol*. **2008**, 199, 150.

(62) Topez, T.; Hernandez, J. ; Gomez, R. Bokhimi, X. Boldu, J.L. ; Munoz, E.; Novaro, O.; Garcia-Ruiz, A. *Langmuir* **1999**, 15, 5689.

(63) Bandara, J.; Hadapangoda, C. C.; Jayasekera, W. G. *Appl. Catal. B* **2004**, 50, 83.

(64) Wen, Z.; Yu, X.; Tu, S. T.; Yan, J.; Dahlquist, E. *Bioresour. Technol*. **2010**, 101, 9570.

(65) Topez, T.; Hernandez-Venture, J.; Aguilar, D.H.; Quintana, P J. *Nanosci. Nanotechnol*. **2008**, 8, 6608.

(66) Utamapanya, S.; Klanabune, K. J.; Schlup, J. R. *Chem. Mater*. **1991**, 3, 175.

(67) Kammler, H. K.; Mädler, L.; Pratsinis, S. E. *Chem. Eng. Technol*. **2001**, 24, 583.

(68) Hargreaves, J.S.J. ; Hutchings, G. J. ; Joyner, R. W. ; Kiely, C. J. *J. Catal*. **1992**, 135, 576.

(69) Che, A.; Tench, J. *Adv. Catal*. **1983**, 32, 1.

(70) M. Anpo, Y. Yamada, Y. Kubokawa, *J. Chem. Soc. Commun*. **1986**, 50, 714.

(71) Pacchioni, G.; Ferrari, A.M.; *Catal. Today* **1999**, 50, 533.

(72) Ding, Z.; Lu, G.Q.; Greenfield, P. F. *J. Phys. Chem. B* **2000**, 104, 4815.

(73) Smith, W. R.; Ford, D. G.; *J. Phys. Chem*. **1965**, 69, 3587.

(74) Zhang, L.; Ji, H.; Lei, Y.; Xia, W. *appl. Surf. Sci*. **2011**, 257, 8402.

(75) Smith, W. R.; Ford, D. G *J. Phys. Chem*. **1965**, 69, 3587.

(76) Zhang, L.; Ji, H.; Lei, Y.; Xiao, W. *appl. Surf. Sci*. **2011**, 257, 8402.

(77) Shrestha, K. M.; Sorensen, C. M.; Klabunde, K. J. *J. Phys. Chem*. C **2010**, 114, 14368.

(78) Jones, G. W.; Lewis, B.; Seaman, H. *J. Am. Chem. Soc*. **1931**, 53, 3992.

(79) D. Urzica, E. Gutheil *Z. Phys. Chem*. **223**, 651, (2009).

(80) Fissan, H. J. *Combust. Flame* **1971**, 17, 355.

4.6. Supporting Information

Fig.4.S1. pXRD patterns of MgO-TiO_2 (2:1) prepared by (a) flame synthesis (b) aerogel method.

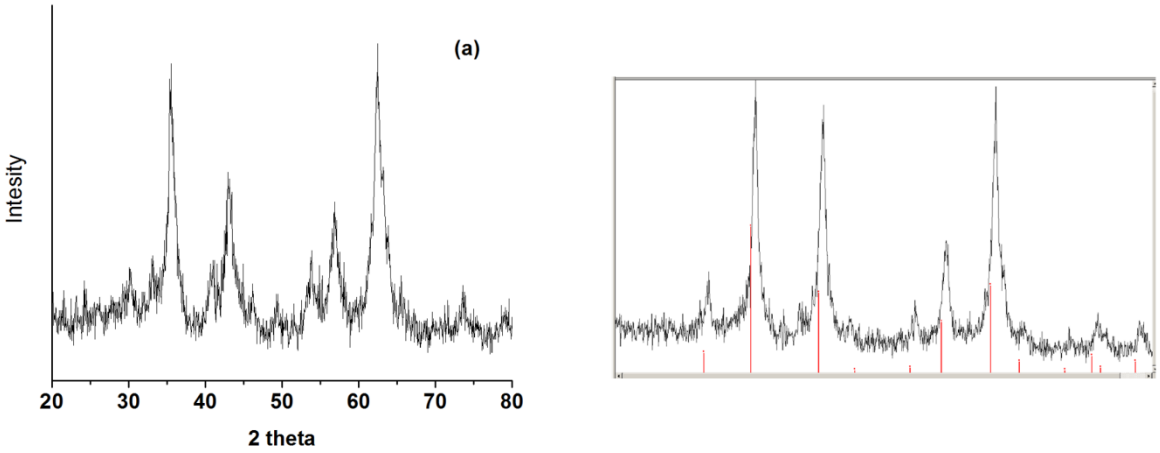

Fig.4.S1a. Formation of $MgTi_2O_4$ (Right: red pattern from JCPDS file no. 16-215).

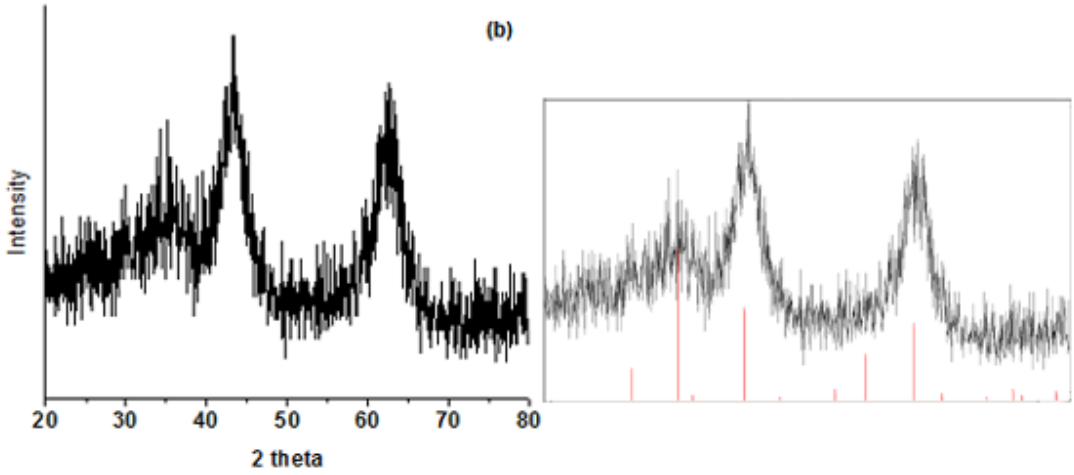

Fig.4.S1b. Formation of $MgTi_2O_4$ (Right: red pattern from JCPDS file no.16-215).

Fig.4.S2. pXRD patterns of MgO-TiO_2 (1:1) prepared by (a) flame synthesis (b) aerogel method.

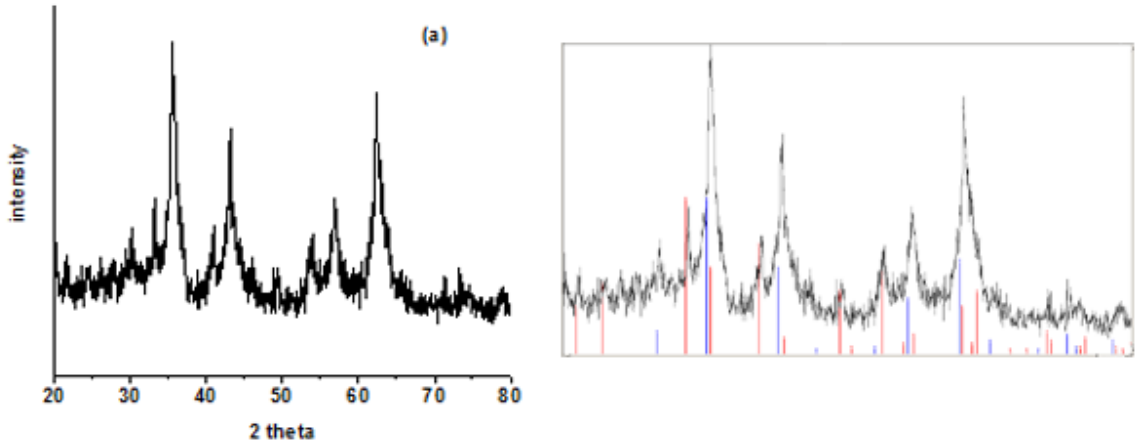

Fig.4.S2a. Formation of $MgTi_2O_4$ (Right: blue pattern from JCPDS file no. 16-215) and $MgTiO_3$ (Right: red pattern from JCPDS file no. 6-494).

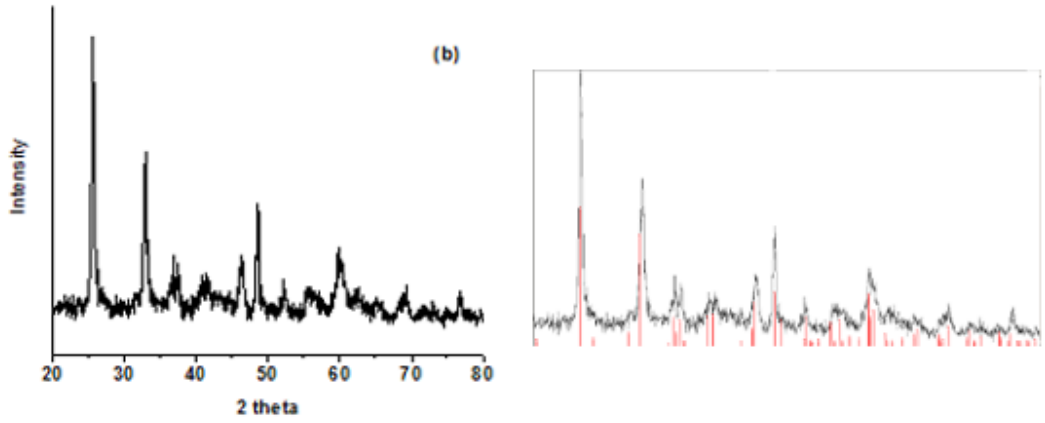

Fig.4.S2b. Formation of $MgTi_2O_5$ (Right: Red pattern from JCPDS file no. 35-792).

Fig.4.S3. pXRD patterns of MgO-TiO_2 (1:2) prepared by (a) flame synthesis (b) aerogel method.

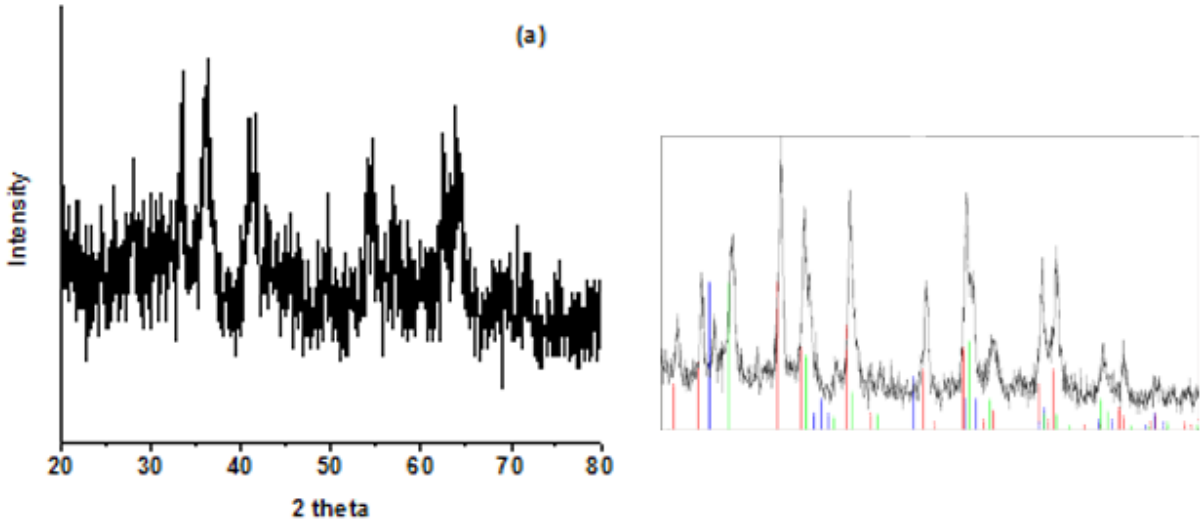

Fig.4.S4a: Formation of $MgTiO_3$ (Right: Red pattern from JCPDS file no. 6-494), Rutile (Right: Green pattern from JCPDS file no. 21-1276), and Anatase (Right: Blue pattern from JCPDS file no. 21-1272).

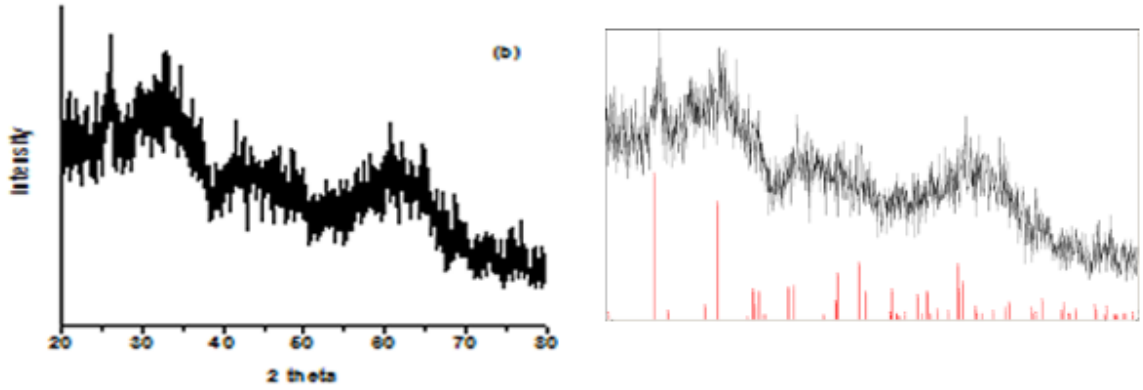

Fig.4.S3b. Formation of $MgTi_2O_5$ (Right: Red pattern from JCPDS file no. 35-792).

Fig.4.S4. EDX data for MgO-TiO_2 with 1:50 and 1:100 mole ratios prepared by aerogel and flame synthesis.

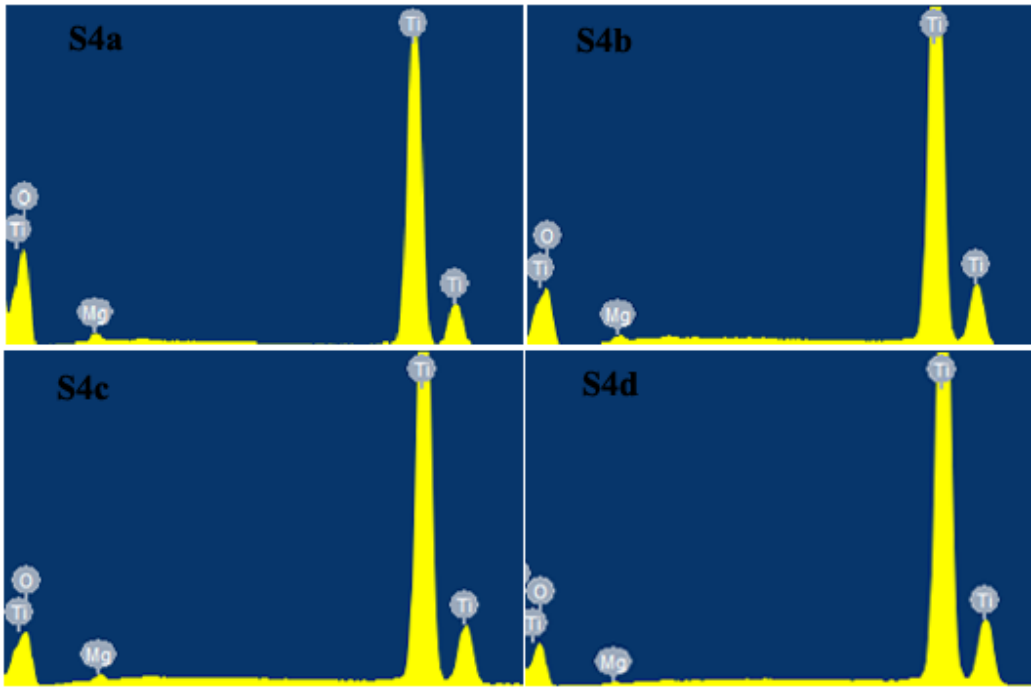

Fig.4.S4a. Mole ratio of Mg and Ti = 1: 52 for MgO-TiO_2 aerogel sample with mole ratio of 1:50.

Fig.4.S4b. Mole ratio of Mg and Ti = 1: 98 for MgO-TiO_2 aerogel sample with mole ratio of 1:100.

Fig.4.S4c. Mole ratio of Mg and Ti = 1: 87 for MgO-TiO_2 sample with mole ratio of 1: 50 prepared by flame synthesis.

Fig.4.S4d. Mole ratio of Mg and Ti = 1: 396 for MgO-TiO_2 sample with mole ratio of 1:100 prepared by flame synthesis.

Fig.4.S5. FTIR spectra of TiO_2, MgO-TiO_2 (1:50), and MgO-TiO_2 (1:1) prepared by flame synthesis.

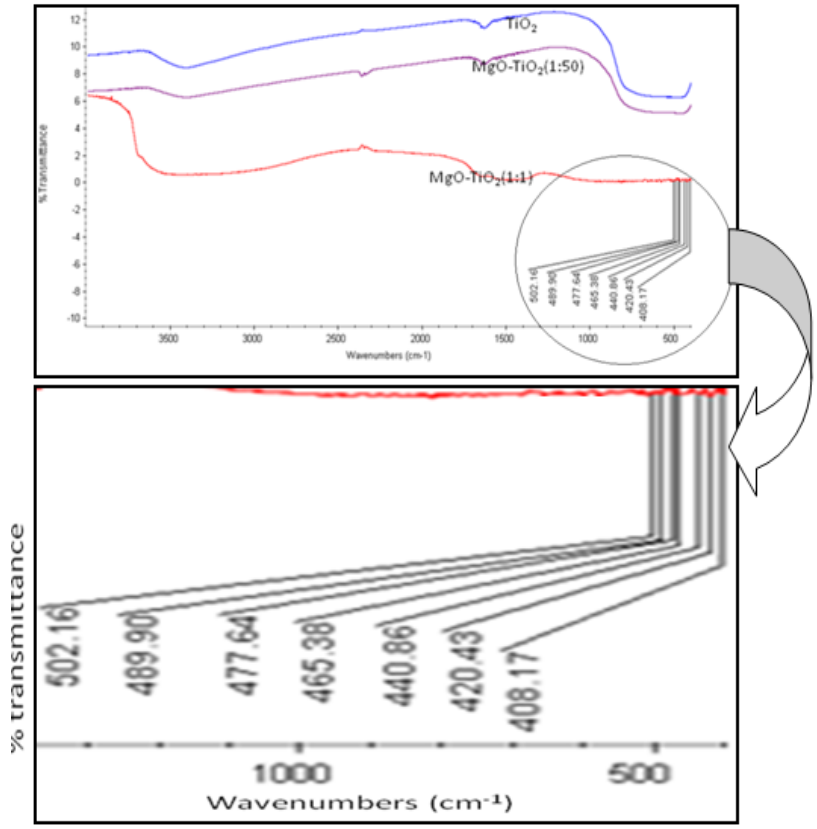

Fig.4.S6: FTIR spectra of TiO_2, MgO-TiO_2 (1:50), and MgO-TiO_2 (1:1) prepared by aerogel method.

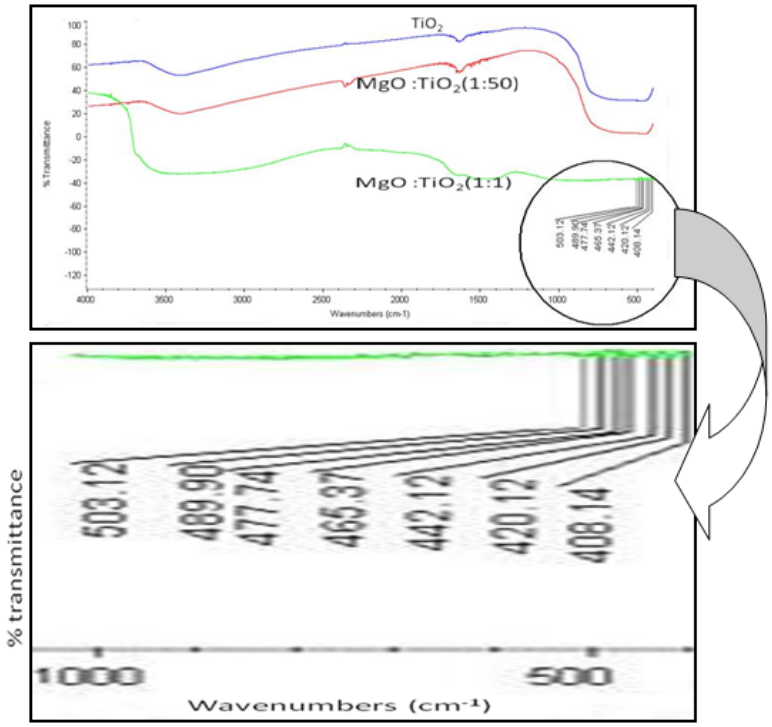

Fig.4.S7(Reproduced): Measurement of CO_2 produced from photocatalytic oxidation of acetaldehyde under UV light by Degussa P25, TiO_2 (as-synthesized), and MgO-TiO_2 mixed oxides with ratios of 1:1, 1:20, 1:50, and 1:100 as photocatalysts prepared by (a) flame synthesis (b) aerogel method.

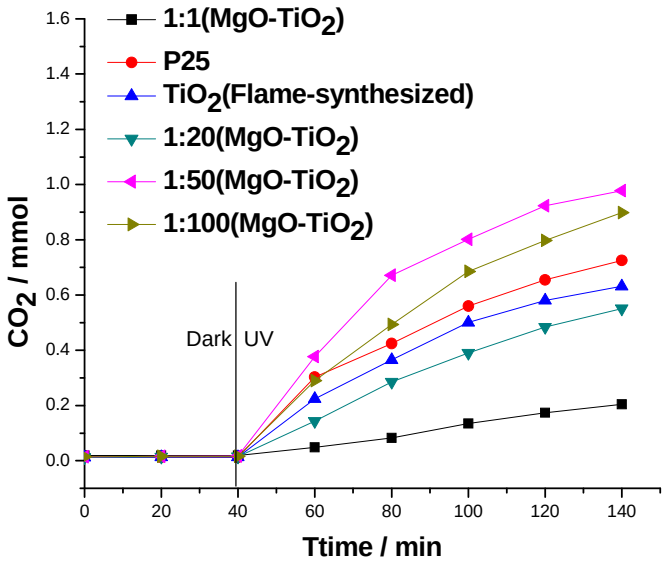

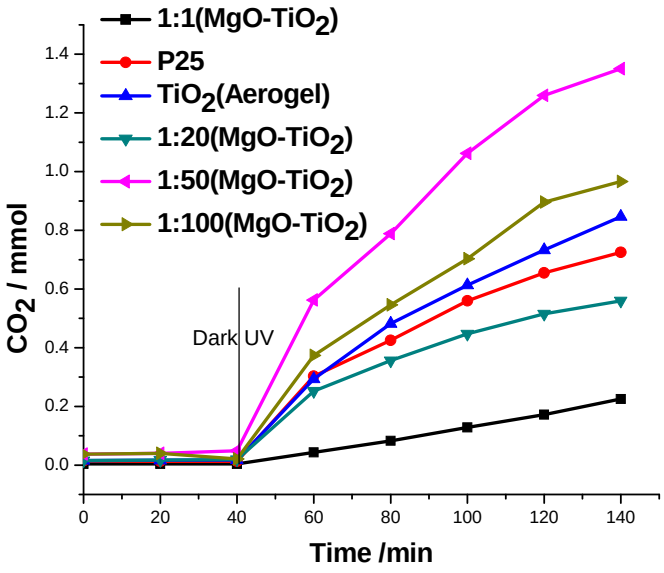

Chapter 5 - Synthesis of Silica Aerosol Gels by Detonation and Flame Synthesis, and Comparison of Their Properties

5.1 Introduction

Traditionally, micrometer size silica-based materials have been widely using in research and industry.[1] They are used as pigments, catalyst substrates, stationary phases in chromatography, pharmacy, ceramics, chemical mechanical polishing, thin film substrates, electronic and thermal insulators, and humidity sensors.[2] Moreover, they are used as stabilizers, coatings, glazes, emulsifiers, strengtheners, and binders. In recent decades, silica nanomaterial has been attractive to researchers in research and development since the nanomaterial might have superior properties compared with bulk SiO_2 material.[3-5] Silica nanoparticles can be dispersed in liquid to improve their suspension behavior although size-dependent physical properties of silica are not too remarkable since silica is an insulator; however, these SiO_2 nanomaterials with chemical functional species are remarkable, the high surface area of smaller silica nanoparticles with functional materials can be exploited for various purposes.[6-11] Amorphous silica material is generally considered as stable and non-toxic.[12] Thus, silica nanomaterials have attracted a great deal of interest because of many potential applications in industries—electronic devices, insulators, catalysis—and pharmaceuticals—enzymes, encapsulation, drug delivery and cell markers—in the field of biochemistry.[13] Silica nanoparticles are also used as additives in plastic and rubbers so that mechanical properties can be improved.[14] So synthesis of silica nanomaterial is important. There are various methods for the synthesis of SiO_2 nanoparticles.[15-18] The sol-gel process has been widely used. In this process, mostly alkoxides of silicon is hydrolyzed; various

parameters—starting materials, amount of water, nature of catalyst, pH, nature of solvent, temperature, time of reaction, aging period, drying method—would play an important role.[19-22] Stober, et al. first reported a pioneering method for the spherical and monodisperse silica nanoparticles from aq. alcohol solution of silicon alkoxide.[23] In this method, ethoxysilane in alcohol of low molecular weight is hydrolyzed in presence of ammonia as a base catalyst so as to get silica nanoparticles. The method has been modified in many ways for the synthesis of monodispersed SiO_2 nanoparticles. The hydrolysis is carried out either in acidic or basic medium at different conditions. Furthermore, SiO_2 nanoparticles with high specific surface area have been prepared by using surfactants. Although state-of-art nanoparticles are prepared by this method, many things should be controlled. There are some limitations— longer reaction time, control of particle size, aggregation and agglomeration, impurities—when the synthesis is carried by sol-gel method; so researchers have also investigated other methods. One of the widely investigated methods is flame synthesis.[24] Flame synthesis is continuous and economically more viable than the sol-gel method; so we can produce more sample in a short span of time by flame synthesis. We need not pay more attention to the effect of pH, surfactant, aging period, and catalyst. Another interesting method could be detonation for the synthesis of nanoparticles;[16] the detonation is a quick batch method so that the method might be worthwhile for the synthesis of nanoparticles under appropriate conditions. Both flame synthesis and detonation are one step dry processes. We need not think about removal of solvent and supercritical drying. In flame synthesis and detonation methods, samples are prepared at relatively high temperature in comparison to the samples prepared with sol-gel method. Samples prepared high temperature might have the possibility of new properties. Sorensen et. al. synthesized silica nanoparticles/nanogels called aerosol gels by detonation using silane gas as a silica precursor;[16]

however, the precursor is toxic and extremely flammable and the precursor is difficult to handle. In this context, we synthesized silica aerosol gels by detonation using a liquid silicon precursor in the same laboratory which was much easier to handle. Furthermore, we synthesized aerosol gels by flame synthesis using different silica precursors. One of the objectives was to compare the properties of silica aerosol gels prepared in both closed and opened environments.

5.2 Experimental Section

5.2.1 Materials

a. Oxygen gas (Linweld)
b. Hexamethyl disiloxane (Sigma Aldrich)
c. Carbon dioxide (Linweld)
d. Dimethoxydimethylsilane (Alfa Aesar)
e. Nitrogen (Linweld)
f. Oxygen gas (Linweld)
g. Methane gas (Linweld)

5.2.2 Synthesis of Silica Aerosol Gels by Detonation. The detonation method was carried out in a cylindrical aluminum reaction chamber with internal diameter 10.2 cm, internal length 11.4 cm, and thickness 3.5 cm so that volume of cylinder was around 931 cc. The detonation chamber had two ports on the side wall; one with pressure gauze and valve for evacuation and filling of desired gases. Another port was for septum with valve for the injection of liquid precursor. Furthermore, there was also a spark plug for initiating the detonation inside the chamber (Fig. 5.1). During the experiment, the reaction chamber was first cleaned and dried. Then the lid was fitted air tightly. The chamber was evacuated to remove air and then filled with pure oxygen. The evacuation and filling of oxygen gas were carried out three times to flush out air. After evacuation, a desired amount of hexamethyl disiloxane (HMDSO) was injected

through a port containing a septum. Then the port was closed using valve. Then oxygen gas was again filled as oxidizer and the valve was closed. After filling the precursor and oxygen gas, the thermocouple was kept in contact with the detonation chamber to note a temperature. The chamber was wrapped with glass wool. Then it was heated to the desired temperature. After attaining the desired temperature, an electric spark was generated inside the detonation chamber using electric solenoid valve(s) with wired electric switch from a remote, safe place. After the detonation sound was heard, about one hour was waited to open the chamber so as to cool. Then white fluffy material was found to be settled mainly at the bottom and some thin coating on the wall of the chamber; some small thin lumps were hanging from the wall of the chamber.

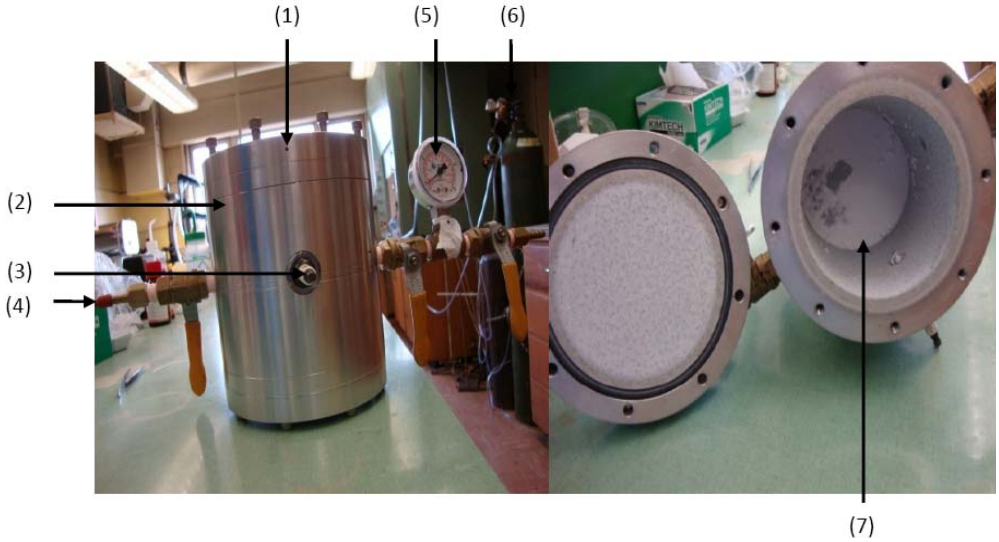

(1)Thermocouple connection point (2) Detonation Chamber (3) Spark plug connection (4) Precursor injecting port (5) Pressure gauze (6) Gas Cylinder (7) Silica formed by detonation.

Figure 5.1 Digital photos of detonation chamber in closed and opened states

Furthermore, many control reactions were carried out. Various amount of HMDSO were injected into the chamber at different in different experiments, and detonation was carried out heating at different temperatures. In a particular experiment, 200 μL HMDSO was injected inside the chamber and the calculated amount of oxygen was filled up so that the precursor could be reacted completely to get silica particles. The detonation was also carried out using CO_2 as background gas.

5.2.3 Flame Synthesis of Silica Aerosol Gels. SiO_2 aerosol gel samples were also prepared by flame synthesis. During the flame synthesis, a silicon precursor, dimethoxydimethylsilane (DMDMS) or HMDSO, were dissolved methanol. In a particular experiment, 3 mL DMDMS was dissolved in 10 mL methanol. The solution was transferred to a tube containing an ultrasonic nebulizer fixed at the bottom of the tube which was extracted from an ultrasonic humidifier (Model V5100 NS; PN 32GB5100B09, Kaz, Inc.). The solution was converted into mist with the help of the ultrasonic nebulizer; the mist along the flow of ultra high pure (UHP) nitrogen (rate = 2 L/min) was driven to the flame of a burner. The flame of the burner was prepared by passing industrial oxygen (10 L/min) and methane (4 L/min) gases. The outer cold surface of a steel bowl with a flat bottom containing ice water was set at the height of 10 cm above the nozzle of the burner so as to collect a deposit of white mass by the thermophoresis process. After 1h, the deposited sample was scrapped out and collected (Fig.5.2).

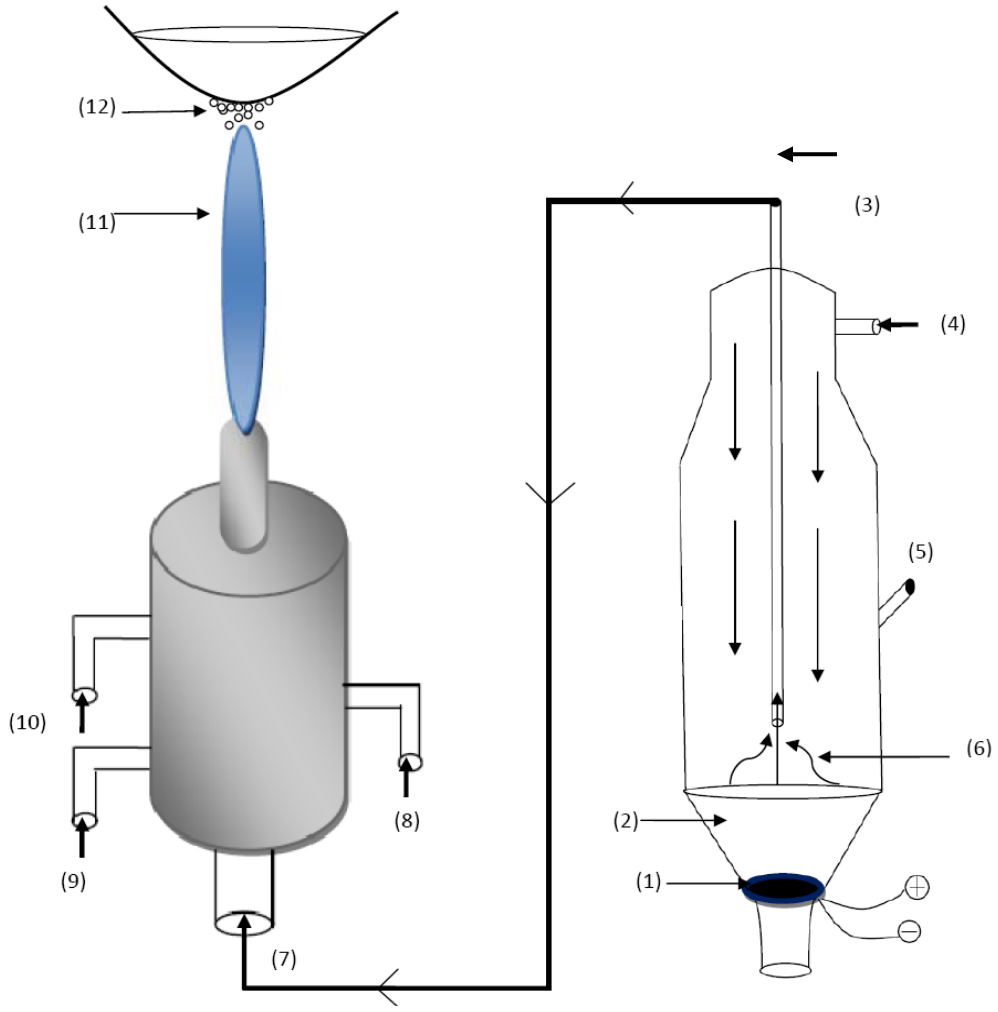

(1)Ultrasonic Nebulizer (2) Precursor solution (3) Mist of precursor driven by nitrogen gas (4) Inlet for nitrogen gas (5) Port for injecting precursor solution (6) Rising mist (7) Inlet for precursor mist driven with nitrogen gas (8) Inlet for methane gas (9) Inlet for oxygen gas (10) Inlet for nitrogen as sheath on the flame (11) Flame (12) Silica aerosol gel.

Figure 5.2 Flame synthesis of silica nanoparticles.

5.2.4 Characterization. (i) Powder X-ray Diffraction (pXRD): Some as-synthesized silica samples were characterized by powder X-ray diffraction. The instrument was Bruker AXS diffractometer D8. The light source was CuKα radiation with applied the voltage of 40 kV and current of 40 mA.

(ii) Transmission Electron Microscopy (TEM): The sizes and morphologies of these silica samples were observed by a TEM. TEM experiments were carried out by using a transmission electron microscopy, Phillips 100 at the biology department of Kansas State University (KSU).

(iii) Brunauer-Emmet-Teller (BET) method: Surface area, pore volume and pore diameter of these materials were measured by using BET N_2 adsorption and desorption experiments. The measurements were carried out using Microsorb II 2300 and Quantachrome NOVA 1200 instrumentation. The samples were cooled to 77 K using liquid nitrogen during the measurement

5.3 Result and Discussion

5.3.1 Silica aerosol gel by detonation. HMDSO (boiling point = 101 ^{o}C) was heated and converted into vapor. When electric spark was produced, HMDSO would react with oxygen explosively in the detonation chamber. As sufficient oxygen was filled, it was supposed that there was complete combustion of HMDSO vapor with the reaction:

$$Si_2C_6H_{18}O + 12O_2 \rightarrow 2SiO_2 + 6CO_2 + 9H_2O \qquad (5.1)$$

When the temperature of the reaction chamber fell down to room temperature, the lid of the chamber was opened and a white fluffy mass was collected and analyzed. The density of the fluffy mass was calculated by measuring mass and volume; the density was found to be around 25 mg /cc, close to a previously reported value.[16]

5.3.1.1 pXRD Analysis

The sample was characterized with pXRD which showed a characteristic peak for silica (Fig.5.3a); the pXRD spectrum implied that the silica was almost in an amorphous form.

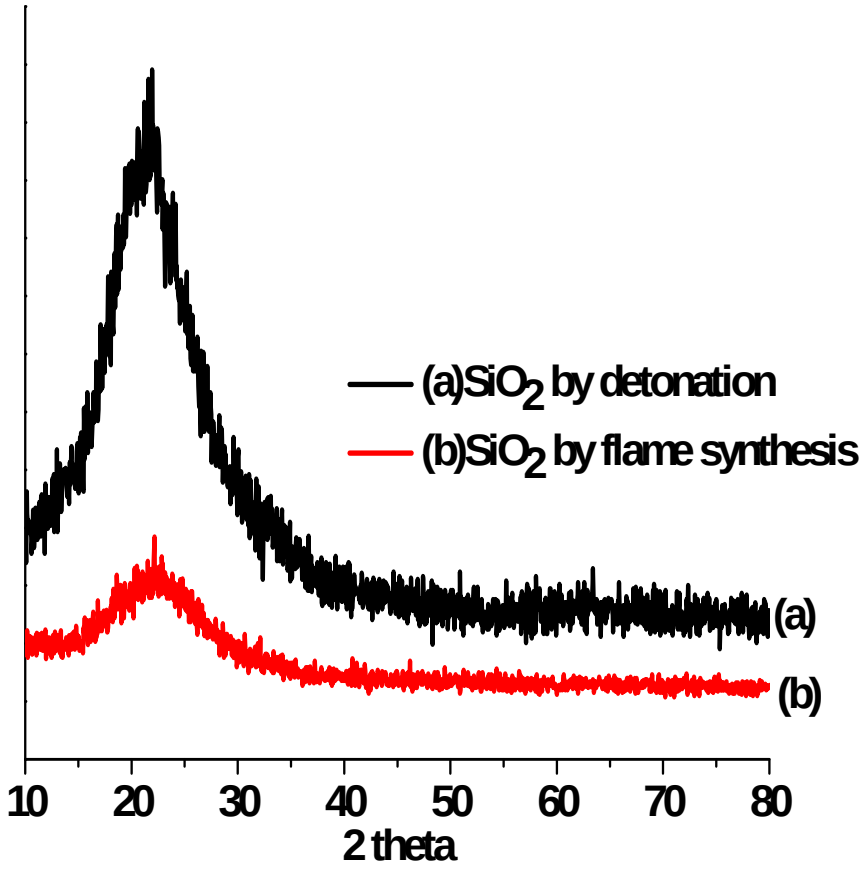

Figure 5.3 pXRD patterns of SiO_2 samples prepared by (a) detonation (b) flame synthesis.

When the same amount of HMDSO was heated at different temperatures using the same quantity of oxygen for the detonation, different amounts of silica particles were found. When detonation was carried out at lower temperature, less silica sample was found; however, at higher temperature, more amount of SiO_2 was obtained (table 5.1). The low amount of silica at lower temperature might be due to the incomplete combustion of the precursor as the there might not be complete evaporation of the precursor for the detonation.

Table 5.1 Yield percentages of SiO_2 with variation of the precursor and temperature prepared by detonation.

No. of Obs	HMDSO(μl)	Temp. (^oC)	Yield %
1	1000	101	50
2	500	101	58
3	250	101	60
4	1000	60	33
5	500	60	35
6	250	60	34

5.3.1.2 Transmission Electron Microscopy Analysis

The SiO_2 aerosol gels prepared by detonation were characterized by TEM imaging, which show that there was formation of spherical SiO_2 nanoparticles. From the TEM images, we found polydispersed nanoparticles with in the range of ~ 75-200 nm when 200 μL silicon precursor was injected inside the reaction chamber and heated at 101 ^oC. The individual silica particles were found to be connected with the adjacent particles so as to form a long chain of nanoparticles in the form of a gel which is termed as aerosol gels (Fig.5.4).

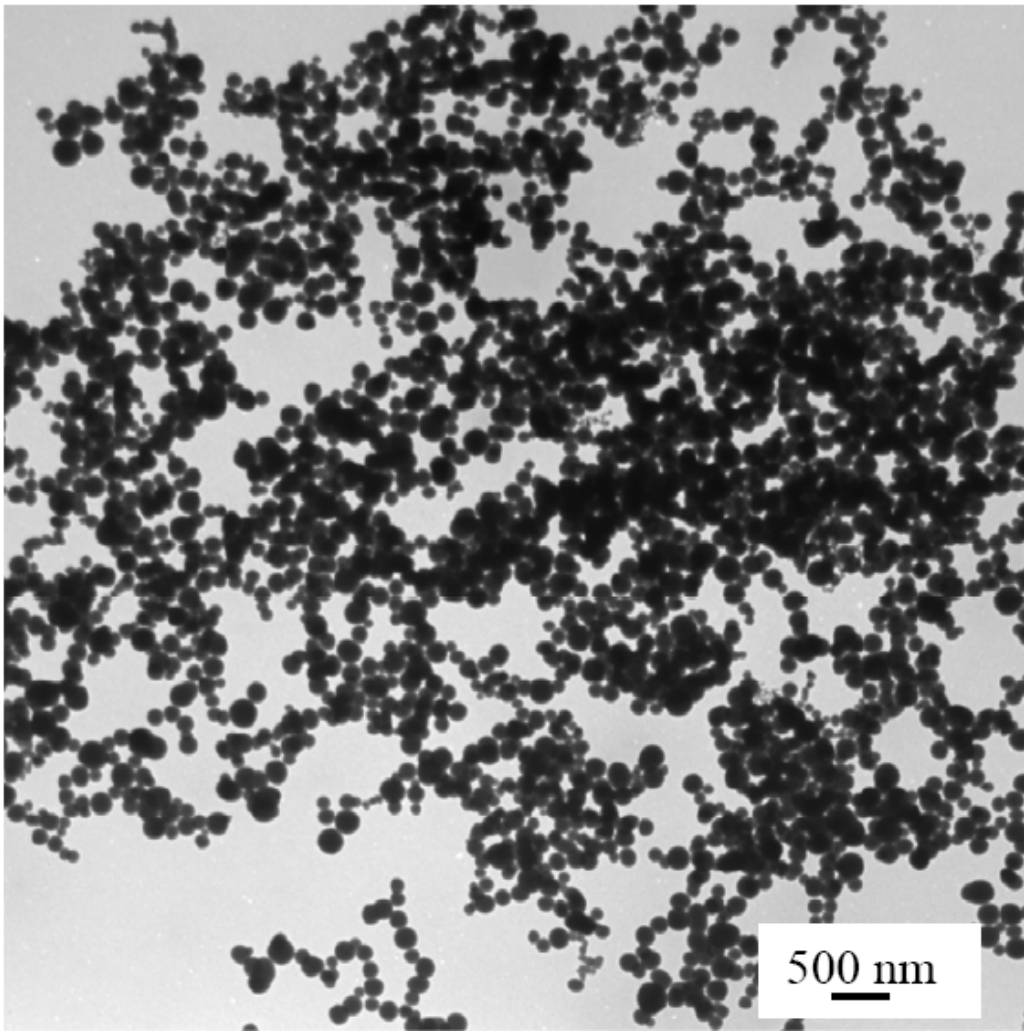

Figure 5.4 SiO_2 nanoparticles prepared by detonation using 200 µL HMDSO heated at 101 ^oC in pure oxygen.

When the amount of precursor was increased to 500 µL with sufficient oxygen for the reaction, the size of silica particles were found to be increased. We observed wide a variation in particle size from ~ 60 nm to ~ 800 nm, as not as a well defined gel of silica particles (Fig. 5.5); in the figure, we can see individual spherical silica particles and their collection.

Moreover, another detonation was also carried using relatively low amount of precursor, 200 μL HMDSO, with carbon dioxide as a background gas and oxygen as an oxidizer; the partial pressures of both gases were one atmospheric pressure before the detonation. In this case, we found significantly smaller silica particles; the size of silica particles was in the range of ~ 5-40 nm (Fig. 5.6).

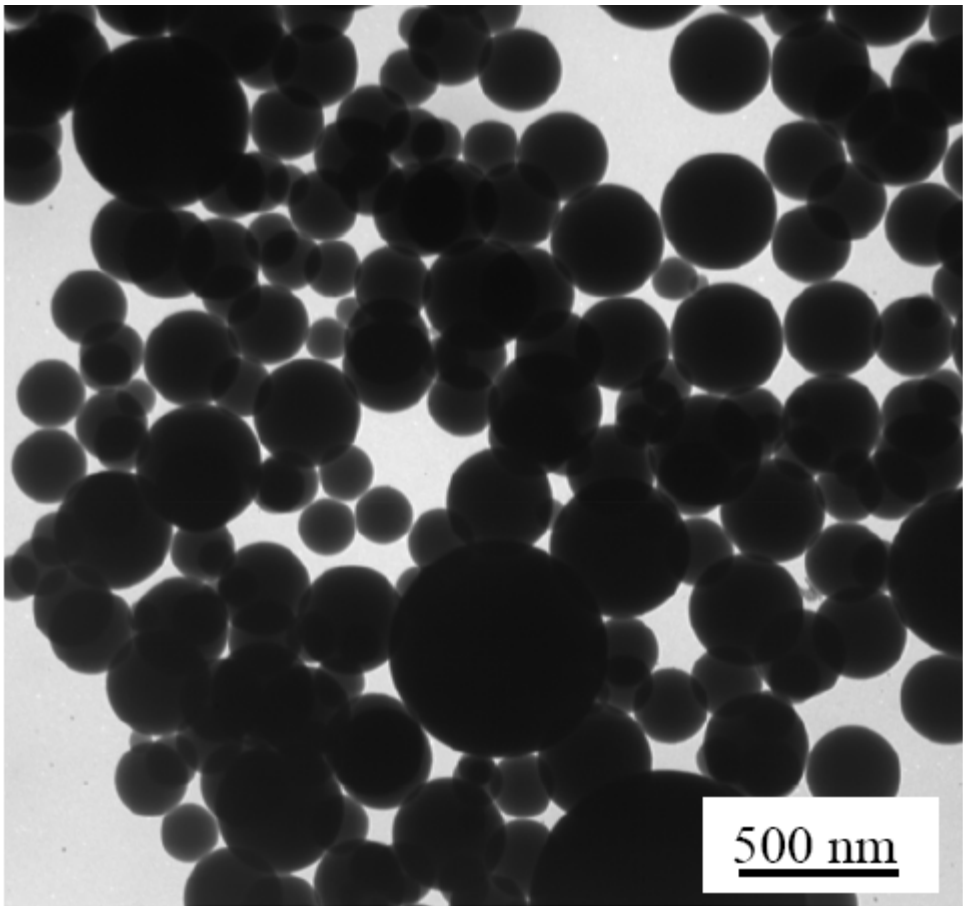

Figure 5.5 SiO_2 nanoparticles prepared by detonation using 500 μL HMDSO heat at 101 ^oC in pure oxygen.

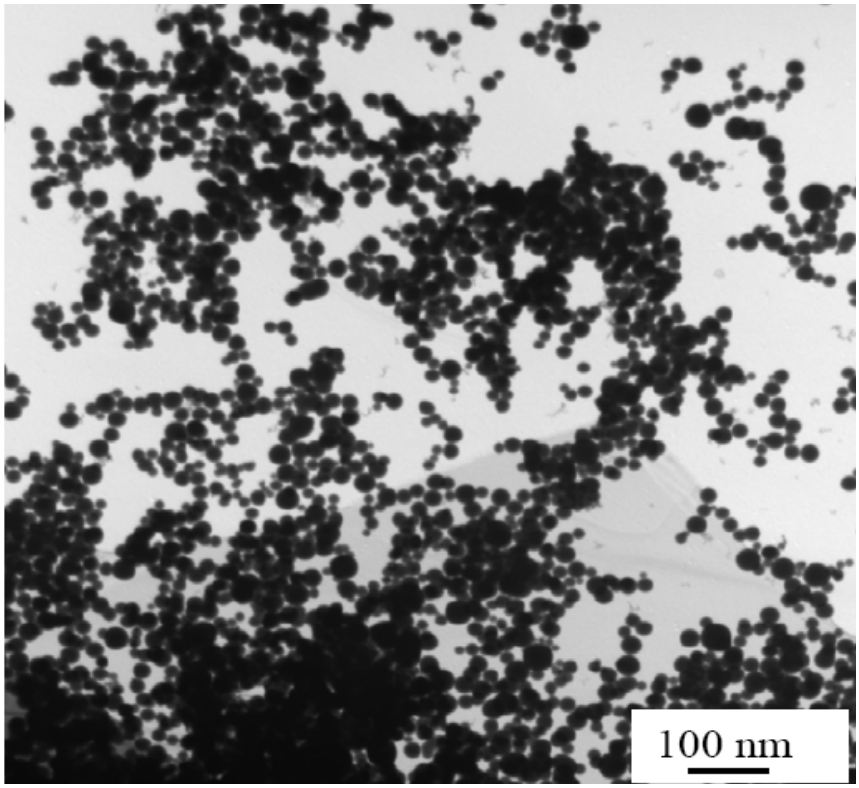

Figure 5.6 SiO_2 nanoparticles prepared by detonation using 200 µL HMDSO heated at 101 ^oC with CO_2 as background gas in pure oxygen.

Table 5.2 BET data of silica nanoparticles

Sample	Area (m^2/g)	Pore volume (cc/g)	Pore Diameter (nm)
SiO_2 by detonation (200 µL DMDSO as precursor)	52	0.082	1.7
SiO_2 by detonation (500 µL DMDSO as precursor)	39	0.062	1.7
SiO_2 by flame synthesis (DMDSO as precursor)	155	0.421	1.7
SiO_2 by flame synthesis (DMDES as precursor)	190	0.332	1.7

The SiO_2 samples were characterized with Brunaur-Emmet-Teller (BET) analysis with nitrogen gas as adsorbate so as to measure specific surface area, pore volume and pore size (table 5.2). The diameter of SiO_2 samples showed that the samples were microporous.

During the detonation reaction, there would be the formation silica molecules. After detonation, the immediate silica molecules combined to give bigger primary particles in the nanoscale range. As prepared by detonation, particles hold excess kinetic and thermal energy, and take a relatively long time to dissipate the energy by those particles in the closed system. It is speculated that the silica particles took the spherical shape due to high temperature, and tendency to minimize the surface energy. During the explosion, there should be formation of smoke of these primary particles. Then the primary particles were headed to aggregate by two processes: coalescence and non-coalescence. By the non-coalescent process, aerosol gels must have formed; gelation is the random aggregation of non-coalescing particles so as to form the branched fractal aggregates.[16] A right condition for a gelation is the gelation time (t_{gel}) which should be shorter than other characteristic times such as settling time or wall deposition time. The gelation time depends upon particle size (a) and volume fraction (f_v) of the particulates as expressed by equation 5.2.[24]

$$t_{gel} = K^{-1}a^3/f_v^{2.5} \qquad (5.2)$$

K is the aggregation rate constant. The equation shows that the greater the particle size, the longer will be the gelation time; so the smaller particle size is favorable for the formation of aerosol gel. Furthermre, the greater the volume fraction, shorter will be the gelation time; the volume fraction was calculated about 10^{-4}. When detonation was carried out using a relatively low amount of silicon precursor with only oxygen gas, there was the formation of low amount of SiO_2; this would be the favorable condition for the formation of aerosol gels due to the formation

smaller particles and large volume fraction. There was the formation of aerosol gels by the interconnection of primary silica nanoparticles (Fig. 5.4). When the detonation was carried using carbon dioxide as a background gas in addition to the precursor, 200 μL, and oxygen, the size of the primary particle was found to be decreased significantly, and again good gelation was found (Fig. 5.6). It is speculated that carbon dioxide, the heavy background gas, could have helped to dissipate energy of primary silica nanoparticles during the Brownian motion, and this could decrease the coalescence of primary nanoparticles. When the detonation was carried out with a amount of silicon precursor, 500 μL, in comparison to previous cases without any background gas, relatively bigger spherical particles were formed. The formation of bigger particles can be considered as normal since more primary silica particles were formed in the beginning in the same volume leading to less volume fraction which caused the coalescence of many primary particles with high energy to form big particles. These big particles are unfavorable for forming aerosol gels as described in equation 5.2. Instead of aerosol gel, we could see the collection of individual bigger particles (Fig. 5.5).

5.3.2 Silica aerosol gels by flame synthesis

When the mixture of silicon precursor and oxygen was allowed to react in a flame, a white solid mass was formed. The sample probably is supposed to formed by following reaction 5.3; the reaction was carried out between dimethoxydimethyl silane and oxygen.

$$Si(OCH_3)_2(C_2H_5)_2 + 10\ O_2 \rightarrow SiO_2 + 8\ H_2O + 6\ CO_2 \qquad (5.3)$$

5.3.2.1 pXRD Analysis

The pXRD pattern showed the formation of silica particles; the sample was found to be almost amorphous in nature (Fig.5.2b).

5.3.2.2 Transmission Electron Microscopy Analysis

The silica samples prepared by flame synthesis were also examined by TEM. We can see spherical and non-spherical particles; spherical particles were found to be relatively bigger. The well defined spherical particles were in the range of ~ 20-100 nm (Fig. 5.7a); in addition to

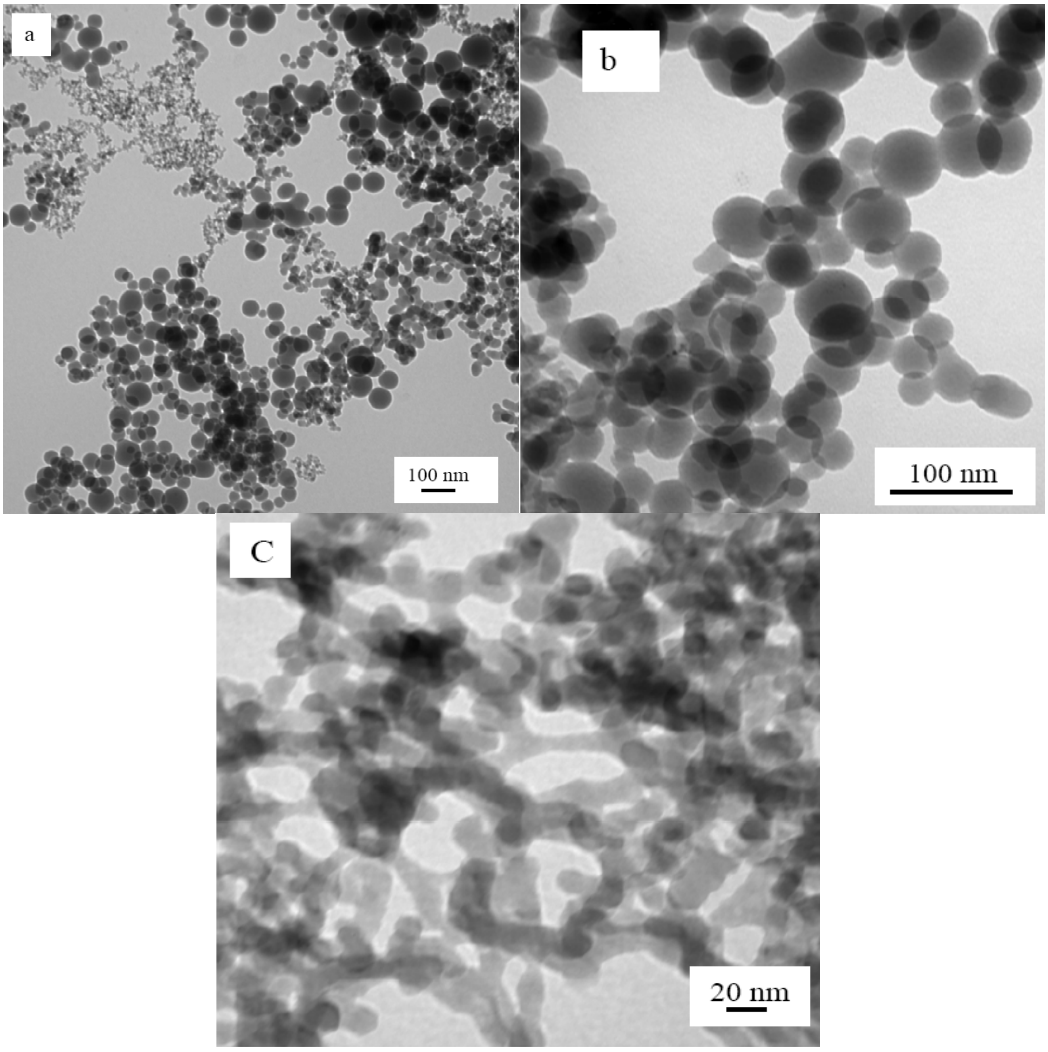

Figure 5.7 Silica nanoparticles prepared by detonation using DMDMS as precursor.

spherical shape, there were also some bigger oval shape silica particles with clearly two different diameters along two perpendicular directions (Fig. 5.7b). In the same TEM image of silica (Fig. 5.7a), smaller non-spherical particles can be clearly observed; these smaller particles had no well defined shape, and were found to be well interconnected to each other so as to form aerosol gels (Fig. 5.7c). In a gel, a narrow neck and slightly expanded form could be observed. The thickness of the narrow neck and expanded form were found to be in the range ~ 5-20 nm. The well defined gels were formed by smaller silica particles than the bigger particles.

The silica samples were also obtained by using HMDSO during the flame synthesis; the main objective of using another silica precursor was to observe the effect of changing precursor. The sample was also characterized by TEM. We observed similar patterns in TEM images as observed in the sample prepared by using DMDMS as the precursor (Fig. 5.8). We could clearly see three types of particles— big spherical, oval, and small non-spherical particles. Big spherical and oval silica particles were in the range of ~ 20-140 nm. The small particles were found to be interconnected to each other forming a gel (Fig. 5.8b). As in previous cases, smaller particles could form well defined gels compared with bigger particles.

BET measurement indicated that the specific surface areas of SiO_2 samples prepared by the flame synthesis were relatively greater than the samples prepared by detonation (table5.2). The samples were found to be mesoporous. The structure of the flame is complex; there are different zones with different temperatures. When the solution of silicon precursor is introduced into the flame, silica nanoparticles are formed at different temperatures. At the hotter zone,

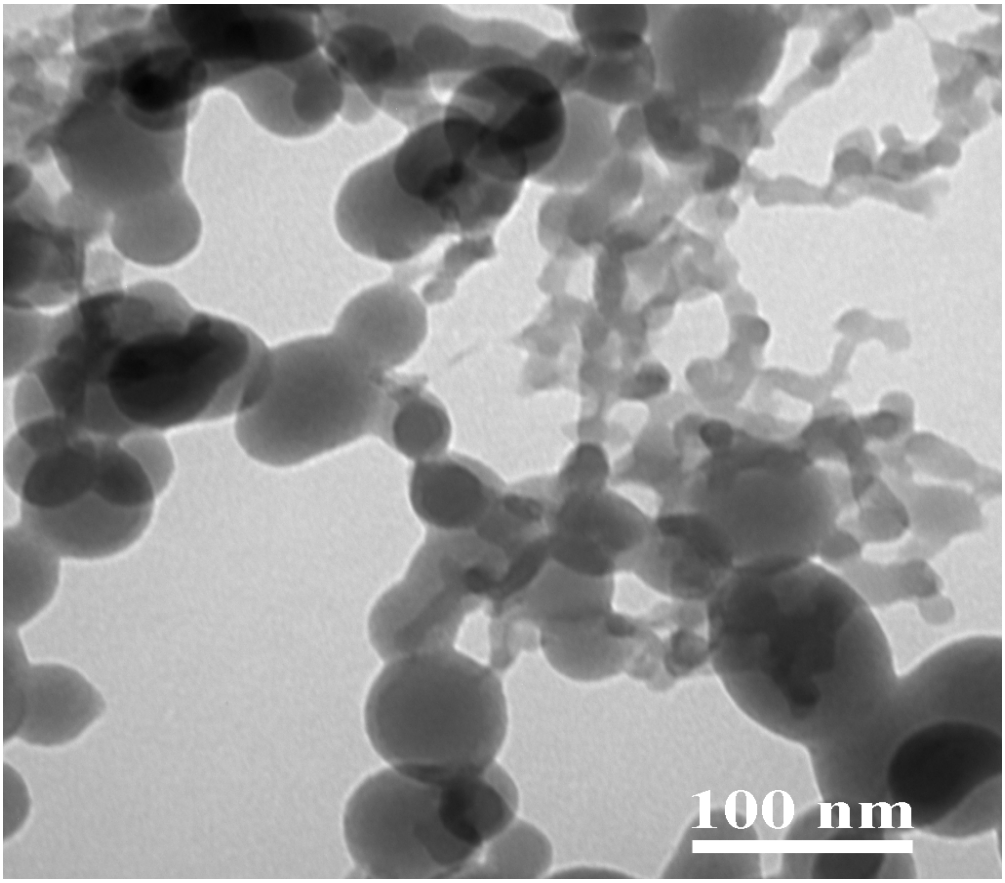

Figure 5.8 Silica nanoparticles prepared by flame synthesis using HMDSO as a precursor.

silicon precursor would react quickly producing a large number of silica particles at a short span of time. Moreover, these particles at higher temperatures would have more kinetic and thermal energy; it is more likely that coalescence of these particles to form bigger spherical particles would occur. So we observed bigger spherical particles in the TEM image of silica particles prepared by flame synthesis. At the medium range temperature zone, the primary particles could coalescence to form bigger particles, and have the tendency to give spherical particles; however, their thermal and kinetic energy should be relatively lower. So it might be that oval shapes would form. At relatively lower temperature zone of the flame, the rate of reaction of silicon precursor with oxygen to form silica particles might be lower; the kinetic and thermal energy of the

particles might be also lower. It is speculated that they would have more tendency to form the aerosol gel rather than coalescence. This might be reason to form the aerosol gels of smaller non-spherical silica nanoparticles.

Silica nanoparticles prepared by different methods—detonation, flame synthesis, sol-gel method—were compared. Literature shows that silica nanoparticles are prepared by sol-gel method with or without surfactant. Silica nanoparticles synthesized by sol-gel method in a particular condition had similar shape and size, and some cases they were monodispersed.[1,25, 26] The shape and size were found to be dependent on various factors such as solvent, surfactant, pH, catalysts. Silica nanopartilces prepared by flame synthesis have different shape and size; such variation in shape and size are likely due to complex nature of the the flame. Indeed, the flame of a burner has generally different temperature zones; it is supposed that various temperature zones would lead to various size and shape of silica nanoparticles as silica particles would have different amount of energy at different temperature zones. In our investigation, we found spherical, oval, and non-spherical particles. The shapes of silica particles prepared by flame synthesis are close to reports in literature prepared by different precursors.[27] The shapes of silica particles are almost independent of precursors as we prepared silica aerosol gels by flame synthesis using two silica precursors: DMDMS and HMDSO. We found silica particles prepared by detonation using HMDSO were spherical, and the nature of shape of silica particles has almost similar to the nature of silica particles previously reported by Sorensen et al. in the same laboratory prepared by using silane, an extremely flammable silica precursor.[16] The size of particles were found to dependent on the amount of precursor and background gas, and formation of silica aerosols was found to be dependent upon particle size and volume fraction.

5.4. Summary

Silica aerosol gels were prepared by detonation and flame synthesis, the closed and opened system respectively. During the detonation, a liquid silica precursor, hexamethyl disiloxane, was used. The silica aerosol gels prepared by this method consisted of spherical nanoparticles. The amount of the silica precursor, affecting the volume fraction, played an important role in the case of formation of aerosol gel and the size of nanoparticles. Larger amounts of the precursor gave relatively larger size particles which are not favorable for the formation of silica aerosol gels. Furthermore, the background gas, such as carbon dioxide, could reduce the particle size of silica nanoparticles, which were found to be favorable for the formation of aerosol gels. One of the important aspects of this result is that the toxic and extremely flammable silica gas precursor can be replaced during the detonation. Silica aerosol gels were prepared by flame synthesis as an opened process. Since a flame structure is complex in nature, there were formations of silica nanoparicles with different shapes—spherical, oval, and non-spherical—and size; the spherical and oval silica particles were relatively larger. These are supposedly formed at relatively higher temperature zones of the flame. The non-spherical particles were relatively small which supposedly formed at relatively lower temperature and might be more favorable to form aerosol gels than bigger particles. It was found that there was almost no effect of changing the silica precursor during the flame synthesis. Since these silica materials were almost amorphous form; they could have many potential applications.

5.5 References

1. Jin, Y.; Lohstreter, S.; Pierce, D. T.; Parisien, J.; Wu, M.; Hall III, C.; Zhao, J. X. *Chem. Mater.* **2008**, 20, 4411.

2. Green, D. L.; Lin, J. S.; Lam, Y. F.; Hu, M. Z. C.; Schaer, D. W.; Harris, M. T. *J. Colloid Interface Sci*. **2003**, 266, 346.

3. Wang, L.; Wang, K.; Santra, S.; Zhao, X.; Hilliard, L. R.; Smith, J.; Wu, Y.; Tan, W. *Anal. Chem.* **2006**, *78*, 646.

4. Yao, G.; Wang, L.; Wu, Y.; Smith, J.; Xu, J. Z.; W.; Lee, E.; Tan,W. *Anal. Bioanal. Chem.* **2006**, *385*, 518.

5. Burns, A.; Ow, H.; Wiesner, U. *Chem. Soc. Rev.* **2006**, 35, 1028.

6. Sun, Y.; Yan, F.; Yang, W.; Zhao, S.; Yang, W.; Sun, C. *Anal. Bioanal. Chem.* **2007**, *387*, 1565.

7. Shang, W.; Nuffer, J. H.; Dordick, J. S.; Siegel, R. W. *Nano Lett.* **2007**, *7*, 1991.

8. Roach, P.; Farrar, D.; Perry, C. *J. Am. Chem. Soc.* **2006**, 128, 3939.

9.Montalti, M.; Prodi, L.; Zaccheroni, N.; Battistini, G.; Marcuz, S.; Mancin, F.; Rampazzo, E.; Tonellato, U. *Langmuir* **2006**, 22, 5877.

10. Vertegel, A. A.; Siegel, R. W.; Dordick, J. S. *Langmuir* **2004**, 20, 6800.

11. Lundqvist, M.; Sethson, I.; Jonsson, B. H. *Langmuir* **2004**, *20*, 10639.

12. Barbe, C.; Bartlett, J.; Kong, L.; Finnie, K. ; Lin, H. Q.; Larkin, M.; Calleja, S.; Bush, A.; Calleja, G. *Adv. Mater*. **2004**, 16 (20), 1-8.

13. Jafardadeh, M.; Rahman, I. A.; Sipaut, C. S. *J. Sol. Gel. Sci. Technol*. **2009**, 50, 328.

14. H. D. Jang Aerosol *Sci. Technol*. **1999**, 30, 477.

15. Dorcheh, A. S.; Abbasi, M. H. *J. Mater. Process. Technol*. **2009**, 199, 10.

16. Dhaubhadel, R.; Rieker, T. P.; Chakrabarti, A.; Sorensen, S. M. *Aerosol Sci. Technol.* **2012**, 46, 596.

17. Panda, S. S.; Mishra, D. P.; Upadhyaya *Powder Technol*. **2009**, 191, 169.

18. Stark, W. J.; Pratnisis, S. E. *Powder Technol*. **2002**, 126, 103.

19. Chu, L.; Tejedor-Tejedor, M. I.; Anderson, M. A. *Microporous Mater.* **1997**, 8, 207.

20. Meixner, D. L.; Dyer, P. N. *J. Sol-Gel Sci. Technol.* **1999**, 14, 223.

21. Colomer, M. T.; Anderson, M. A. *J. Non-Cryst Solids* **2001**, 290, 93.

22. Enomoto, N.; Kumagai, A.; Hojo, J. *J. Ceram. Soc. Jpn*. **2005**, 113, 340.

23. Tabatabaei, S.; Shukohfar, A.; Aghababazadeh, R.; Mihabibi, A. *J. Phys. Conf. Ser.* **2006**, 26, 371.

24. Dhaubhadel, R.; Gerving, C.S.; Chakrabarti, A.; Sorensen, S. M. *Aerosol Sci. Technol*. **2007**, 41, 804.

25. Thomassen, L. C. J.; Aerts, A.; Rabolli, V.; Lison, D.; Gonzalez, L.; Kirsch-Volders, M.; Napierska, D.; Hoet, P. H.; Kirschhock, C. E. A.; Martens, J. A. *Langmuir* **2010**, 26, 328.

26. Sujuki, K.; Ikari, K.; Imai, H. *J. Am. Chem. Soc*. **2004**, 126, 462.

27. Cho, K.; Chang, H.; Kil, D. S.; Park, J.; Jang, H. D.; Sohn, H. Y. *Aerosol Sci. Technol.* **2009**, 43, 911.